University of Kentucky
UKnowledge

Theses and Dissertations--Pharmacy | College of Pharmacy

2016

RNA Nanotechnology for Next Generation Targeted Drug Delivery

Fengmei Pi
University of Kentucky, fengmei.pi@uky.edu
Digital Object Identifier: https://doi.org/10.13023/ETD.2016.432

Right click to open a feedback form in a new tab to let us know how this document benefits you.

Recommended Citation

Pi, Fengmei, "RNA Nanotechnology for Next Generation Targeted Drug Delivery" (2016). *Theses and Dissertations--Pharmacy*. 65.
https://uknowledge.uky.edu/pharmacy_etds/65

This Doctoral Dissertation is brought to you for free and open access by the College of Pharmacy at UKnowledge. It has been accepted for inclusion in Theses and Dissertations--Pharmacy by an authorized administrator of UKnowledge. For more information, please contact UKnowledge@lsv.uky.edu.

STUDENT AGREEMENT:

I represent that my thesis or dissertation and abstract are my original work. Proper attribution has been given to all outside sources. I understand that I am solely responsible for obtaining any needed copyright permissions. I have obtained needed written permission statement(s) from the owner(s) of each third-party copyrighted matter to be included in my work, allowing electronic distribution (if such use is not permitted by the fair use doctrine) which will be submitted to UKnowledge as Additional File.

I hereby grant to The University of Kentucky and its agents the irrevocable, non-exclusive, and royalty-free license to archive and make accessible my work in whole or in part in all forms of media, now or hereafter known. I agree that the document mentioned above may be made available immediately for worldwide access unless an embargo applies.

I retain all other ownership rights to the copyright of my work. I also retain the right to use in future works (such as articles or books) all or part of my work. I understand that I am free to register the copyright to my work.

REVIEW, APPROVAL AND ACCEPTANCE

The document mentioned above has been reviewed and accepted by the student's advisor, on behalf of the advisory committee, and by the Director of Graduate Studies (DGS), on behalf of the program; we verify that this is the final, approved version of the student's thesis including all changes required by the advisory committee. The undersigned agree to abide by the statements above.

Fengmei Pi, Student

Dr. Peixuan Guo, Major Professor

Dr. David Feola, Director of Graduate Studies

RNA NANOTECHNOLOGY FOR NEXT GENERATION TARGETED DRUG DELIVERY

DISSERTATION

A dissertation submitted in partial fulfillment of the requirements for the degree of Doctor of Philosophy in the College of Pharmacy at the University of Kentucky

By

Fengmei Pi

Lexington, Kentucky

Co-Directors: Dr. Peixuan Guo, Professor of Pharmaceutical Sciences

and Dr. Eric Munson, Professor of Pharmaceutical Sciences

Lexington, Kentucky

2016

Copyright © Fengmei Pi 2016

ABSTRACT OF DISSERTATION

RNA NANOTECHNOLOGY FOR NEXT GENERATION TARGETED DRUG DELIVERY

The emerging field of RNA nanotechnology is developing into a promising platform for therapeutically application. Utilizing the state-of-art RNA nanotechnology, RNA nanoparticles can be designed and constructed with controllable shape, size for both RNA therapeutics and chemical drug delivery. The high homogeneity in particle size and ease for RNA therapeutic module conjugation, made it feasible to explore versatile RNA nanoparticle designs for preclinical studies.

One vital module for therapeutic RNA nanoparticle design is RNA aptamer, which can enable the RNA nanoparticles find its specific target for targeted drug delivery. A system of screening divalent RNA aptamers for cancer cell targeting was developed. The system utilized a highly stable three way junction (3WJ) derived from phi29 bacteriophage packing RNA (pRNA). Instead of using one random loop for aptamer SELEX as traditionally, the divalent RNA nanoparticle library contains two variable loops for substrate binding, similar to protein antibodies. The presence of two binding sites on one aptamer greatly enhanced its affinity, and the thermodynamically stability of pRNA-3WJ motif enables controllable RNA folding of each loop. The selected RNA

antibody against epithelial adhesion molecule (EpCAM) A9-8 can deliver therapeutic anti-miR21 to EpCAM positive cancer cells *in vitro*. The feasibility of using RNA aptamer for targeted chemical drug delivery is explored. A phosphorothioate bond modified DNA (thio-DNA) aptamer targeting annexin A2 was utilized as ligand to build nucleic acid nanoparticles for ovarian cancer targeted drug delivery. A DNA/RNA hybrid nanoparticle was generated by conjugating the thio-DNA aptamer to pRNA-3WJ motif. The DNA/RNA hybrid nanoparticles showed favorable property for delivering doxorubicin to ovarian cancer cells *in vitro*, also targeted to ovarian cancer xenograft in bio-distribution study *in vivo*. Utilizing the spatial orientation of pRNA-3WJ, cholesterol modification on the arrow tail of pRNA-3WJ can display RNA nanoparticle on the surface of exosomes/extracellular vesicles (EV) for active targeting. Taking the advantage of RNA ligand for specific targeting; and exosome for efficient membrane fusion, cytosol homing and functional siRNA delivery; the RNA ligand decorated exosomes were constructed for specific delivery of siRNA to cancer cells. PSMA aptamer-displaying exosomes and encapsulated survivin siRNA ($PSMA_{apt}$/EV/siSurvivin) showed efficient gene silencing both in cell culture and animal trials. After systemically injection of $PSMA_{apt}$/EV/siSurvivin to prostate cancer xenograft mice, cancer growth was almost completely blocked. These results suggest the advance of RNA nanotechnology can further drive its way towards clinical application as a novel next generation drug delivery system.

KEYWORDS: RNA Nanotechnology, Phi29 packaging motor, aptamer, SELEX, exosomes, prostate cancer, ovarian cancer

Fengmei Pi

Student's Signature

11/14/2016

Date

RNA NANOTECHNOLOGY FOR NEXT GENERATION TARGETED DRUG DELIVERY

By

Fengmei Pi

Dr. Peixuan Guo
Director of Dissertation

Dr. Eric Munson
Co-Director of Dissertation

Dr. David Feola
Director of Graduate Studies

11-15-2016
Date

To my parents and family for their continued support

ACKNOWLEDGMENTS

Firstly, I would like to thank my thesis advisor, Dr. Peixuan Guo, for his continual support and guidance throughout my PhD studies. I would like to thank Dr. Guo for providing the opportunity to study in such a well-developed laboratory, working in the intriguing research. Secondly, I sincerely appreciate Dr. Guo's mentoring through my research, and providing invaluable advice, experience, and guidance.

Additionally, I would like to thank my committee members, Dr. Eric Munson, Dr. Todd Porter, Dr. Jianhang Jia and Dr. Mark Evers. They gave me valuable advice, help and assistance through my research, qualifying exam, and dissertation defense. Their instruction through my graduate studies proved indispensable in all aspects of my graduate work.

Furthermore, I would like to thank the Center for Clinical and Translational Science at the University of Kentucky for the opportunity to participate in the center and gain valuable knowledge and insight in my cancer related research. Special thanks to Dr. Lisa Privittee, Dr. Piotr Rychahou, Dr. Bin Guo, and Dr. Thiviyanathan Varatharasa for their insight into my research projects.

I would like to thank the members, past and present, of the Peixuan Guo laboratory, as their willingness to share their experience and knowledge in the field proved to be fundamental developing my research and scientific career. I would like to give special thanks to Dr. Dan Shu, Dr. Farzin Haque, Dr. Yi Shu, Dr. Hui Zhang, Dr. Gian Marco De-Donatis, Dr. Randal Rief, Dr. Daniel Binzel, Dr. Ashwani Sharma, Dr. Emil Khisamutdinov and Dr. Mario Vieweger for their training and valuable insight in

my experiments and data throughout my research. I would have not made it through this endeavor without their assistance and kindness. Additionally, I would like to thank all past and present members of the Guo laboratory; Dr. Dan Shu, Dr. Hui Zhang, Dr. Ashwani Sharma, Dr. Mario Vieweger, Dr. Taek Lee, Dr. Chad Schwartz, Dr. Gian Marco De Donatis, Dr. Mehdi Rajabi, Dr. Jia Geng, Dr. Huaming Feng, Dr. Daneil Binzel, Dr. Xijun Piao, Dr. Zhi Zhou, Dr. Xiaofang Jia, Shaoying Wang, Hui Li, Zhengyi Zhao, Danny Jasinski, Erfu Yan, Yanqi Xie, Zhouxiang Ji, Concong Xu, Zheng Cui, Hongran Yin, Sijin Guo, Zhefeng Li, Le Zhang, Hongzhi Wang, and Megan Heitkemper. I truly believe my success would not have happened without the strong team work present in the Guo laboratory.

I appreciate and would like to acknowledge all other faculty and staff members throughout my graduate career, especially graduate coordinator Catina Rossoll and director of graduate studies Dr. Jim Pauly, Dr. David Feola at the College of Pharmacy in University of Kentucky. I thank them for their assistance in my transition to work as a visiting scholar in Dr. Guo's lab in the Ohio State University to finish my Ph. D. thesis study. Additionally I would like to thank them for organizing class schedules, and facilitating my graduate studies.

Finally, I would like to thank and show my appreciation to my parents Zhihua Pi and Quanrong Xu, my husband Song Wang, along with many others for their continued love, encouragement, and support through my everyday struggles. They have meant the world to me through this process and continue to play essential roles in who I am today.

The work in the thesis dissertation was supported by the National Institute of Health under grants R01EB012135, U01CA151648 to Peixuan Guo, and CCTS grant UL1TR000117 to Peixuan Guo and Mark Evers.

TABLE OF CONTENTS

Acknowledgments iii

Table of Contents v

List of Tables vii

List of Figures viii

List of Abbreviations x

Chapter 1: Introduction and Literature Review 1

Brief Summary: 1

Hypotensis: 4

Literature Review: 4

1.1 Nanotechnology and drug delivery 4

1.2 Aptamers and Nanotechnology 12

1.3 Extracellular Vesicles and drug delivery 19

Chapter 2: Development of High-Affinity Thermo-Stable Divalent RNA Antibody for Cancer Cell Targeting and Delivery 27

Abstract: 27

Introduction: 28

Materials and Methods: 28

Results and Discussion: 35

Conclusion: 52

Acknowledgement: 52

Chapter 3: Nanoparticle Orientation to Control RNA Loading or Surface Display of Extracellular Vesicles for Efficient Cell Targeting, siRNA Delivery and Cancer Regression 53

Introduction: 53

Materials and Methods: 54

Results and Discussion:..... 61
Conclusion..... 80
Acknowledgement:..... 83

Chapter 4: RNA nanoparticles harboring annexin A2 aptamer can target ovarian cancer for tumor specific doxorubicin delivery 84
Abstract: 84
Introduction: 85
Materials and Methods 87
Results and Discussion 93
Conclusion:..... 108

Chapter 5: Discovery of a New Method for Potent Drugs Development Using Power Function of Stoichiometry of Homomeric Biocomplexes or Biological Nanomotors ... 111
Abstract: 111
Introduction: 112
5.1 Rationale for selection of multi-subunit biocomplexes as efficient drug targets .. 114
5.2 Inhibition efficiency as a power function of target stoichiometry proved by Phi29 viral assembly system..... 126
5.3 Wide-spread distribution of biomotors with multiple subunits or high order stoichiometry 129
5.4 Targeting biocomplexes for developing potent drugs..... 133
Conclusion and Future perspective 138
Acknowledgement..... 144

Chapter 6: Future Direction and Current State of the Field..... 145
Conclusion and Future Direction: 145
Current Staet of The Field:..... 147

Reference 149

LIST OF TABLES

Table 1. Current exosomes based drugs under clinical trial……26

Table 2. Probability of obtaining complexes containing M copies of drugged and N copies of undrugged subunits Formation ……121

LIST OF FIGURES

Figure 1.1. Schematic drawing shows the basic steps of SELEX. 14

Figure 2.S1. Primary sequence of bivalent RNA nanoparticle library.. 32

Figure 2.1. Physiochemical and biological properties of the bivalent RNA antibody constant measurements.....39

Figure 2.S2. Sequence alignment and secondary structure analysis to identify final RNA Ab.....42

Figure 2.S3.Comparing the binding affinity of selected 3 sequences with MCF7 cells *in vitro* 43

Figure 2.2. Determination of apparent dissociation constants (Kd) of RNA-Ab with cells.....46

Figure 2.3. Testing the cell entry of RNA-Ab by confocal microscopy.....48

Figure 2.4. Determination of apparent dissociation constants (Kd) for loop deleted RNA-Ab with EpCAM positive MCF7 Cells. 50

Figure 2.5. RNA-Ab mediated delivery of anti-miRNA21 to EpCAM positive cancer cells.....52

Figure 3.1. RNA nanotechnology for decorating native EVs 65

Figure 3.S1.Physopchemical characterization for EVs and RNA nanoparticles.....67

Figure 3.2. Difference between arrow head and arrow tail cholesterol.....71

Figure 3.S2. RNA nanoparticles can be displayed on EVs outer surface by cholesterol anchoring.....73

Figure 3.3. Specific binding and siRNA delivery to cells *in vitro* with PSMA aptamer displaying EVs 76

Figure 3.S3.Western blot detect the knockdown of survivin protein by EVs.....77

Figure 3.4. A*nimal* trials using ligands displaying EV for tumor inhibition 79

Figure 4.1. Characterization of endo28-3WJ DNA/RNA hybrid nanoparticles 95

Figure 4.2. Loading doxorubicin into Endo28-3WJ nanoparticles and its *in vitro* release 98

Figure 4.3. The binding and internalization of Endo28-3WJ to annexin A2 positive cells 101

Figure 4.4. *In vitro* delivery of doxorubicin by Endo28-3WJ-Sph1 nanoparticles to cells 103

Figure 4.5. Cell cytotoxicity assay for Endo28-3WJ-Sph1/Dox intercalates *in vitro* .105

Figure 4.6. *In vivo* targeting of Endo28-3WJ to ovarian cancer xenograft in mice model 107

Figure 5.1 The morphology and stoichiometry of Phi29 DNA packaging motor.. 120

Figure 5.2 The relationship between the stoichiometry of homomeric target complex (Z) and target complex inhibition effect (IC)... 125

Figure 5.3 Comparing Phi29 viral assembly inhibition efficiency by targeting components with different stoichiometry.... 128

Figure 5.4.Widespread biomotors or nanomachines are composed of multisubunit complex.... 132

Figure 5.5.Examples of homomeric multisubunit complex as drug target for developing potent drugs.... 137

LIST OF ABBREVIATIONS

2'-F	2'-Fluoro RNA Modification
-OH	Hydroxyl
-NH2	Primary amine
3WJ	Three Way Junction
$\Delta G°$	Change in Gibbs Free Energy
DNA	Deoxy Nucleic Acid
dsDNA	Double Stranded Deoxy Ribonucleic Acid
EtBr	Ethidium bromide
FBS	Fetal Bovine Serum
K_D	Dissociation Constant
miRNA	Micro Ribonucleic Acid
mRNA	Messenger Ribonucleic Acid
PAGE	Polyacrylamide Gel Electrophoresis
PCR	Polymerase Chain Reaction
pRNA	Packaging Ribonucleic Acid
PSMA	Prostate Specific Membrane Antigen
RISC	RNA-Induced Silencing Complex
RNA	Ribonucleic Acid
RNAi	Ribonucleic Acid Interference
RNase	Ribonuclease
rtPCR	Real Time Polymerase Chain Reaction
C_t	Total Concentration
siRNA	Small Interfering Ribonucleic Acid
PBS	137 mM NaCl, 2.7 mM KCl, 100 mM Na_2HPO_4, 2 mM KH_2PO_4, pH 7.4
TBE	89 mM Tris-borate, 2 mM EDTA
TBM	89 mM Tris, 200 mM Borate Acid, 5 mM $MgCl_2$
TMS	50 mM Tris pH 8.0, 100 mM NaCl, 10 mM $MgCl_2$
EV	Extracellular Vesicles
PEG	Poly Ethylene Glycol
SELEX	Systemic Evolution of Ligands by Exponential Enrichment
ESCRT	Endosomal Sorting Complex Required for Transport
TSG101	Tumor Susceptibility Gene 101 Protein
Alix	ALG-2-interacting Protein X
CD40	Cluster of Differential 40 Protein
IL4	Interleukin 4
HIV-1	Human Immunodeficiency Virus 1
CD63	Cluster of Differential 63 Protein
STAU	Staufen
AGO2	Argonaute 2

TNRC6A	Trinucleotide Repeat Containing Gene 6A
RVG	Rabies Virus Glycoprotein
Lamp	lysosome associated membrane glycoproteins
BACE1	Beta- Secretase 1
Let7	Lethal-7
EGFR	Epidermal Growth Factor Receptor
TLR3	Toll Like Receptor 3
MHC	Major Histocompatibility Complex
GMP	Good Manufacture Practicing
GM-CSF	Granulocyte macrophage Colony stimulating factor
UC	Ultracentrifugation
EpCAM	Epithelial cell adhesion molecule
Ab	Antibody
DHFBI	3, 5-difluoro-4-hydroxybenzylidene imidazolinone
LNA	Locked nucleic acid,
UV	Ultraviolet
FDA	Food and Drug Administration
AMD	Age related Macular Degeneration
VEGF	Vascular endothelial growth factor
4-1BB	CD137, tumor necrosis factor receptor superfamily member 9
CTLA-4	Cytotoxic T-lymphocyte-associated protein 4
EDTA	Ethylenediaminetetraacetic acid
SDS	Sodium dodecyl sulfate
kDa	Kilodalton
Dox	Doxorubicin
MexB	Multidrug resistance protein MexB
AcrB	Recombinant Aerobic respiration control sensor protein ArcB
ABC	ATP-binding cassette
TMD	Transmembrane domains
NBD	Nucleotide-binding domain
ATP	Adenosine triphosphate
IMPDH	Inosine monophosphate dehydrogenase
FabI	Fatty acid biosynthesis 1
ASCE	Additional Strand Catalytic E
IC_{50}	Half maximal inhibitory concentration
LD_{50}	Median lethal dose
AFM	Atomic Force Microscopy
NTP	Nucleoside triphosphate
GDP	Guanosine diphosphate
GMP	Guanosine monophosphate
IMP	Inosine monophosphate
GPCR	G-Protein-Coupled Receptors
CNS	Central Nervous System
Bpm	Burkholderia pseudomallei

Chapter 1: Introduction and Literature Review

BRIEF SUMMARY:

Chapter 1 begins this thesis with an overview on the RNA nanotechnology and its application for targeted drug delivery. First the current status and promise of nanotechnology and RNA nanoparticles for drug delivery system are examined. Next the status of RNA aptamers development, the advancement of aptamer selection method, its application and advantages for clinical application are discussed. Finally, Extracellular vesicles (EVs) as an emerging field in therapeutics and diagnosis is introduced, including its biogenesis, native functions in biological organism, regulation of its secretion. The application extracellular vesicles as new generation therapeutics as well as drug delivery vehicles are discussed.

Chapter 2 looks at the development of bivalent RNA aptamers targeting to cancer stem cell marker epithelial cell adhesion molecule (EpCAM). The highly stable three way junction (3WJ) derived from phi29 DNA packaging motor pRNA was utilized as a core motif to construct an antibody shaped RNA library with two random regions for binding region selection. The extracellular domain of EpCAM protein was used as target for RNA aptamer selection. The selected divalent 2'F-pyrimidine modified RNA aptamers can bind specifically to its target with K_D value around 100nM. The selected EpCAM aptamer can bind to EpCAM positive cancer cells and specifically delivery locked nucleic acid (LNA) based anti-miR21 into cancer cells and induce cancer cell apoptosis.

Chapter 3 studies how to utilize the orientation of pRNA-3WJ to control RNA loading or surface display on extracellular vesicles for efficient cancer cell targeting,

siRNA delivery and cancer regression. Placing a membrane anchoring cholesterol molecule at the arrow tail of pRNA-3WJ resulted displaying of RNA aptamer or folate ligand on to the surface of extracellular vesicles. Taking advantage of the RNA aptamer ligand for specific targeting and EVs for efficient membrane fusion, the resulting RNA aptamer-displaying EVs were used for specific delivery of siRNA with efficient gene silencing resulting in complete blockage of cancer growth. Animal studies showed that the nanometer scale ligand-displaying EVs specifically localized in tumor xenografts without accumulating in healthy organs. Efficient gene silencing was observed both in cell culture and animal trials from systemic administration of Prostate Membrane Specific Antigen (PSMA) aptamer-displaying EVs loaded with survivin siRNA.

Chapter 4 studies the application of RNA aptamer harboring nanoparticles for ovarian cancer targeted delivery of chemotherapeutics doxorubicin. A multifunctional RNA nanoparticle harboring phosphorothioate bond modified DNA aptamer targeting annexin A2 protein, and GC rich sequence for intercalating doxorubicin was designed and constructed. The highly stable pRNA-3WJ structural motif provides a rigid core to the RNA architecture and disfavors misfolding of aptamers when conjugated to other oligonucleotides, while keep their affinity and functions intact. Thus, this nanoparticle design is of significance utility for aptamer mediated targeted delivery. The nanoscale RNase-resistant RNA nanoparticles remained intact after systemic injection in mice and accumulated specifically to tumors with little or no accumulation in healthy organs 6 h post-injection. The RNA nanoparticle/doxorubicin intercalates showed enhanced toxicity to ovarian cancer cells with annexin A2 overexpressing, but reduced toxicity to annexin A2 negative cells in cell toxicity assay. These results suggest that the constructed

nanoparticle can potentially enhance ovarian cancer targeted doxorubicin delivery for cancer treatment at lower doses with enhanced efficacy.

Chapter 5 studies the discovery of a new method for potent drug development using power function of stoichiometry of homomeric biocomplexes or biological nanomotors. Targeting multisubunit homomeric biological motors with a sequential action mechanism, highly potent drugs can be developed. Inhibiting multisubunit tragets with sequential actions resembles breaking one bulb in a series of Christmas lights, which turns off the entire string. Besides the drug binding affinity, the potency of drug inhibition depends on the stoichiometry of targeted biological complexes. As biomotors with multi-subunits are widespread in viruses, bacterial and cells, this approach should have general application in the development of inhibition drugs with high efficiency. Most viral DNA packaging motors contain a high-stoichiometry machine composed of multiple components that work cooperatively and sequentially. Thus, it is an ideal target for potent antiviral drug development.

Chapter 6 briefly summarizes the major findings in the way of RNA nanotechnology for pharmaceutical application discussed in this thesis dissertation. Furthermore, the future direction of this work is described providing a prospective on research that is still needed to move forwards the application of RNA nanotechnology. Finally, the current state of RNA nanotechnology is discussed looking at the major hurdles that have been solved and look at how the recent advancements can drive RNA nanotechnology into the cancer therapy.

HYPOTHESIS:

The 3WJ motif from Phi29 bacteriophage packaging RNA (pRNA) provides a stable RNA scaffold for the construction of nanoparticles for the treatment of cancers.

LITERATURE REVIEW:

1.1 Nanotechnology and drug delivery

Nanotechnology is a young scientific field that represents a vast variety of disciplines ranging from fundamental material science to many applied sciences including pharmaceutics. The application of nanotechnology in medicine is referred to as nanomedicine, which has profound impact to improve the efficacy of chemotherapeutics and gene therapeutics, also improve diagnostic sensitivity for early disease diagnosis(1) by enhancing tumor targeting and reduce its systemic toxicity, given the premise of developing intelligent drug delivery systems.

Nanomedicine field is undergoing a revolution in the recent years. A wide variety of nanoparticle materials are studied and used in nanomedicine. The varieties of material include liposomes, polymeric micelles, dendrimers, quantum dots, iron oxide particles, carbon nanotubes, and nucleic acid based nanoparticles (2-4). The most exciting concept of nanomedicine research is the emerging of multifunctional nanoparticles. They normally include multiple mix and matched functionalities, include components of ligand for targeting nanoparticles to a specific location; linkers and core structures that give the nanoparticle defined shape and size; therapeutic or diagnostic cargoes that either encapsulated or conjugated to the nanoparticles; and sometimes with a proper coating material to improve its bioavailability and biocompatibility(3). For example, chemical drugs can be loaded into traditional nano-delivery systems such as micelle (5), polymer

nanoparticles (6), liposome (7), carbon nanomaterials (8), quantum dots (9,10), and gold nanoparticles (11) for *in vivo* tumor targeted imaging and therapy. Nanomedicine is also harnessed for the delivery of gene therapeutics including RNAi drugs.

RNA interference is an innate cell machinery to regulate gene expression by noncoding RNA, which mainly includes small interfering RNA (siRNA) and micro RNA (miRNA). The short single stranded miRNAs can form duplexes with its complementary mRNA sequences in the 3'untranslated region. RNAi inhibits specific target gene expression either by mRNA degradation or translation inhibition. MiRNA mediated mRNA degradation normally occurs only when the miRNA perfectly matches its target mRNA; partially complementary to target mRNA sequence inhibits the mRNA translation with even a single nucleotide base change (12). The challenges to apply RNAi based therapies include their cellular uptake, bio-distribution, stability, off-target effect and toxicity *in vitro* and *in vivo*. The negative charge of RNAi molecules makes them difficult to cross cell plasma membrane (13). To enhance cellular uptake of RNAi, traditional transfection techniques, such as electroporation, gene gun, microinjection, and viral transfection can be employed *in vitro*; but not for *in vivo* systemically administration. To facilitate clinical application of RNAi treatment, passive tissue targeting and active cellular targeted delivery strategies are explored. Passive targeting strategies mainly utilize positively charged natural or artificial polymer materials forming complex with negatively charged RNAi for delivery. Stable nucleic acid-lipid particles (SNALP) are lipid based nanoparticles which encapsulate RNAi payloads by forming complex between the cationic lipid with negative charged RNA(14). The concern for SNALPs is its accumulation in liver and toxicity for liver, kidney and immune system(15), thus it is not

used for human testing. 1.2-dioleoyl-sn-glycero-3-phosphatidylcholine (DOPC) (16), histidine-lysine peptides (17), atelocollagen rich in positively charged amino acids (17) have been used for siRNA delivery through passive targeting by EPR effect. Active cellular targeting is a very promising direction for systemic delivery. Different approaches have been studied for loading siRNA to achieve target cell specific delivery. Cholesterol siRNA conjugates mainly targets liver(18); N-acetylgalactosamine modified dynamic polyconjugates mainly targets the asialoglycoprotein receptor on hepatocytes(18); RGD (Arg-Gly-Asp) peptide modified PEI (polyehtyleneimine) complex mainly targets integrins which is a receptor highly expressed on cancer cells and extracellular matrix around tumor(18); transferrin conjugated PEG-cylodextrin containing poly-cationic (CDP) particles targets transferrin receptors expressed on many tumors(19); the specific ligand expressed as fusion proteins composed of mAb fragments with positively charged human truncated protamine targets specific receptor expression cells(20); aptamer siRNA chimeras also provided a new platform for specific cell targeted siRNA delivery(21). The siRNA delivery systems under clinical trials now are mainly CDP nanoparticles, SNALP liposomes for systemic administration, and local administration by intravitreal injection or inhalation (13).

The well-known EPR (enhanced permeability and retention) effect is a major mechanism for nanomedicines getting accumulated in tumors and thus distinguishes the nanomedicine from traditional small chemical drugs. In fact, whether EPR effect is sufficient to achieve the desired enhanced therapeutic effect in human is questioned. EPR effect only offers around 2-fold increase tumor environment than normal organs in fact (22), as the tumor microenvironment is quite complex. The tumor vasculature usually has

incomplete endothelial lining thus having larger pores leading to higher vascular permeability and hydraulic conductivity (23). However, there are multiple barriers to the nanodelivery systems to reach tumor cells, except for the clearance by mononuclear phagocyte systems (MPS) for larger nanoparticles or by kidney glomerular filtration for smaller nanoparticles, the abnormal tumor vasculature, the high interstitial fluid pressure in tumor tissue, the solid mechanical stress produced by tumor growth and abnormal extracellular matrix in tumor tissue all created barriers for extravasation of nanoparticles to penetrate into tumors(22). Methods to improve the EPR effect of nanodelivery systems including modulating the tumor blood flow, modulating the tumor vasculature and stroma and killing the cancer cells to reduce barrier functions are under intensive study(24). A very promising way to improve the therapeutic effect of nanomedicine stratagem call Near infrared photo immunotherapy involves using a targeted monoclonal antibody conjugated to a photon absorber IR Dye 700, where the EGFR targeting antibody directed nanoparticles to bind tumor cell membrane, 24 h post administration, the tumor was exposed to NIR light at 690 nm thus induces nearly immediate necrotic tumor cell death(25).

Birth of RNA nanotechnology

Advancement in nanotechnology paved the way for developing more sophisticated drug delivery systems for transporting varieties of bio-functional molecule to the desired site for diagnosis and treatment. The field of DNA nanotechnology had significant progress recent years, DNA nanostructures have been employed as smart imaging agents or delivery platforms on living organisms. Nucleic acid based nanoparticles have advantage over inorganic nanoparticles for *in vivo* application

including their high purity, easy production and reproducibility, biocompatibility and biodegradability (26).

DNA nanotechnology was initialized by Nadrian C. Seeman in early 1980s, after the discovery of double-helical, G quadruplexes, X or Y-shaped DNA (27). Three dimensional nanostructures can be designed and constructed with single strand and double stranded DNA sequences, with confined shape and structure, exploiting the Watson-Crick base paring principle. Sticky ends of DNA were used as toeholds for self-assembly process, thus the building blocks of DNA nanoparticles can be precisely controlled(28). Novel DNA origamis was constructed with a 7249nt long circular plasmid DNA from virus M13mp18 with more than 200 short DNA oligoes as staple strands(29), which can fold the long single strand DNA at specific sites to a designed shape. To apply for clinical use, DNA nanostructures must meet several essential requirements, such as they should remain intact after exposing to blood plasma, no immunogenicity. A major challenge the DNA nanotechnology field facing now is the serum stability of DNA nanoparticles, Although it was found that the rigid tetrahedron DNA structures(30), compact DNA nanotubes(31) and DNA origami nano arrays(32) have improved nuclease resistance, most DNA nanoparticles have a half- life. Although most DNA structures are more stable at high Mg^{2+} concentration condition, such condition is not available *in vivo*(33).

RNA nanotechnology is also a newly emerging field, with an evidence showing that RNA nanoparticles can be assembled from bottom up assembly in 1998 (34), led by Peixuan Guo. Dimer, trimer and hexamer pRNA nanoparticles were constructed using the reengineered RNA fragment from phi29 DNA packaging motor packaging RNA, using

the intermolecular interaction between two loops of each reengineered pRNA molecule(34,35). This was an early proof of concept study for RNA nanotechnology. The RNA nanotechnology field went into a rapid development phase after overcoming the barricade of enzymatically and thermodynamically instability of RNAs by chemical modifications. These include modification on bases such as 5-BrU and 5-IU (36), modification on the phosphate linkage such as phosphothioate and boranophosphate (37), modifications on the 2'-OH group with 2'-fluoro, 2'-o-methyl, 2'-amine (38-41), and locked nucleic acid (42) which is modified by forming an extra bridge between 2'-O and 4'-C. 2'F pyrimidine modified RNA nanoparticles showed enhanced serum stability, the 2'F-pRNA 3WJ nanoparticles are stable in 50 % serum after 8 hours incubation at 37 °C (43), in contrast, unmodified pRNA-3WJ are degraded in 50 % less than 1 h. LNA or other chemical modification also greatly enhanced RNA particles enzymatically stability substantially(4).RNA nanoparticles constructed with the modified RNA strands have enhanced serum stability and also thermodynamical stability (44). The same pRNA-3WJ structure formed by 2'F-pyrimidine modified RNA strands showed higher thermodynamic stability than unmodified RNA, following by DNA, which was verified by as the dissociation constant (apparent K_D) value for 2'F-RNA, RNA and DNA pRNA-3WJ nanoparticles to be 4.5 nM, 11.4 nM and 47.7 nM respectively; as well as the entropy value ($\Delta G°_{37}$) to be -36, -28 and -15 kcal/mol for 2'F-RNA, RNA and DNA based pRNA-3WJ structure (44).

Several toolkits have been developed as principles for RNA nanoparticle construction. The toolkit 1 utilized a biomimetic strategy learned from phi29 pRNA hexamer structure, the hand in hand interaction between adjacent pRNA molecules. The

pRNA folds into a complex structure including a helical ds-RNA domain with open 5'/3' end and interlocking regions with two loops which was described as left hand and right hand of pRNA. Interaction between the right hand and left hand loop from two pRNA molecules promote a dimer formation(34,45,46). This mechanism has been utilized to construct pRNA trimer, tetramer, pentamer and hexamer(47,48).

The toolkit2 utilizes palindrome sequence forming foot-to-foot interaction based higher ordered RNA nanoparticles. A palindrome sequence reads the same from either 5' end to 3'end direction or from 3'end to 5'end direction. Palindrome sequences can be added to the end of helix domain of pRNA nanoparticles to form foot-to-foot dimer, foot-to-foot trimer, foot-to-foot tetramer and so on(4).

The toolkit3 utilizes the highly thermodynamically stable pRNA-3WJ domain as a core structure, and forming multivalent RNA nanoparticles by extension its arms. This branched pRNA 3WJ nanoparticle have been shown to be able to carry three different functional modules including fluorescent dye for *in vivo* tracking of nanoparticles, an RNA aptamer for active targeting, and a siRNA or miRNA sequence for functional gene expression modulation(43,49,49-52) . The similar principle was also extended to forming a X-shaped motif which can carry four pieces of siRNA sequences and achieve synergetic effect for gene knockdown(53).

Toolkit4 utilize more native tertiary RNA motifs to build varieties of three dimensional RNA structures. The flexible pRNA-3WJ motif was utilized to construct two dimensional RNA triangles, square, pentagon and hexagon structures (54,55), and even the three dimensional RNA tetrahedron (56), prism (57) structure. Geary et al. design and constructed an RNA sheet using 180° and 120° kissing-loop (KL) motifs from HIV-1

DIS and RNAi/ii inverse loop (58), and dovetail motifs (59). A 2D hexagonal lattice structure was created by connecting multiple tiles with kissing loop interactions. The formed RNA structure called RNA origami can be folded during cotranscription without request for annealing process. Nasalean et al. built an RNA filament structure by assemble H-shaped RNA nanoparticle based on four way junction motif with loop-loop interaction (60). Otherwise, similar strategy for DNA nanoparticle design such as using Watson-Crick base paring and cross over can also be used for RNA nanostructures.

Toolkit 5 utilizes DNA/RNA hybrids to construct nanoparticles with functional controlled release of fragment RNA (61). As the DNA and RNA have different thermodynamic properties, which can be used to tune triggered dissociation of the DNA/RNA hybrids (62-64).

RNA nanotechnology is getting more and more attention recently as they seem to be the most appropriate carrier for functional RNA molecules, such as RNA aptamers which can specifically bind to cancer cell marker for disease diagnosis and drug delivery (43,65), siRNA and miRNA for RNAi therapy (66), or immune modulator CpG oligos for immunotherapy (54). Intense studies on RNA nanotechnology for pharmaceutical application are ongoing, including large scale production, and its immune modulation properties, as well as its pharmacodynamics properties. MiRNA therapy includes miRNA mimics and miRNA inhibitors. The miRNA inhibitors bind to a single stranded mature miRNA to block its function, thus chemical modification on the anti-microRNA sequence the hurdle of chemical and enzymatically stability can be solved. Substitution of the 2'-OH group in the ribose ring with 2'-O-methyl, 2'-O-methoxyethyl, or 2'- fluoro groups have shown increased the stability of anti-miRs (67). Successful delivery of LNA

modified anti-miR21 seed sequence by RNA nanoparticles harboring EGFR targeting aptamer showed promising result in regression of breast cancer in mice study(66). For the miRNA mimics delivery, it is more challenging. The synthetic miRNA mimics must be double stranded and processed into RNA induced silencing complex (RISC) to be functional. Nanodelivery systems which can enhance its cancer cell targeted delivery, and augment successful endosomal escape are important factors for miRNA therapeutics.

1.2 Aptamers and Nanotechnology

Aptamers are single stranded DNA or RNA oligonucleotides which can fold into variety of complex secondary structures and thus bind to diverse targets including small molecules, peptides, proteins and even whole cells with high affinity and specificity. Aptamers are generated from an *in vitro* selection process called SELEX (Systematic Evolution of Ligands by EXponential enrichment) (68). Aptamers mimics antibody in the property of binding to target molecule with high affinity and specificity, while it exhibits significant advantages in terms of its stability, ease of synthesis and its small size.

1.2.1 SELEX method

In vitro selection process, like finding a needle from a large haystack, starts with construction of a large pool containing 10^{13} to 10^{16} random nucleic acid sequences followed by iterative selection and amplification processes to get rid of the non-binding sequences, while amplify and enrich the target binding sequences (**Figure 1.1**). The selection process is usually monitored by the affinity of library to its target after each round of selection. The end point of selection is usually marked with non-increasing affinity of the library comparing to the previous round. The final round library is then sequenced for aptamer identification.

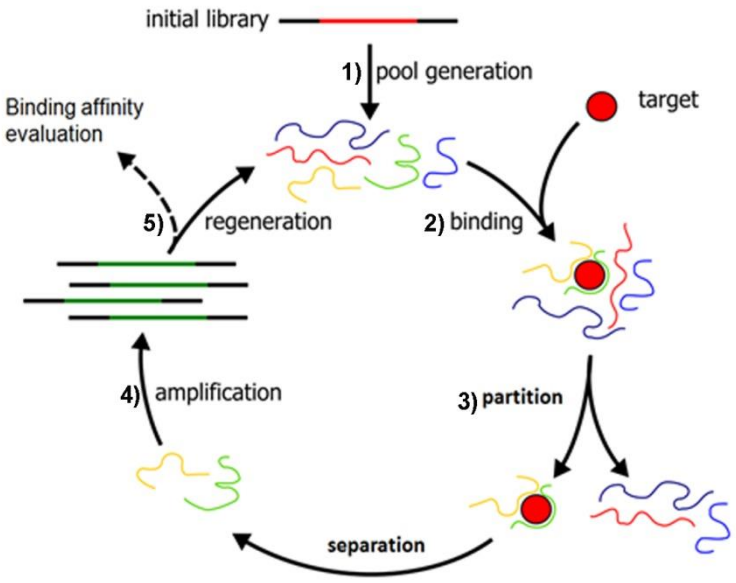

Figure 1.1. Schematic drawing shows the basic steps of SELEX. 1). A library contains multiple sequences is constructed by *in vitro* transcription or chemical synthesis 2). The library RNAs are subjected to binding reaction with the target molecule; 3). The mixture of library and target complexes is then subjected to partition by method of selection; 4). Remove the nonbinding sequences, the target binding sequences are then recovered and amplified 5). Prepare library for next round of selection.

The target for aptamer selection varies from small chemical entities such as malachite green (69,70), 3, 5-difluoro-4-hydroxybenzylidene imidazolinone (DHFBI) (71,72), to peptide, protein and cells. Through the invention of SELEX method in 1990s by Tuerk and Gold (73), great efforts have been made to the methodology to improve its success rate. One key step in SELEX process is the partition of the targeting binding sequence from the non-binding sequences. To this end, nitrocellulose filter was used as partition media to keep the protein bound nucleic acid sequences on the filer while remove the non-binding sequences (74); later, functionalized magnetic beads were developed as media to immobilize the target molecule thus recover the target binding sequences on the beads(75). Considering the in silico folding of proteins might be different from their folding when expressed on cell membrane, cell SELEX(76) and tissue SELEX(77) were later adopted by scientists to find aptamers that can be directly used clinically.

Another important step in SELEX process is sequencing. In traditional method the last round library is usually cloned into vectors and single clones were randomly picked up for Sanger sequencing (78). This step seems like trying one's luck to get high affinity aptamer. Recently, with the development of next generation sequencing technology, next generation sequencing method has been utilized to aid SELEX (79,80). Millions of sequences from amplified library can be analyzed at the mean time with deep sequencing technique. The chance of finding an aptamer is increased by this method, which also can be used to monitor the process of SELEX rather than a blinded operation.

To select an aptamer with high binding affinity to its target *in vitro* is usually not the final goal for a SELEX project. A useful aptamer should be resistant to nuclease

digestion, also can bind its target *in vivo* for application. To this end, large efforts have been made, such as chemically modify the library during selection or the final aptamer post selection to improve stability of the aptamer. Modification on both the sugar phosphate backbone and the nucleobases of a RNA molecule can increase its stability, and also expand its chemical functionality, increase the library diversity. Replacing the phosphate-sugar backbone with phosphorothioate(81) or bridging the 2'-O and 4'-C of the ribose forming locked nucleic acid (LNA) (82) can greatly increase the aptamer stability against nuclease digestion(83). Examples of backbone modification on aptamers include using 2'-amino-pyrimidines(84,85), 2'-Fluoro-pyrimidine(86,87), 2'-O-methyl purine(88), Locked nucleic acids(89), 4'-thio-pyrimidine(90) or mixed modified nucleotides(91) during *in vitro* transcription for library preparation. Y639F T7 RNA polymerase can be used for most pyrimidine modified library preparation (83); KOD Dash DNA polymerase can be used for LNA modified library preparation (89). 2'-Fluoro pyrimidine modification is widely used for aptamer selection, the final VEGF aptamer on market was selected using this protocol. But several 2'-amino pyrimidine modified RNA aptamers are difficult to be synthesized in large scale thus they were abandoned from therapeutic candidates (92). 2'-O-methyl is a common post transcriptional modification on mRNA in nature, thus aptamer with 2'-O-methyl modification is easier to get approved by FDA.

Modification on bases of RNA oligonucleotides can increase their enzymatically stability, and also possibly enhance their catalytic functionality. It was reported that incorporating an imidazole ring with nearly neutral pKa to library pool could enhance their catalytic function (93). An RNA amide synthase was selected from RNA library

including 5-imidizol uridine (94). Including 5'-bromo and 5'-iodo modified pyrimidine into aptamer sequence can aid the UV crosslinking of aptamer to its target(83). 6-aminohexyl adenosine was incorporated into RNA library during SELEX for ribozyme selection (95).

Modification on the termini of an aptamer was also explored to increase its stability and *in vivo* half life time (96). It was reported that capping the 3'end of thrombin binding aptamer with locked nucleotides increased its stability against nuclease in human serum (97). The incorporation of 2'4'-LNA to the 3'end of DNA aptamer was achieved by terminal deoxynucleotidyl transferase (TdT)(98).

1.2.2 Aptamers for therapeutics

The first aptamer drug was approved by FDA in 2004, which is an RNA aptamer against vascular endothelial growth factor (VEGF) -165 for wet age related macular degeneration (AMD) treatment (99). This aptamer drug was developed targeting VEGF165. By targeting VEGF165, the aptamer can block its interaction with VFGF receptor presenting in eye blood vessels, and inhibit angiogenesis. Three separate SELEX experiments were carried out in NeXstar Pharmaceuticals for its development (84,100). The first unmodified RNA aptamer was isolated from a library with 30 random nucleotides in 1994 (84). Subsequently, a 2'-NH_2 pyrimidine modified RNA aptamer was isolated and modified with 2'-O methyl on purine bases poste selection to increase its nuclease resistance (100). Later, the 2'-F pyrimidine modified RNA aptamer was selected with further improved affinity, the aptamer was modified with 2'-O methyl on purine bases poste selection to enhance its nuclease resistance *in vivo*. The 2'-F pyrimidine, 2'-O methyl RNA aptamer was selected for final drug development as Pegaptanib (100,101).

Another aptamer targeting α-thrombin protein is being developed to an anti-coagulation drug by blocking the interaction between fibrinogen and thrombin (102), which is under phase II clinical trial by ARCA Biopharma Company (103).

The potential of using aptamer for immunotherapy has also been explored. DNA aptamer-lipid probe was used to modify cell surface through noncovalent link for specific cell targeting (104). This method can be used to engineer immune effector cells for cancer therapy. DNA nanoscaffolds with double star shape or linear brunch shape templated multivalent bispecific aptamer showed the ability to bridge two kinds of cell specifically together (105). Oligonucleotide aptamers against immune modulation proteins such as 4-1BB, CTLA-4 can also be developed as immune modulation drugs (106).

1.2.3. Aptamers for targeted drug delivery

Besides being directly used as drugs, aptamers are also used as bullet for targeted drug delivery. Targeted therapy can improve cancer treatment by increasing efficacy, reducing toxicity and side effects. Aptamers have been widely used in targeted delivery for chemotherapy and gene therapy. Two main types of aptamer modified drug delivery systems are the aptamer nanomaterial conjugates and aptamers functionalized nucleic acid nanoparticles (107).

Aptamers conjugated to varieties of nanoparticles can be used for targeted drug delivery. Gold nanoparticles, silica nanoparticles, graphene or fullerene carbon based nanoparticles have all been functionalized with aptamers for active targeting (104,107). Multivalent aptamer decorated gold-silver nanorods can increase its target cell binding affinity; can be potentially used for cellular imaging (108). Gold nanorods decorated with

multiple prostate cancer targeting aptamers showed potential for targeted photo thermal therapy targeting prostate cancer (109). Porous hollow magnetite nanoparticles decorated with PEG functionalized with aptamer can load doxorubicin into the nanoparticles, and direct nanoparticles to cancer cells through receptor mediated endocytosis, release drug in the acidic lysosomal(110).

Aptamers fused to DNA or RNA nanoparticle can act as drug carriers by loading chemotherapeutic agents through intercalation reaction (111), and nucleic acid based therapeutics such as miRNA or siRNA through strand extension (52,66). But this should be done without sacrificing the overall folding and affinity of both aptamer and the drug conjugate (43,48,53).

1.2.4 Advantages and challenges for developing aptamer to drugs

There is significant advantage for using aptamers in diagnosis and disease treatment. Aptamers are selected from an *in vitro* process without the request for animals, and can be chemically synthesized which will ensure controllable quality assurance comparing to the batch variations normally noticed in antibody production. One concern of nucleic acid based aptamers for *in vivo* application is the stability. Its stability against nuclease was greatly improved by using chemical modified RNA oligonucleotides to instead of native nucleic acid. Modified RNA library can be prepared by substituting the 2'-OH group in pyrimidines with 2'-Fluoro, 2'-OH groups in purines with 2'-O methyl groups (84,100). But there are still other challenges towards its clinical application. One is the quick kidney elimination of aptamer after systemic administration, as the size of aptamers usually falls in the range of less than 10nm and can be cleared by renal glomerular filtration. Methods to increase the aptamer size are explored, including adding

poly ethylene glycol (PEG) or cholesterol onto the RNA aptamers (112) to increase its size thus the half life time *in vivo*. The toxicity of aptamer *in vivo* is not well studied yet, although it is believed that protein free aptamers are less immunogenic than antibodies, but Macugen has shown some side effects in AMD patient (112).

1.3 Extracellular Vesicles and drug delivery

Extracellular vesicles (EVs) are membrane surrounded particles secreted by almost all cell types. EVs are also known as intercellular messenger organelles by mediating intercellular communication and exchanging biological signals between cells. EVs play important role in regulating both physiological and pathological process. The following part will discuss about the biogenesis, the mechanism regulating EV releasing, function of exosomes as well as their application for therapeutics delivery system.

1.3.1 Exosome biogenesis

EVs can be classified into three classes according to their biogenesis: microvesicles, exosomes, and apoptotic bodies. Microvesicles are small membrane bound fragments generated by outward budding from the plasma membrane. They have a very heterogeneous population with size ranging from 100 to 1000 nm; while exosomes are vesicles from the endosome membrane when multivesicle bodies fuse with the plasma membrane at the end of endocytosis-recycling process (113), with size ranging from 50 to 140 nm. Exosomes are normally characterized by highly enriched tetraspanin proteins including CD9, CD63, CD81 or CD82. They are proposed as exosome markers from proteomic analyses (114). During the exosome biogenesis, the first step is formulation of intraluminal vesicles following the inward budding of late endosome membranes. The endosomal sorting complex required for transport (ESCRT) assembled into 4 complexes

named ESCRT-0, 1, 2, 3 to capture and transport the sorted protein and other contents in late endosome into ILVs. Both ESCRT dependent and independent mechanisms are involved in the biogenesis of exosome (115). Protein TSG101 and Alix are certainly involved in the ESCRT complex formation and exosome biogenesis; they are also recognized as protein markers for exosomes (116).

1.3.2 Mechanisms regulating exosome release

Releasing of exosomes from donor cells is regulated by various conditions. Savina et al. found that increasing intracellular Ca^{2+} concentration could stimulate exosome secretion from a hematopoietic cell line K562, which was experimentally proved that treating cells with monensin stimulated exosome release (117). Activating cellular signals also can stimulate exosome secretion. Triggering CD40 /IL4 receptor in murine B cells caused releasing high level of exosomes, although releasing exosome is not a constitutive activity of B cells (118). Hypoxic condition also promotes exosome release from cells. It was observed that culturing different breast cancer cell lines under hypoxia condition or experimentally activation hypoxia signaling increased exosome release (119). Riches et al. reported that exosome release is also affected by the presence of exosomes in a feedback regulatory mechanism. Presence of exosomes in mammary epithelial cells microenvironment could inhibit secretion of exosome from breast cancer cells (120). Stimulating dendritic cells with HIV-1 virus also trigger release of exosomes, which was found to be activated by stimulating the dendritic cell immune receptors(121).

1.3.3 Function of exosomes

Living cells communicate through multiple pathways. Direct cell interactions and secreting soluble factors are two well-known methods for communication between cells.

Releasing of membrane derived vesicles also named extracellular vesicles is a newly discovered way for cellular communication. Extracellular vesicles were discovered in the 1980s by two independent labs during studying the fate of transferrin receptor in sheep reticulocyte maturation (122) and pathway for transferrin receptor shedding (123). EVs were later found play important roles in regulating normal physiological process(124), such as stimulation of adaptive immune response(125), stem cell maintenance(126), tissue repairing(127) and blood coagulation(128) in physiological conditions; and promoting tumorigenesis (129), virus infection(130) and spread of amyloid-β-peptides for Alzheimer's disease development (131) in the pathological conditions.

EVs are natural vehicles for mRNA, miRNA, various noncoding RNA, genomic DNA, and proteins delivering between cells (132). Various molecules including siRNA, miRNA, mRNA and proteins are loaded into the lumen of EVs before its secretion (133). Breast cancer cells derived exosomes are found contain miRNA and RNA-induced silencing complex (RISC) for miRNA processing, thus promote tumorigenesis (134). As intercellular communication organelles, exosomes may act as novel tools for disease treatment by various approaches, including (1) immune modulators with immunosuppressive or immune-activating effect or vaccination for multiple disease treatment; (2) drug delivery vehicles for delivering proteins or nucleic acids to recipient cells(135). These clues indicate the future of exosomes for therapeutic applications.

1.3.4 Application of Exosomes

Exosomes as gene delivery tools

Exosomes are natural carrier for various RNA molecules and proteins for cellular communication. Delivery of exosomal RNA has significant effects in modulating the

recipient cell phenotypes. Valadi et al. first reported that exosomes can transfer mRNA and miRNA to recipient cells and the delivered RNA molecules are functional, can be translated into proteins (136). The transfer of miRNA to recipient antigen presenting cells can be directed by T cell derived CD63 positive exosomes, and its unidirectional (137).

EVs have been explored as delivery tools for various therapeutic agents, including small RNA drugs, and chemotherapeutics (137). The most obvious advantage of using exosomes as delivery vehicles for small RNA relies that they have natural homing ability for small RNAs. The proteins and nucleoproteins including STAU1(double-stranded RNA binding protein staufen homolog 1), STAU2, AGO2 (argonaute 2) and TNRC6A(trinucleotide repeat containing gene 6A) associated with exosomes are involved in RNA transport, processing(124). It was reported that exosomes isolated from dendritic cells can deliver siRNA to mouse brain after systemic injection. The exosome donor dendritic cells were reengineered to overexpress rabies virus glycoprotein (RVG) peptide fusion to lysosome associated membrane glycoproteins (Lamp2b), thus the isolated exosomes with neuron specific RVG peptide overexpression on its surface can target brain cells. The re-engineered exosomes loaded with BACE1 siRNA targeting β-secretase (138) can deliver siRNA to wild type mice brain after systemic injection. It had significant therapeutic effect on mice model shown as efficient mRNA and protein knockdown(139). siRNA was loaded into exosomes by electroporation. Exosomes can also transfer viral miRNA from the EBV-infected cells to the uninfected cells when they are co-cultured, and the transferred miRNA was found to be functional (140). The GE peptide positive exosomes from HEK293T cells can deliver let-7a miRNA to recipient

EGFR positive breast cancer cells *in vivo*, and inhibited breast cancer development *in vivo*(141).

Exosomes also fit for chemotherapeutics delivery. Comparing to artificial nanovesicles such as liposomes and nanoparticles for chemotherapeutic delivery, EVs are advantageous in their increased stability *in vivo* as for circulation, and decreased immunogenicity and toxicity (142). The chemo resistance development in most tumor disease is associated with the secretion of exosomes at low pH microenvironment in tumor cells, and drugs such as cisplatin can be eliminated through exosome releasing(143). But if using exosome as vehicles for drugs, it could protect drugs from degradation, and enhance its cellular uptake can as increased uptake of exosomes was also observed at low pH conditions (144). Exosomes are considered as promising antitumor drug carriers (142). Chemical drug paclitaxel can be packaged into exosomes and released into cell culture medium by treating mesenchymal stromal cells with paclitaxel. The isolated paclitaxel loaded exosomes showed strong anti-proliferative efficiency on pancreatic tumor cells *in vitro* (145). A recent study showed that encapsulating paclitaxel into exosomes increased its cytotoxicity towards multi-drug resistant cells around 50 times *in vitro*, high paclitaxel loading efficiency to exosomes was achieved using a sonication method (146). Encapsulating doxorubicin into exosomes did not increase its *in vitro* cytotoxicity on cancer cells, but it did reduce its cardiac toxicity in xenograft mice model *in vivo* (147). All these studies showed that exosomes are promising delivery systems for chemotherapeutics.

Exosomes as immune therapeutics

Besides as gene therapy delivery vehicles, Exosomes are also developed as immune modulatory therapeutics. Exosomes can generate CD8+ anti-tumor T cells responses to maximize activation of specific T cells and enhance their anti-tumor immunity. Tumor associated ascites-derived exosomes in combination with TLR3 agonists has been used as immunotherapy for ovarian cancer treatment in a clinical trial (148). As tumor derived exosomes contain large amount of tumor associated antigens (149), and MHC class I molecules for antigen presentation. Tumor derived exosomes also showed vaccination effect for eradicating tumors in mice model (149).

Current questions to be solved for developing exosomes into immune therapeutic includes: the method for preparation of GMP grade exosomes and to identify which immune adjuvant to be used (148). One study showed that CpG adjuvants are proper candidate for dendritic cells derived exosomes in vaccine therapy (150). Ascites-derived exosomes in combination with the granulocyte macrophage colony stimulating factor (GM-CSF) has been evaluated in phase 1 and phase 2 clinical trials for treating colorectal cancer. Phase 1 clinical trial in 2008 with 40 patients concluded the ascites-derived exosomes in combination with GM-CSF is feasible and safe (151). More exosome related clinical trials on going are summarized in table 1(142).

Table 1. Current exosomes based drugs under clinical trial

Disease	Exosome source	Isolation	modification	Ref
Melanoma, CT1, n=15	Autologous monocyte derived dendritic cell EVs, SC.	UC with sucrose cushion	MAGE3 loaded	(152)
Non-small cell lung cancer, CT1, n=13	Autologous monocyte derived dendritic cell EVs, SC.	Filtration/UC sucrose cushion	Peptide loaded	(153)
Colon cancer, CT1, n=40	Autologous ascites derived EVs, SC.	UC sucrose cushion	Unmodified with or w/o GM-CSF	(154)
Colon cancer, CT1, n=35	Plant nanovesicles	Filtration/UC	Curcumin, exogenous loading	NCT01294072
Type I diabetes, CT1, n=20	Umbilical cord blood MSC-EVs			NCT02138331
Non-small cell lung cancer, CT2, n=2	Autologous IFN-γ matured monocyte derived dendritic cell EVs, intradermal	Ultrafiltration/ UC sucrose cushion	Peptide loaded	(155)
Malignant pleural effusion, CT2, n=30	Tumor cell derived microparticles as vector for chemotherapeutics drug delivery		Chemotherapeutic drugs, exogenous loading	NCT01854866

1.3.5 Prospective

Although the study on exosomes is still in its young stage, exosomes already showed great advantage in solving some difficult questions in drug delivery field. Exosomes can cross the blood brain barrier, can be engineered to achieve specific targeting effect, can bypath the endosome trapping for RNAi drug delivery as naturally evolved functional machinery in cells. Although there is challenge towards the clinical application, such as the above motioned yield and GMP production difficulty, and also unknown immunogenicity towards the recipient in long term. Hopefully great promise will be made in the future.

Copyright © Fengmei Pi 2016

Chapter 2: Development of High-Affinity Thermo-Stable Divalent RNA Antibody for Cancer Cell Targeting and Delivery

This chapter (with some modification) is under preparation. Special thanks to Dr. Ashwani Sharma for help and assistance in preparation of data for Figure 2.S1.

ABSTRACT:

Widely used protein antibody contains two binding sites providing immense biomedical applications with high affinity and specificity. RNA aptamers expanded the field of antibodies, but have low specificity which is partly attributed to their monovalent nature thus limiting their biomedical application. Divalent aptamers fusing two aptamers into a single unit have been reported but such fusion causes refolding and structure alteration affecting their affinity and specificity. Inspired by nature and using state-of-art RNA nanotechnology platform, we report here a novel divalent RNA antibody (RNA-Ab) design utilizing unusual thermodynamic stability of the pRNA three-way junction (3WJ) of phi29 DNA packaging motor. The highly stable 3WJ provides a rigid core to the RNA architecture similar to antibodies keeping both the loops separated for independent target binding, and further disfavor misfolding of RNA-Ab when conjugated to oligonucleotide therapeutics, keeping affinity and functions of attached functionalities intact. Using this 3WJ based nanotechnology design; we describe the selection and characterization of serum and thermodynamically stable divalent RNA-Ab against a prominent cancer marker EpCAM with high affinity and specificity

INTRODUCTION:

RNA nanotechnology is a rapidly growing field, which involves the programmable and addressable designs of RNA 3D architectures. A large number of highly ordered RNA structures including triangles (54), square (55), pentamers (54), hexamers (47,48) and boiling resistant hexacubic arrays (156) have been constructed and shown to perform diverse biological functions. Recently, our lab has discovered unusually stable three-way junction (3WJ) motif of pRNA that assembles with high affinity from three different RNA strands and is resistant to denaturation by 8 M urea (43). Utilizing this highly stable 3WJ motif as core, several nanostructures harboring different functional modules such as RNA aptamers, ribozymes, siRNA etc. have been constructed which are shown to retain their folding and functionality for specific cell binding (43,53), catalytic activity (43), gene silencing (53,157), and fluorogenic properties (72,158)both *in vitro* or in animal models.

MATERIALS AND METHODS:

Cell lines

HT29, HCT116, KB cells, CD4+ Jurkat cells, and MDA-MB-231 cells were purchased from American Type Culture Collection (ATCC). KM-20 cells were generously provided by Dr. Piotr Rychohou (University of Kentucky, USA). All cell lines were maintained in water jacketed CO_2 incubator at 37 °C with 5 % CO_2. KB cell and $CD4^+$ Jurkat cells were cultured in RPMI1640 medium supplemented with 10% fetal bovine serum (FBS, Hyclone). HT-29 and HCT-116 cells were cultured in McCoy's 5A medium supplemented with 10 % FBS. KM-20 cells were cultured in MEM medium supplemented with 10 % FBS, 10 ml/L of sodium pyruvate, 10 ml/L non-essential amino

acid, 20 mL/L of MEM essential vitamin mixture. MDA-MB-231 cells were cultured in DMEM medium supplemented with 10 % FBS, MCF-7 cells were cultured in EMEM medium supplemented with 10 % FBS and 1 % of bovine insulin.

Library builds up

The 116 nt DNA library with 60 random bases was chemically synthesized in one micromole scale from (W. M. Keck Oligonucleotide synthesis Facility, Yale University). The sequence of ssDNA library (**Figure 2.S1**) consist two random regions that are flanked by known primer-binding regions and a conserved middle region which can fold with the primer binding region to form the complete 3WJ assembly. The ssDNA library was PCR amplified with primers L6F1 and L6R1 to generate the double-stranded DNA template. The dsDNA was then *in vitro* transcribed to 2'Fluoro pyrimidine modified RNA library using Y639F T7 polymerase for selection process. To maintain the diversity of the library, 30 pmol of DNA (2×10^{13} sequences) was amplified in a 10ml PCR reaction. The PCR products were purified by MinElute PCR purification kit (Qiagen) to remove the primers and free nucleotides. The purified dsDNA library (5 µg) was *in vitro* transcribed into initial 2'-fluoro-pyrimidine modified RNA library in a 100 µL reaction, treated with DNaseI and used directly for *in vitro* selection.

ssDNA libraryDNA: 5'- GGA GGC ACC ACG GCT GGA TCC GGA TCA ATC ATG GCA A-N30- T TGC CAT GTG TAT GTG GG-N30- CCC ACA TAC TTT GTT GAT CCT TGG TCA TTA GGA TCG-3'

L6F1DNA: 5'-GTA TAA TAC GAC TCA CTA TAG GG C CGG ATC AAT CAT GGC AA3'

L6R1DNA: 5'-GGA TCA ACA AAG TAT GTG G3'

Sph1-L6R1DNA: 5’- CTC CCG GCC GCC ATG GCC GCG GGA TTG GAT CAA CAA AGT ATG TGG-3’

Cy5-Sph1 DNA: 5’-Cy5/CTC CCG GCC GCC ATG GCC GCG GGA TT-3’

LNA21-Sph1: 5’ +G+A+T+A+A+G+C+TCTCCCGGCCGCCATGGCCGCGGGAT-3’

3WJa-Sph12’F RNA: 5’-uuG ccA uGu GuA uGu GGG AAu ccc GcG Gcc AuG Gcc GGG AG-3’

3WJa 2’F RNA: 5’- uuG ccA uGu GuA uGu GGG-3’

3WJb 2’F RNA: 5’-ccc AcA uAc uuu Guu GAu cc-3’

3WJc 2’F RNA: 5’-GGA ucA Auc AuG GcA A-3’

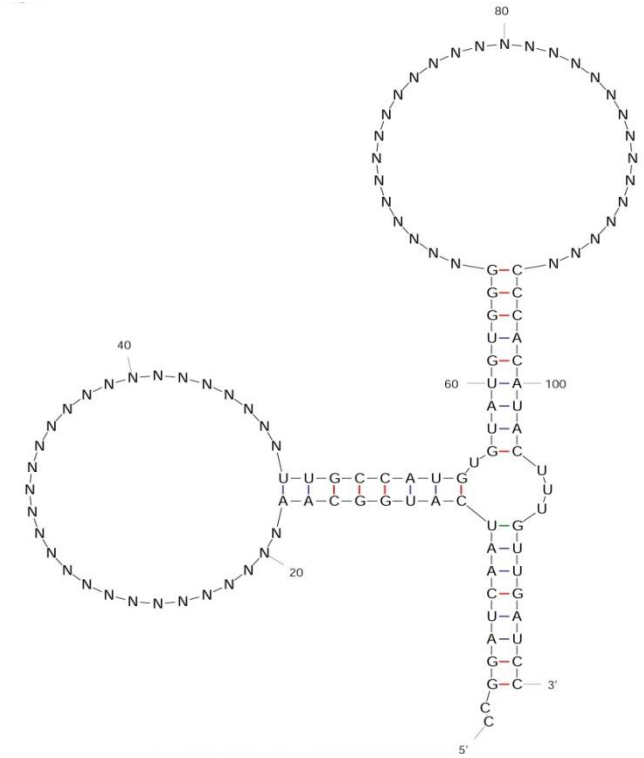

Figure 2.S1. **Primary sequence of bivalent RNA nanoparticle library**. The library contains two random regions for target binding selection and a pRNA-3WJ scaffold providing a rigid Y shaped structure mimicking antibody.

Protein immobilization

The extracellular fragment of EpCAM protein (Met1-Lys265) with poly histidine at its C terminal was purchased from Sino Biological Inc. 5μg of His-tagged EpCAM protein was immobilized to 3 μL of dynabeads® his-tag isolation (Invitrogen) in 100 μL of binding buffer at 4 °C overnight following the manufacturers protocol. A poly-Histidine peptide was immobilized to magnetic beads following the same procedure for negative selection.

In vitro selection

20 μg of 2'F-RNA library was first incubated with 3 μL of His-peptide immobilized dynabeads as negative selection to remove non-specific binding sequences. 20 μg of yeast tRNA was added in the binding buffer to reduce non-specific reaction. This RNA library taken from supernatant of negative selection tube was then incubated with 5 μg of EpCAM protein immobilized magnetic beads with yeast tRNA in SHMCK buffer (110 mM NaCl, 20 mM HEPES, 1 mM $MgCl_2$, 1 mM $CaCl_2$, 5 mM KCl, pH 7.4) at room temperature for 3 h as positive selection. The beads were washed 3 times with SHMCK buffer after incubation. The target-bound RNA sequences on magnetic beads were directly reverse transcribed into DNA by Thermoscript^{TM} Reverse transcriptase (Invitrogen), followed by PCR amplification. Then 2'-F RNA was generated by *in vitro* transcription for next round of SELEX. During the SELEX process, the protein concentration, incubation times were decreased gradually or the washing time was increased gradually to increase the stringency of selection to acquire aptamer with high affinity.

The enriched library after 7 to 9 rounds of SELEX process was reverse transcribed, PCR amplified for 7 cycles with Taq polymerase (Promega) and agarose gel purified, cloned into the pGEMT vector plasmid (Promega). Plasmid DNAs from the selected individual clones were extracted from E Coli cells with Genejet plasmid purification kit (Fermentas), and sequenced by Advanced Gene Technology Center (University of Kentucky). The aptamer sequences were analyzed with Cluster W2(159), random regions were aligned using MultAlin (160) and secondary structures were predicted using M-Fold software (161).

Flow cytometry analysis

Plasmid DNA from clones were PCR amplified with primer L6F1 and sph1-L6R1 to extend its 3'end with extra 26 nucleotides for fluorescent labeling. 2'F RNA was *in vitro* transcribed and purified from 8 M urea, 8% polyacrylamide gel by crush and soak method, followed by ethanol precipitation. To label the 2'F RNA with Cy5 fluorescent dye, a 5'-Cy5 modified DNA oligo Cy5-Sph1 (IDT) complimentary to the extended 3`end region of corresponding 2'F RNA sequence was hybridized by heating at 80°C for 5 min and step cool down to 4 °C.

Cells cultured in T-75 flask were harvested with 0.25 % trypsin. Around 2×10^5 cells were incubated with different concentration of Cy5 labeled 2'F RNA nanoparticles in OptiMEM medium for 1 h at 37 °C, protect from light. Cells were then washed three times and suspended in PBS for analysis by flow cytometry.

Confocal microscopy method

Cells were grown in cover glass (Fisher Scientific) in 24 well bottom culture dishes in its complete medium overnight. On the day of testing, cells were washed with OptiMEM medium twice, incubated with Cy5 labeled 2'F RNA nanoparticles at 37 °C for 1 hr. After that cells were washed with PBS twice, fixed with 4% paraformaldehyde (Microscopy Sciences) in PBS at room temperature for 20min; then washed with PBS and permeabilized with 0.05 % Triton X100 in PBS at room temperature for 3 min; the cells were stained with $Alexa_{488}$ Phallodin (Invitrogen) at room temperature for 20 min and washed with PBS, air dried. Cell nucleus was stained with DAPI gold anti fade (Invitrogen) for confocal microscopy imaging with FluoView FV 1000-Filter Confocal Microscopy System (Olympus) (Available from University of Kentucky, Markey cancer center) .

Inhibition of endocytosis

The inhibition of endocytosis assay was carried out as described before (87), briefly pretreat cells in a potassium depletion buffer (50 mM HEPES, 140 mM NaCl, 2.5 mM $MgCl_2$, and 1 mM $CaCl_2$) or in a hypertonic buffer (potassium depleted buffer plus 3 mM KCl and 450 mM sucrose) at 37 °C for 1 hr, then incubate cells with the RNA nanoparticles for test. The cells were treated the same way as for confocal microscopy assay. Potassium depletion buffer or hypertonic buffer was used for the following wash steps.

Design and construction of EpCAM RNA Ab harboring anti-miR21

The locked nucleic acid (LNA) modified oligonucleotides targeting the seed sequence of microRNA 21 (miR21)(66,162) was tested as model nucleic acid

therapeutics for A9-8 RNA-Ab mediated delivery effect. A 26 nucleotide (nt) sequence named sph1 was added to the 3'end of 7 nt LNAs for nanoparticle assembly, named LNA21-Sph1. The LNA21-Sph1 was synthesized by EXION Company. The A9-8 harboring LNA oligo nanoparticle was prepared by hybridizing LNA21-sph1 to A9-8-Sph1 2'F-RNA by heating to 80 °C for 5 min and step cool down to 4 °C. Control nanoparticle harboring anti-miR21 was prepared by hybridizing 3WJa-sph1 2'F-RNA with LNA21-sph1 at 80 °C for 5 min and step cool down to 4 °C, then mix with 3WJb 2'F-RNA and 3WJc 2'F-RNA at equal molar ratio at room temperature.

Dual luciferase assay to analyze delivery of anti-miR21 by A9-8

Cells were seeded in 24 well plates in its complete medium at density of 2×10^5 cells/mL. PsiCheckTM-2 plasmid which contains miR21 seed sequence at 3'-UTR region of Renilla Luciferase reporter gene was constructed (Promega) (66,162). The plasmid was transfected to cells with Lipofectamine 2000 (Life technologies). Four hours post transfection the cell medium was changed to complete growth medium and incubated for another 2 h. Then the nanoparticles diluted in 200 µL of serum free medium were added, 4 h later complete medium was added. The cells were lysed after 24 h and test for Luciferase and Renilla expression by dual luciferase assay system (Promega). At least three biological repeats were performed.

RESULTS AND DISCUSSION:

RNA aptamers have been extensively investigated since 1990 (163). They are of significant utility for targeted delivery of oligonucleotide therapeutics because of their ability to bind specifically to different protein targets. However, there are still challenges towards its medical application. One challenge especially for targeted therapeutics

delivery is their low affinity for substrate interaction (164), which might be caused by its monovalent nature, or misfolding of aptamer-conjugates which sacrifice function of both aptamer and attached oligonucleotide therapeutics conjugate such as siRNA or miRNA. Another challenge is rapid clearance of RNA aptamer from circulation which is attributed to their relatively small size (165). Significant efforts have been done in recent past to overcome these limitations. To enhance the affinity of aptamer, Muller et al.(166) were the first to demonstrate a multivalent approach by linking together two aptamers that bind to distinct epitopes on thrombin protein through a poly (A) linker and showed improvement on affinity over the monovalent aptamer. To reduce renal clearance of aptamers, adding significant mass by linking aptamer end to polyethylene glycol (PEG)(101), to streptavidin via 3`biotin and by attaching Fc tail of IgG has been shown promising results (167). To overcome the folding problem Berezhnoy et al.(168) has recently reported that fusing siRNA with lower melting temperature to 3`end of aptamer has minimal effect on overall folding of the aptamer conjugate.

These literature findings emphasize the need of a novel scaffold which can increase aptamer target binding affinity by its multivalence, increases its size to enhance its bioavailability *in vivo*, and can be directly conjugated with oligonucleotide therapeutic without interrupting the folding of both parties. To meet these requires, we propose here a novel divalent RNA-Ab design based on thermodynamically stable antibody shaped pRNA-3WJ motif (26,43) for RNA based andibody development (**Figure 2.1**). The design utilizes the highly stable three way junction (3WJ) motif of phi29 DNA packaging motor pRNA which provides a rigid core structure similar to constant region of antibodies, allowing both loops to fold independently. Moreover, the 3WJ core adds

significant size to RNA antibody nanoparticle to disfavor renal clearance (169) and provides a handle to attach variety of drugs or therapeutic oligonucleotides like miRNA and siRNA without attenuating RNA-Ab`s activity or specificity. The design is generally applicable for *in vitro* selection of RNA-Ab virtually against any target, and can be advantageous in the development of RNAi based therapeutics or sensing platforms.

Using this design, we generated a nuclease resistant RNA-Ab against the cancer stem cell marker epithelial cell adhesion molecule (EpCAM), a transmembrane protein overexpressed in many cancer cells including stem cells. The selected RNA-Ab specifically binds to cancer cells overexpressing EpCAM with low K_D in nM range for different cell lines. Both RNA-Ab loops participate in binding and RNA-Ab was further shown to deliver anti-miR21 to breast and colon cancer cells.

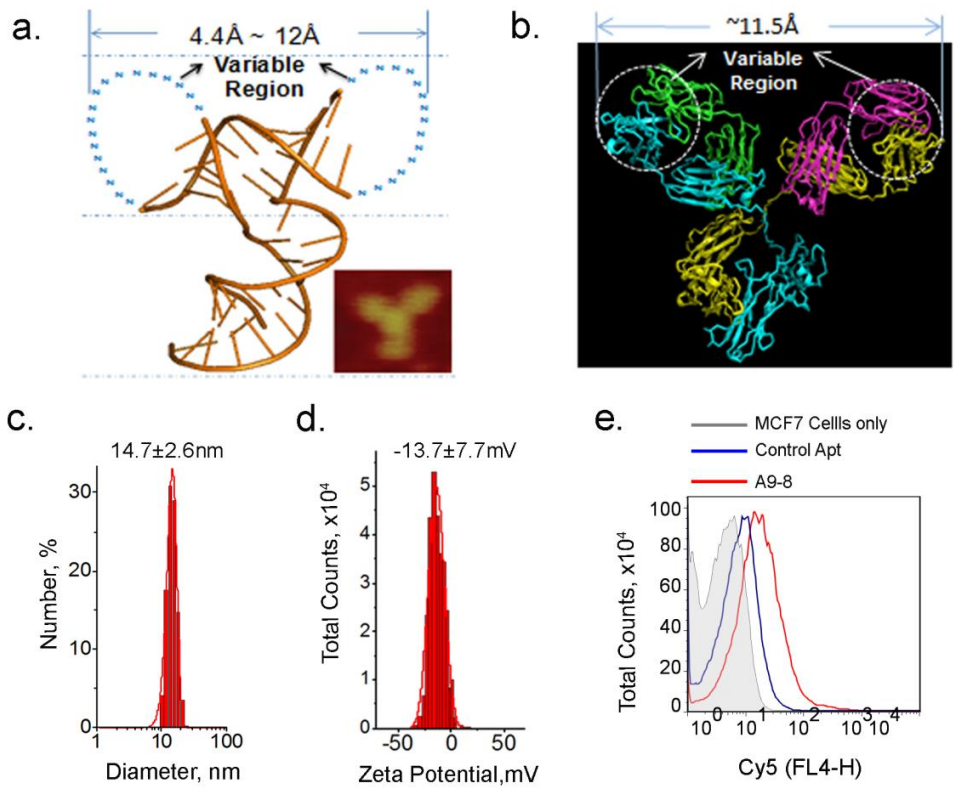

Figure 2.1. Physiochemical and biological properties of the bivalent RNA antibody. a. RNA-Ab design based on 3WJ crystal structure with two random loop sequences conjugate to 3WJ core motif of phi29 pRNA(43) b. A crystal structure of an intact monoclonal antibody for phenobarbital (PDB ID: 1IGY), c. DLS measurement of size distribution and d. zeta potential of selected RNA-Ab. e. Representation of a typical flow cytometry binding analysis comparison of Cy5 Labeled sequences to EpCAM positive MCF-7 cells. Gray represnts cell only, blue control aptamer sequence (50 nM) and red RNA-Ab A9-8 (50 nM).

To select a protein antibody shaped RNA aptamer (**Figure 2.1**), the thermodynamically stable pRNA-3WJ core was used as the constant region. Two random sequences were placed to the two arms of the 3WJ, mimicking two heavy chains of protein antibody serving as the two variable regions. The two random loops on either side of the 3WJ will provide bivalency and thus strong specificity to the target. Moreover, the thermodynamically stable 3WJ core will help maintain independent folding of each loop, providing overall stability. This design is advantageous since the third arm mimics the Fc complement binding domain on protein antibodies, thus can be attached with various therapeutic functionalities such as siRNA or miRNA without any detrimental effect on the folding of either RNA-Ab or the attached functionality. 2'-fluoro pyrimidines modified RNA library was used to enhance the serum stability of the RNA-Ab.

Epithelial cell adhesion molecule (EpCAM) was chosen as the target that is highly expressed on the most malignant epithelial cancers. In normal epithelia, EpCAM is only expressed on basolateral gap junctions, thus not accessible to various antibodies or drugs while in epithelial cancers, it is distributed homogenously on cell surface (170). Studies have revealed the importance of EpCAM in cancer biology, including processing of cell migration, cell proliferation (171), cancer cell invasion and metastasis (172). EpCAM protein is rapidly internalized when it is bound to antibodies, thus the RNA antibody against EpCAM will suit for payloads delivery by receptor-mediated endocytosis (173).

To select an RNA-Ab against EpCAM protein, we used magnetic beads based SELEX protocol as discussed above. An initial 2'-F RNA library containing 2×10^{13} species was incubated with the EpCAM attached magnetic beads for first round SELEX. A total of nine rounds of selection against EpCAM recombinant protein were carried out.

The negative selections were introduced in the first and seventh rounds. For negative selection, RNA library was passed through only His 6- peptide attached to magnetic beads. A total of 9 rounds of selection were performed and the selective pressure was stepwise modified by decreasing target concentration and incubation time. The progress of the selection was determined by filer binding assay(174). The selection rounds showed enrichment in filter binding assay till 8^{th} rounds and thus selection process was stopped after performing an extra round at 37 °C to get the highest binding sequence at biological temperature. The last round library was cloned into pGEM-T vector and 20 clones were sequenced and analysed for their secondary structure predictions. The data showed some repeating sequences (**Figure. 2.S2a**). Three different sequences were chosen based on their secondary structures (using M-fold (161)) or number of repeats and were tested for their cell binding ability using flow cytometry (**Figure. 2.S2b**). The clone A9-8 now on referred as RNA-Ab showed the best results for cell binding in flow cytometry (**Figure 2.S3**) and was chosen for further studies.

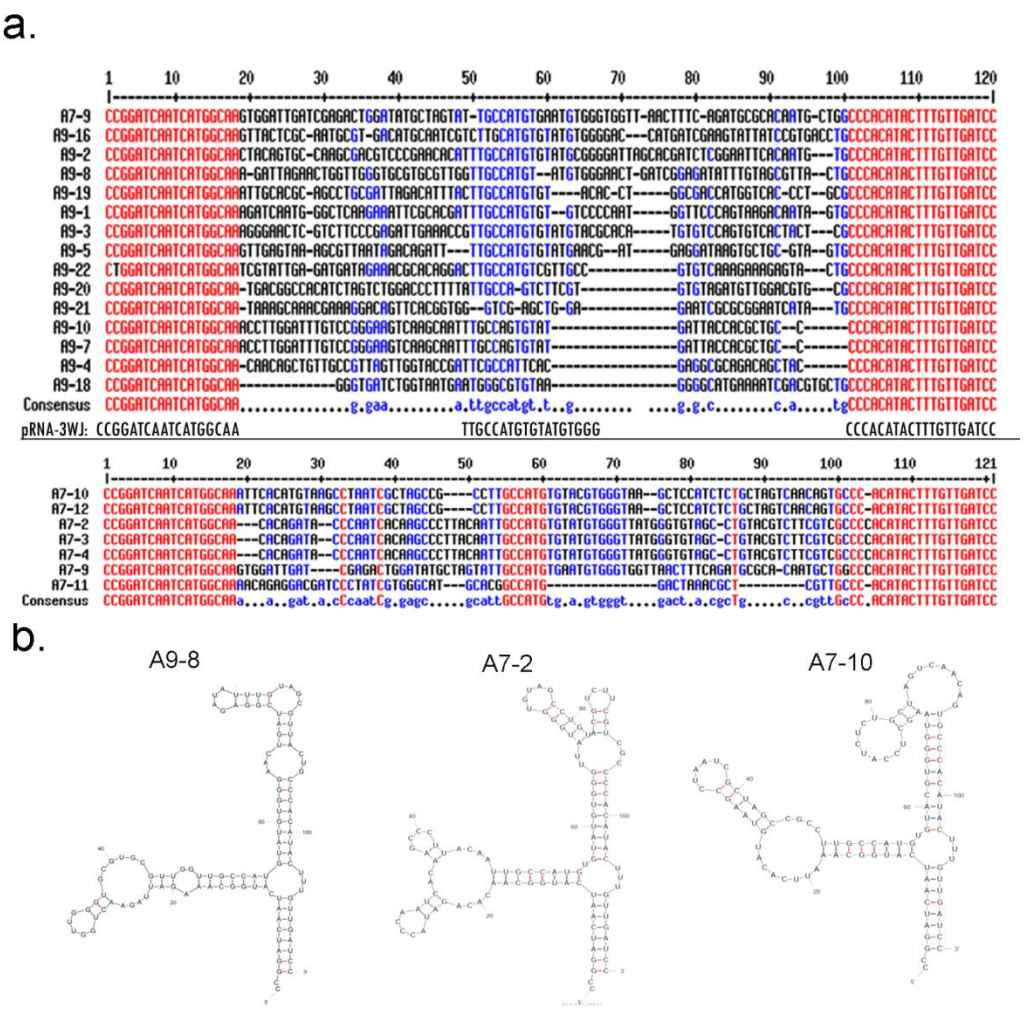

Figure 2.S2. Sequence alignment and secondary structure analysis to identify final RNA-Ab. a. Sequence alignment of picked clones after 7th and 9th round of SELEX using MultiAlin. A9-8 in 9th round library reserved all 3WJ sequences, and A7-2, A7-10 showed multiple repeats were chosen for further analysis. B. Secondary structure A9-8, A7-2, A7-10 calculated by M-fold.

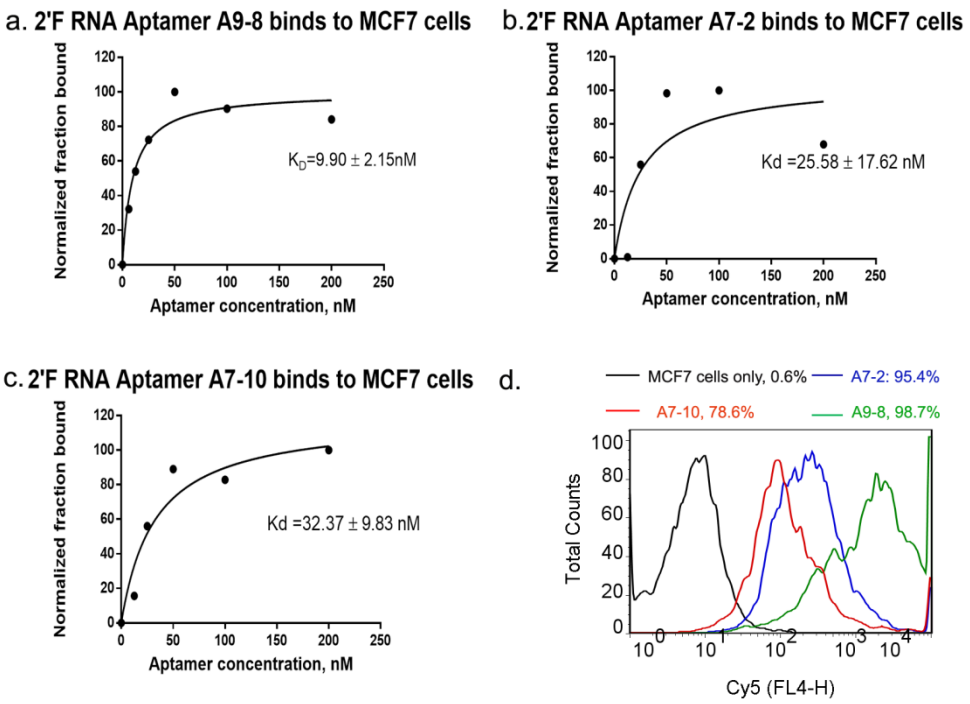

Figure 2.S3. Comparing the binding affinity of selected 3 sequences with MCF7 cells *in vitro*. a. Sequence A9-8 showed an apparent K_D of 9.90 nM to MCF7 cells, b. Sequence A7-2 showed an apparent K_D of 25.58 nM to MCF7 cells, c. Sequence A7-10 showed an apparent K_D of 32.37 nM to MCF7 cells in flow cytometry analysis. d. Comparing the binding of 3 sequences to MCF7 cells at the concentration of 50 nM by flow cytometry. The result is consistent with apparent K_D test, A9-8 showed the strongest binding affinity among the three sequences.

Generally, nanoparticles with a size of 10-100 nm are optimal for drug delivery due to slow renal clearance and improved *in vivo* circulation time avoiding liver and spleen cleaning up (175). We determined the nanoparticle size distribution of selected RNA-Ab against EpCAM protein using dynamic light scattering with Malvern Nanosizer. RNA-Ab showed a mean size of 14.25 ±0.05 nm as shown in **Figure 2.1**. The 3WJ structural core motif adds significant size and mass to bring it to optimal nm size range for slow renal clearance, and thus consequently high tumour localization is anticipated as previously shown by 3WJ constructs(169).

The binding affinities of selected RNA-Ab A9-8 with different EpCAM positive cell lines were determined by flow cytometry with cy5-labeling. Breast cancer cell lines MCF-7(87,176), MDA-MB-231(87) and colon cancer cell lines HT-29 (87,177), HCT-116 (178) and KM-20 were tested as EpCAM positive cell lines; Jurkat cell line(179), which does not express EpCAM was tested as negative cell line. The cells were incubated with varying concentration of RNA-Ab or the control scramble sequence, and the binding of RNA-Ab to EpCAM positive cells was observed as shown in a typical histogram in **Figure 2.1d**. RNA-Ab A9-8 binds significantly higher to EpCAM positive cell MCF7 than control 3WJ 2'F RNA nanoparticle, which was assembled by mixing equal molar ratio of 3WJa, 3WJb, and 3WJc 2'F RNA. The normalized bound cell ratio against aptamer concentration was plotted in a graph and fitted to one site specific binding curve to determine the apparent dissociation constants (K_D) of RNA-Ab with different cell lines as shown in **Figure 2.2**. The nonspecific binding from control sequence to cells was subtracted for K_D analysis. The data shows that RNA-Ab binds specifically to different EpCAM positive cell lines with apparent K_D values in nM range and showed non-specific binding to EpCAM negative Jurkat cells as represented by a linear binding curve (**Figure 2.2f**). RNA-Ab showed the highest binding affinity at K_D of 9.90 ± 2.15 nM (**Figure. 2.2d**) to human breast cancer cells line MCF7.

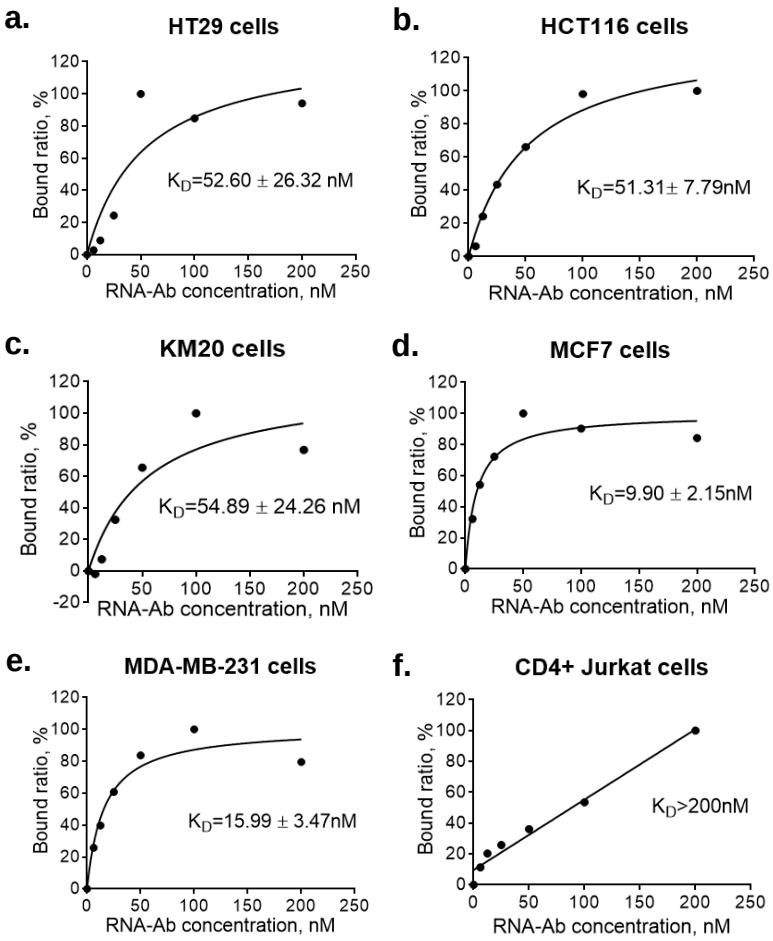

Figure 2.2. Determination of apparent dissociation constants (K_D) of RNA-Ab with cells. The binding curves for RNA-Ab with EpCAM positive cell lines (a-e) and negative cell line (f). The straight line in 'F' represents non-specific binding and thus very high K_D values (> 200 nM).

The specific cell binding and entry of RNA-Ab A9-8 to EpCAM positive cells was further confirmed by confocal microscopy showing cellular distribution. The RNA-Ab A9-8 gets internalized into the cells through receptor-mediated endocytosis and thus does not require any transfection reagent. Moreover RNA-Ab A9-8 specifically bind to EpCAM positive breast cancer cell lines MCF-7 as well as colon cancer cell lines HT-29 and HCT-116, whereas no binding was observed for EpCAM negative Jurkat cells (**Figure 2.3**). The magnified view of cells shows that the Cy5-labeled RNA-Ab was localized in the cell cytoplasm, whereas under similar conditions the control sequence showed very low binding. To test whether RNA-Ab A9-8 can be internalized to cell cytoplasm following binding, the receptor mediated endocytosis pathway was blocked by treating MCF-7 cells under potassium depletion condition (87). Incubating Cy5-labeled RNA-Ab with the MCF-7 cells that pre-treated with potassium depletion buffer, the RNA-Ab did not enter into the cell cytoplasm but rather bound only to the cell membrane forming a circle around the cell membrane (**Figure 2.3a**). In contrast, incubating RNA-Ab under normal condition with MCF-7 cells, it gets internalized and distributed as shown by dispersed dots near cell nucleus. Thus, it can be concluded that the RNA-Ab gets internalized into the cells after binding to receptors on the cell surface membrane.

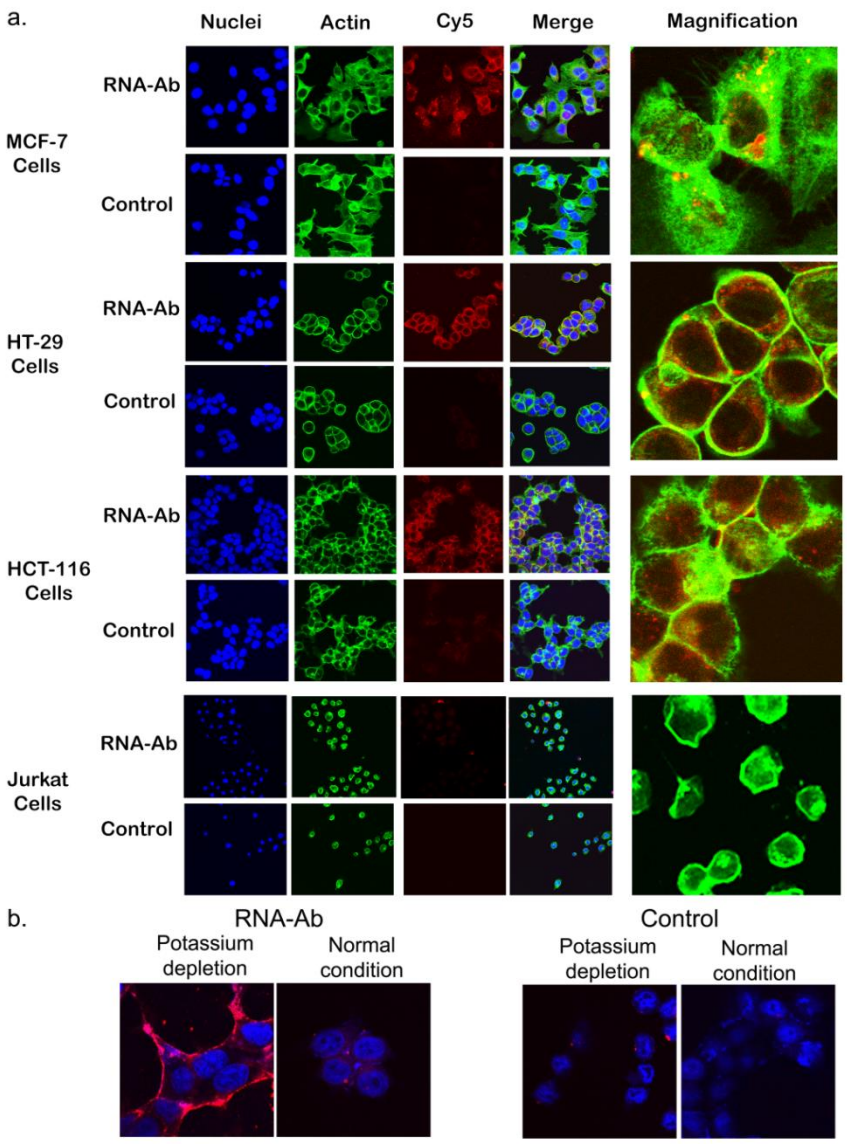

Figure 2.3. The cell entry of RNA-Ab tested by confocal microscopy. a. The binding and subcellular distribution of RNA-Ab to EpCAM-positive cancer cell lines (MCF-7, HT-29, and HCT-116) and to EpCAM negative cell line (Jurkat) b. Binding and subcellular distribution of RNA-Ab and control sequence to EpCAM positive cell line MCF-7 in potassium depletion buffer when receptor mediated endocytosis pathway is blocked and in normal conditions.

To investigate whether both loops of the RNA-Ab participate in binding to the target mimicking a protein antibody, we truncated RNA-Ab by deleting one loop at a time, keeping the other loop intact. This provided two new aptamer structures as shown in **Figure 2.4.** Next, the binding affinity of these one-loop structures towards MCF-7 cells were tested by flow cytometry, the original RNA-Ab was tested as positive control. The structure with only loop 1 showed an apparent K_D around 25 nM (**Figure 2.4a**) while the structure with only loop 2 showed a K_D around 15 nM (**Figure 2.4b**), whereas the original RNA-Ab with both the loops present have a K_D value of around 9.9 nM (**Figure 2.4c**). This shows that both the loops in RNA-Ab bind to its target with high affinity proving bivalent nature of selected RNA antibody. We also tested the binding affinity of recently reported 2'F-RNA aptamer EpDT3 to MCF-7 cells (87), which is the only 2`F-RNA aptamer selected so far against EpCAM. All the loop deleted structures and the full length RNA-Ab showed lower apparent K_D than EpDT3 which showed apparent K_D value around 83 nM to MCF7 cells in our experiment (**Figure.2.4d**).

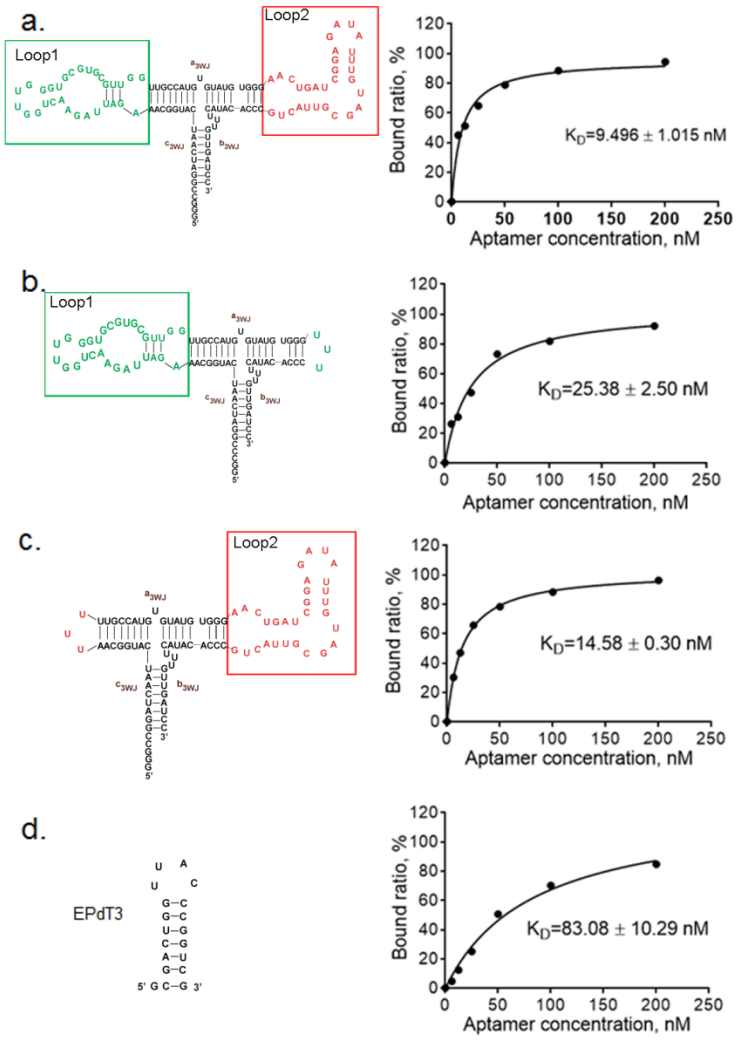

Figure 2.4. Determination of apparent dissociation constants (K_D) for loop deleted RNA-Ab with EpCAM positive MCF7 Cells. a. Loop1 deleted RNA-Ab, b. loop 2 deleted RNA-Ab, c. the full length RNA–Ab, and d. the reported 2'F-RNA aptamer for EpCAM binding affinity comparison

Micro-RNA 21 (miR21) was discovered as an oncogenic miR which targets a number of tumour suppressor genes (180,181). High level expression of miR21 is associated with various types of cancers. A 8-mer tiny locked nucleic acid (LNA), which is complementary to the seed sequence of miR21, has been reported to be able to knock down the miR21 expression, and inhibit the microRNA 21 function *in vitro* and *in vivo* (162). EpCAM protein has been previously shown to act as a cargo to internalize the attached payloads (173). To investigate if the newly developed RNA-Ab A9-8 can specifically deliver anti-miRNA oligonucleotide into EpCAM positive cells, a dual luciferase reporter assay system was used to detect the miR21 level in cells. The perfect-match anti-miR21 sequences were cloned to 3'UTR region of the primary reporter gene Renilla luciferase. The second reporter gene Firefly luciferase was used as internal controls, which allows normalization of the Renilla luciferase expression for endpoint lytic assays. RNA-Ab constructs harbouring anti-miR21-LNA were prepared by hybridizing the LNA oligonucleotide (LNA21-Sph1, **Figure 2.5a**) to the 3'-end extended RNA-Ab. RNA 3WJ nanoparticles harbouring anti-miR21-LNA were constructed as negative control. EpCAM positive breast cancer cell line MCF-7 and colon cancer cell line HCT-116 have high level of miR21 expression (data not shown here). After incubating RNA-Ab miRNA construct with cells, A9-8-LNA significantly reduced miR21 level in cancer cells with a dose depending response. In contrast the 3WJ-LNA, LNA itself, or RNA-Ab did not knockdown the miR21 levels (**Figure 2.5b, c**). Results showed that RNA-Ab A9-8-LNA can deliver its cargo anti-miRNA into cell cytoplasm and significantly knockdown miRNA expression level.

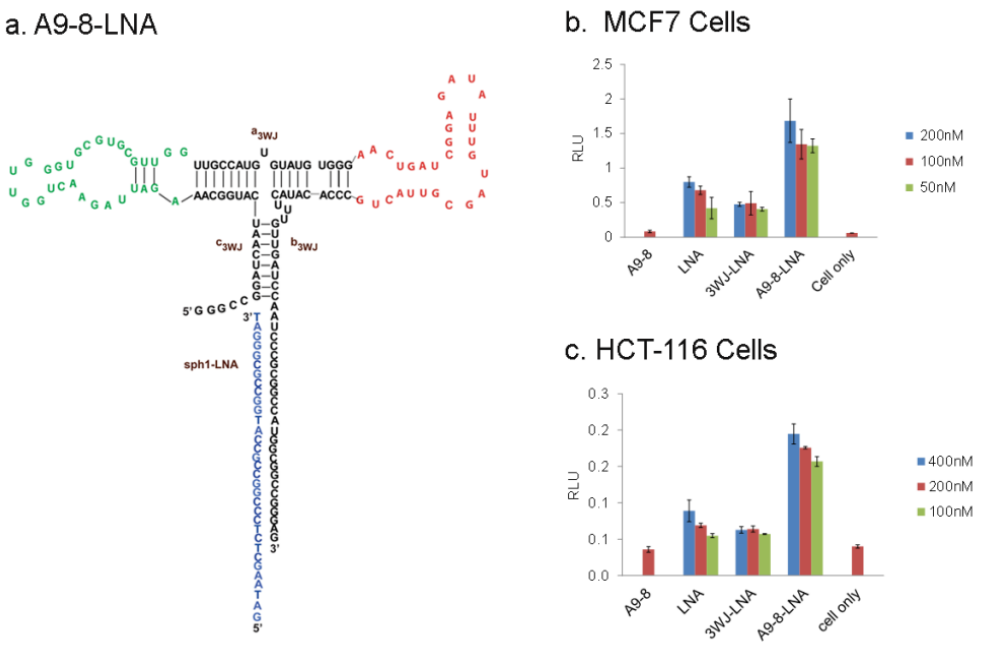

Figure 2.5. RNA-Ab mediated delivery of anti-miRNA21 to EpCAM positive cancer cells. a. The secondary structure of A9-8-LNA nanoparticle, which is assembled from two pieces of oligonucleotides. b. Delivery of anti-miR21 to MCF-7 cells by incubating cells with different concentration of nanoparticles. c. Delivery of anti-miR21 to HCT-116 cells by incubating nanoparticles with cells. RLU is relative Renilla to firefly luciferase unit, which is reversely related to miR21 levels in cells.

CONCLUSION:

In conclusion, the divalent RNA antibody presented here binds its target with high affinity and specificity. The key design feature of the RNA-Ab is highly stable 3WJ core derived from phi29 packaging motor, which provides significant mass and helps to maintain folding of attached oligonucleotide therapeutics for efficient delivery. The design can be used for selection of RNA antibody virtually against any small molecule or protein. Further experiments are underway to show its therapeutic utility in animal models. Although several antibody based immunotherapeutic targeting to various cancer biomarkers have been developed, they suffer from instability, lack of proficient clinical response and discrepancy in quality of antibodies from batch to batch (170). Moreover, the effect of antibody dependent cell mediated cytotoxicity (ADCC), antibody-mediated complement dependent cytotoxicity (CDC) and induction of anti-idiotypic response critically rely on the carbohydrate composition in the CH_2 domain of the antibodies, which can vary largely in batches (170). The RNA-Ab design presented here can be chemically synthesized. It is anticipated to provide improved oligonucleotide therapeutic delivery for various diseases to provide better healthcare.

ACKNOWLEDGMENT:

The authors would like to thank Ashwani Sharma, Yi Shu, and Dan shu for help with the experimental designs. The work was supported by NIH grants EB012135 and EB003730 and funding to Peixuan Guo's Endowed Chair in Nanobiotechnology position from the William Fairish Endowment Fund. The content is solely the responsibility of the authors and does not necessarily represent the official views of NIH.

Copyright © Fengmei Pi 2016

Chapter 3: Nanoparticle Orientation to Control RNA Loading or Surface Display of Extracellular Vesicles for Efficient Cell Targeting, siRNA Delivery and Cancer Regression

This chapter (with some modification) is under revision at *Nature Nanotechnology*. Special thanks to Dr. Daniel Binzel and for help and assistance in assays with prostate cancer cells *in vitro* and Hui Li, Dr. Bin Guo for help and assistance with *in vivo* assays.

INTRODUCTION:

It has been popularly believed that the advantage of nanotechnologies is the top-down and bottom-up construction approaches to make particles in nanometer-scale holding unique and special function. Here we report one more advantage of nanotechnology by controlling the structural orientation to regulate the anchoring of nanoparticles on extracellular vesicles (EVs) membrane for specific cancer targeting and intracellular trafficking. The orientation of arrow shaped RNA nanoparticles on EVs was possible to be controlled. Placing a membrane anchoring cholesterol at the arrow tail resulted in displaying of RNA aptamer or folate ligand onto the surface of EVs. In contrast, placing the chemical at the arrow head resulted in partial loading of RNA nanoparticles into the EVs. Taking advantage of the RNA aptamer ligand for specific targeting and EVs for efficient membrane fusion, the resulting RNA aptamer-displaying EVs were used for specific delivery of siRNA with efficient gene silencing resulting in complete blockage of cancer growth. Animal studies showed that the nanometer scale ligand-displaying EVs specifically localized in tumor xenografts without accumulating in healthy organs. Efficient gene silencing was observed both in cell culture and animal trials from systemic

administration of PSMA (Prostate Membrane Specific Antigen) aptamer-displaying EVs loaded with survivin siRNA.

MATERIALS AND METHODS:

The construction, synthesis and purification of RNA nanoparticles with or without the 2'F modification or Alex647 labeling has be reported (43).

The $PSMA_{apt}$/3WJ/Cholesterol RNA nanoparticle was assembled by mixing equal molar ratio of three RNA oligo strands including a_{3WJ}-Cholesterol, b_{3WJ}-Alexa647 and c_{3WJ}-$PSMA_{apt}$ 2'-F RNA in TES buffer (50 mM Tris, pH8, 5 mM EDTA, 0.05 M NaCl), heating to 85 °C for 5 min, then slowly cooling down to 4 °C. The assembly of RNA nanoparticles was detected in 8 % TBM-Polyacrylamide gel. The sequences of all the RNA strands (lower case letters indicate 2'-F nucleotides) are:

(1) a_{3WJ}: 5'-uuG ccA uGu GuA uGu GGG-3'

(2) a_{3WJ}-sph1: 5'-uuG ccA uGu GuA uGu GGG AAu ccc GcG Gcc AuG Gcc GGG AG-3'

(3) a_{3WJ}-survivin sense: 5'-uuG ccA uGu GuA uGu GGG GcA GGu uCC uuA ucu Guc Auu-3'

(4) a_{3WJ}-survivin sense(scramble): 5'-uuG ccA uGu GuA uGu GGG AAu ccc GcG Gcc AuG Gcc GGG AG-3'

(5) a_{3WJ}-Folate: 5'-(Folate)uuG ccA uGu GuA uGu GGG -3' (custom ordered from Trilink)

(6) a_{3WJ}-Cholesterol: 5'- uuG ccA uGu GuA uGu GGG(Cholesterol TEG)-3' (custom ordered from Trilink)

(7) b_{3WJ}: 5'-ccc AcA uAc uuu Guu GAu ccc-3'

(8) b_{3WJ}-Folate: 5'-(Folate)ccc AcA uAc uuu Guu GAu ccc-3'

(9) b_{3WJ}-Cholesterol: 5'-ccc AcA uAc uuu Guu GAu ccc(Cholesterol TEG)-3' (custom ordered from Trilink)

(10) b_{3WJ}-Alexa647: 5'-(Alexa647)(AmC6)- ccc AcA uAc uuu Guu GAu ccc-3' (custom ordered from Trilink)

(11) c_{3WJ}: 5'-GGA ucA Auc AuG GcA A-3'

(12) c_{3WJ}-$PSMA_{apt}$: 5'-GGA ucA Auc AuG GcA AuG GGA ccG AAA AAG Acc uGA cuu cuA uAc uAA Guc uAc Guu ccc-3'

(13) c_{3WJ}-Alexa647: 5'- GGA ucA Auc AuG GcA A(C6-NH)(Alexa647)-3' (custom ordered from Trilink)

(14) Survivin anti-sense:5'-UGA CAG AUA AGG AAC CUG C-3'

(15) Survivin anti-sense(scramble): 5'-CUC CCG GCC AUG GCC GCG GGA UU-3'

EVs purification:

EVs were purified using a modified differential ultra-centrifugation method(182). Briefly, the fetal bovine serum (FBS) used for cell culture was spun at 100,000 × g for 70 min to remove the existing serum exosome. The supernatant of HEK293T cell culture (EVs enriched medium) was harvested 48 h after cell plating, and was spun at 300×g for 10 min to remove dead cells, followed by spinning at 10,000 × g for 30 min at 4 °C

degree to remove cell debris and/or microvesicles. EVs were concentrated from the culture medium by using an Opti-prep Cushion procedure (183). The Opti-prep cushion offers an iso-osmotic pressure and prevents physical disruption of the exosome. A 200 μL of 60 % iodixanol (Sigma) was added to the bottom of each tube to form a cushion layer. After spinning at 100,000 × g for 70 min at 4 ºC using Beckman SW28 rotor, the EVs migrated and concentrated to the interface layer between the 60 % iodixanol and the EVs enriched medium. 1mL of the fraction close to the interface and cushion was collected. A 6 mL EV solution was further washed with a 30mL PBS in a SW28 tube that contained 50 μL of 60 % iodixanol cushion, and spin at 100,000 × g for 70 min at 4 ºC. The pellets in the cushion were all together collected and were suspended in 1 mL of sterile PBS for further use.

Cell culture, EM imaging, confocal microscopy, DLS measurement, and flow cytometry:

Methods for cell culture, EM imaging, confocal microscopy, DLS and flowcytometry have been reported (43,66,139). HEK293T, KB, LNCaP-FGC, PC-3 cells were obtained from ATCC, LNCaP-LN3 were obtained from MD Anderson Cancer Center. Cell cultures purchased from ATCC were authenticated by Short Tandem Repeat (STR) prior to purchase and LNCaP-LN3 cells were authenticated prior to receiving the cells as a gift. Each cell line was not tested for mycoplasma. While the KB cell line has been listed as a misidentified cell line that has been derived by contamination of HeLa cells, it serves as an ideal model in these studies. KB cells are known to overexpress folate receptor that allows for proper specific targeting through the use of Folate on RNA

nanoparticles. The derivation of the KB cell line will not affect using it as model to test folate receptor targeting property of the RNA displaying EVs.

Nanoparticle Tracking Analysis:

Nanoparticle Tracking Analysis (NTA) was carried out using the Malvern Nanosight NS300 system on EVs re-suspended in PBS at a concentration of 10µg of proteins/ml for analysis. The system focuses a laser beam through the sample suspension. These are visualized by light scattering, using a conventional optical microscope aligned to the beam axis which collects light scattered from every particle in the field of view. Three 10 sec video records all events for further analysis by NTA software. The Brownian motion of each particle is tracked between frames, ultimately allowing calculation of the size through application of the Stokes Einstein equation.

Size exclusion chromatography:

Sephadex G200 gel column was equilibrated with PBS and loaded with fluorescently labeled EV samples. After washing with PBS, fractions were collected with 5 drops per well. The fluorescence intensity Cy5 or $Alexa_{647}$ in the collected fractions was measured using a microplate reader (Synergy 4, Bio Tek Instruments, Inc).

siRNA loading into EVs:

EVs (100 µg of total protein) and RNA (10 µg) were mixed in 100 µL of PBS with 10 µL of ExoFect Exosome transfection (System Biosciences) followed by a heat-shock protocol. Cholesterol modified RNA nanoparticles were incubated with siRNA loaded EVs at 37 ºC for 45 min, then stay on ice for 1 h to prepare the RNA decorated EVs. The decorative RNA nanoparticles were kept at ratio of 10 µg RNA nanoparticles

per 100 μg of EV in protein amount. To purify RNA decorated EVs, 400 μL of RNA decorated EVs was washed with a 5 mL PBS in a SW-55 tube that contained 20 μL of 60 % iodixanol cushion, and spin at 100,000 × g for 70 min at 4 ºC. The pellets in the cushion were all together collected and were suspended in 400 μL of sterile PBS for further use.

FBS digestion experiment:

15μl of the purified $Alexa_{647}$-RNA decorated EVs were mixed with 30 μL of FBS (Sigma), and incubate at 37 °C for 2 h. The samples were loaded into 1 % syner gel for electrophoresis in TAE (40 mM Tris-acetate, 1 mM EDTA) buffer to test the degradation of decorative RNAs. Gel was imaged with Typhoon (GE healthcare) at $Alexa_{647}$ channel.

Assay the effects of $PSMA_{apt}$/EV/siSurvivin on prostate cancer using qRT-PCR:

LNCaP-FGC cells were incubated with 100 nM of the $PSMA_{apt}$/EV/siSurvivin and controls including 3WJ/EV/siSurvivin and $PSMA_{apt}$/EV/siScramble nanoparticles respectively. After 48 h treatment, cells were collected and target gene down-regulation effects were assessed by qRT-PCR. PC-3 cells were used as negative control cell line.

Cells were processed for total RNA using Trizol RNA extraction reagent following manufacture's instruction (Life Technologies). The first cDNA strand was synthesized on total RNA (1 μg) from cells with the various RNAs treatment using SuperScript^{TM} III First-Strand Synthesis System (Invitrogen). Real-time PCR was performed using Taqman Assay. All reactions were carried out in a final volume of 20 μL using Taqman Fast Universal PCR Master Mix and assayed in triplicate. Primers/probe set for human BIRC5 and 18S were purchased from Life Technologies. PCR was

performed on Step-One Plus real time PCR system (Applied Biosystem). The relative survivin mRNA expression level was normalized with 18S RNA as internal control. The data was analyzed by the comparative CT Method (ΔΔCT Method).

Due to the high reproducibility and consistency between cell cultures, in *in vitro* studies it was predetermined that a sample size of at least n = 3 would allow for adequate analysis to reach meaningful conclusions of the data. However, in *in vivo* studies, higher variance are seen in tissue samples; therefore, a higher set of samples is required to compensate for this natural variance. In these studies, n = 4 and the experiment repeated in triplicates was completed. Samples and animals were randomized into groups throughout the whole experiment.

Western blot and antibodies:

LNCaP-FGC cells were incubated with 100 nM of the $PSMA_{apt}$/EV/siSurvivin and controls including 3WJ/EV/siSurvivin and $PSMA_{apt}$/EV/siScramble nanoparticles respectively. After 48 h treatment, cells were collected and lysed with RIPA buffer (Sigma) with a protease inhibitor cocktail (Roche). Primary antibodies used for western blot analysis were rat anti-human surviving antibody (R&D system, AF886), rat anti-human β-actin (Abcam, ab198991), rat anti-human TSG101 (Thermo Scientific, PA5-31260).

Cytotoxicity assay:

The cytotoxicity of $PSMA_{apt}$/EV/siSurvivin was evaluated with a MTT assay kit (Promega) according to the manufacture's protocol. LNCaP-FGC and PC-3 cells were

treated with EVs in triplicate in 96-well plate. After 48hr cell survival rate was analyzed by the MTT assay on microplate reader (Synergy 4, Bio Tek Instruments, Inc).

***In vivo* targeting assay of tumor xenograft after systemic injection of EVs:**

To generate prostate cancer xenograft mice model, male athymic nude Nu/Nu (6-8 weeks old) mice (Taconic) were used. 2×10^6 LNCaP-LN3 cells in 100 μL of PBS mixed with equal volume of Matrigel matrix (Corning life science) was injected to each mouse subcutaneously. When the tumor reached a volume of ~500mm^3, the mice were anesthetized using isoflurane gas (2 % in oxygen at 0.6 L/min flow rate) and injected intravenously through the tail vein with a single dose 2 mg/kg of EVs/mice weight. Whole body imaging (Excitation 650 nm/ Emission 668 nm) was carried out at 1 h, 4 h, and 8 h post EVs administration using IVIS Spectrum Station (Caliper Life Sciences). The mice were euthanized after 8 h, and organs and tumors were taken out for fluorescence imaging to compare the biodistribution profiles of EVs. This animal experiment was done with a protocol approved by the Institutional Animal Care and Use Committee (IACUC) of The Ohio State Univeristy.

***In vivo* therapeutic effect of EVs in prostate cancer mouse models:**

6-8 weeks old male nude mice (Nu/Nu) were purchased from Charles River (Wilmington, MA). The mice were maintained in sterile conditions using IVC System (Innovive). Tumor xenografts were established by subcutaneous injection of 2×10^6 cancer cells mixed with equal volume of Matrigel matrix (Corning life science) in the flank area of the mice. $PSMA_{apt}$/EV/siSurvivin, $PSMA_{apt}$/EV/siScramble and PBS were administered by tail vein injection, at dosage of 0.5 mg siRNA/5 mg EVs per Kg of mice body weight, twice per week for three weeks. Two axes of the tumor (L, longest axis; W,

shortest axis) were measured with a caliper. Tumor volume was calculated as: $V = (L \times W^2)/2$. This animal experiment was done with a protocol approved by the Institutional Animal Care and Use Committee (IACUC) of North Dakota State University. For tumor inhibition assay, n = 10, the mice that did not develop tumor from the beginning were excluded for analysis.

Statistics:

Each experiment was repeated at least 3 times with triplication for each sample tested. The results were presented as mean ± standard deviation, unless otherwise indicated. Statistical differences were evaluated using unpaired *t* test with GraphPad software, and $p < 0.05$ was considered significant.

RESULTS AND DISCUSSION:

Design and construction of arrow shaped RNA nanostructures for display on EVs surface.

The three-way junction (3WJ) (43,184) of the bacteriophage phi29 motor pRNA folds by its intrinsic nature into a flat sheet with three angles of 60°, 120° and 180° between helical regions (**Figure 3.1a.**) (184). The pRNA-3WJ was extended into an arrow shaped structure by incorporating an RNA aptamer serving as a targeting ligand, binding PSMA, a prostate cancer cell-surface receptor. The engineered pRNA-3WJ was used to decorate EVs purified from HEK293T cell culture medium to create ligand decorated EVs. HEK293T EVs were used as they are non-immunogenic and contain minimal intrinsic biological cargoes (185). An Opti-Prep ultracentrifugation method was used to purify EVs (see Methods(182)). Adding the iso-osmotic Opti-Prep cushion layer for ultracentrifugation greatly enhanced reproducibility of exosome purification in yield

(data not shown), as well as lessen physical disruption of exosomes by ultracentrifugation pelleting. A single lipid molecule, cholesterol, was conjugated into the arrow tail of the pRNA-3WJ to promote the anchoring of the 3WJ onto the EV membrane (**Figure 3.1b.**). Cholesterol-tetraethylene glycol (TEG) spontaneously inserts into the membrane of EVs that contain hydrophobic lipid core (186,187). The displaying of the RNA nanoparticles to the surface of the purified EVs was achieved by a simple incubation of the cholesterol-modified RNA nanoparticle with the EVs at 37 °C for one hour. Electron Microscopy (EM) imaging (**Figure 3.1c.**), Nanoparticle Tracking Analysis (NTA) and Dynamic Light Scattering (DLS) revealed that the isolated native EVs were physically homogeneous, with size centering at 110 nm(**Figure 3.1d, Figure. 3.S1a-b**), with a negative zeta potential (**Figure 3.1e**). The purified EVs were further identified by the presence of exosome marker TSG101 (188) by western blot (**Figure 3.S1c**). The yield of purifying EVs from HEK293T cell culture medium was about 10-15 μg of EVs (measured as protein concentration), or 0.1 - 1.9 × 10^9 EV particles (measured by NTA) per 10^6 cells.

EVs hold great promise as emerging therapeutic carriers given its intercellular communication nature. They can enter cells through multiple routes including membrane fusion, tetraspanin and integrin receptor mediated endocytosis, lipid raft mediated endocytosis, or micropinocytosis; but there is no specificity regarding the recipient cells (132,189). In order to confer specific targeting of the EVs to cancer cells, two classes of targeting ligands including folate and PSMA RNA aptamer were conjugated to the 3WJ for display on EVs. Folate is an attractive targeting ligand, since many cancers of epithelial origin, such as head and neck cancers, overexpress folate receptors.(190) PSMA is expressed at an abnormally high level in prostate cancer cells and its expression

is also associated with more aggressive disease (191). A PSMA binding 2'-F modified RNA aptamer (192) was displayed on EVs for enhancing targeting efficiency to prostate cancer cells. For imaging, one of the pRNA-3WJ strands was end-labeled with the near infrared fluorescent dye $Alexa_{647}$ (**Figure 3.1i**). The size distribution and zeta potential of RNA nanoparticle decorated EVs did not change significantly as measured by NTA and DLS (**Figure 3.1f-g**, **Figure 3.S1d)**.

Survivin, an inhibitor of cell apoptosis, is an attractive target for prostate cancer therapy, since its knockdown can decrease tumorigenicity and inhibits metastases.(193) In combination with the survivin siRNA loaded in the EVs(**Figure 3.1i**), the $PSMA_{apt}$/EV/siSurvivin were prepared for evaluating *in vivo* prostate cancer inhibition efficacy (see section 5). To improve the enzymatically stability of siRNA, the passenger strand was 2'-fluorine (2'-F) modified on pyrimidines, while keeping the guide strand unmodified (50,51). For tracking the siRNA loading efficiency in EVs, the survivin siRNA was fused to an $Alexa_{647}$ labeled 3WJ core, and assembled into RNA nanoparticles (**Figure. 3.S1e**). After loading siRNA into EVs, the size of EVs did not change significantly as measured by NTA with a peak around 110 nm (**Figure. 3.1f**). The loading efficiency for siRNA-3WJ RNA nanoparticles was around 80 % (**Figure. 3.s1f**), controls without EVs or with only the ExoFect reagent showed as low as 15 % loading efficiency using the same method.

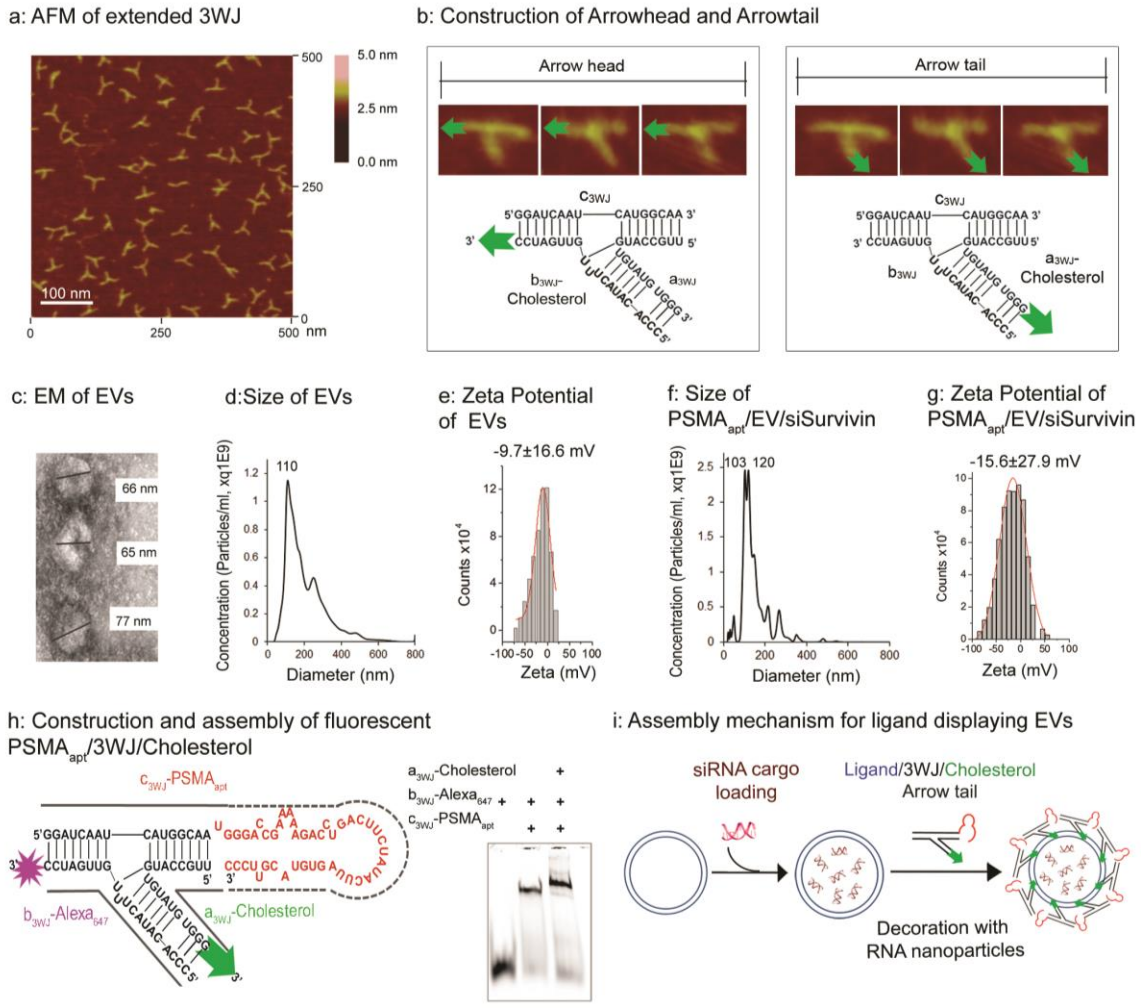

Figure 3.1.: RNA nanotechnology for decorating native EVs. **(a)** AFM image of extended 3WJ of the motor pRNA of bacteriophage phi29. **(b)** Illustration of constructing cholesterol labeled 3WJ on either the arrowhead arm or the arrow tail arm of the 3WJ. **(c)**. Electron microscopy image of EVs from HEK293T cells. **(d)**. NTA profile and **(e).** Zeta potential of EVs from HEK293T cells. **(f)**.NTA profile and **(g)**. Zeta potential of PSMA aptamer displaying survivin siRNA loaded EVs. **(h)**. 2D structure (left panel) and 8 % native PAGE for testing the assembly of Alexa$_{647}$ labeled PSMA$_{apt}$/3WJ/Cholesterol.'+' indicates the presence of the 3WJ component strands. **(i)**. Assembly method for ligand displaying EVs. The native EV purified from HEK293T

cells were loaded with therapeutic siRNA cargoes, and then displaying with RNA nanoparticles harboring cholesterol for membrane anchorage and chemical ligand or RNA aptamer for specific cell binding.

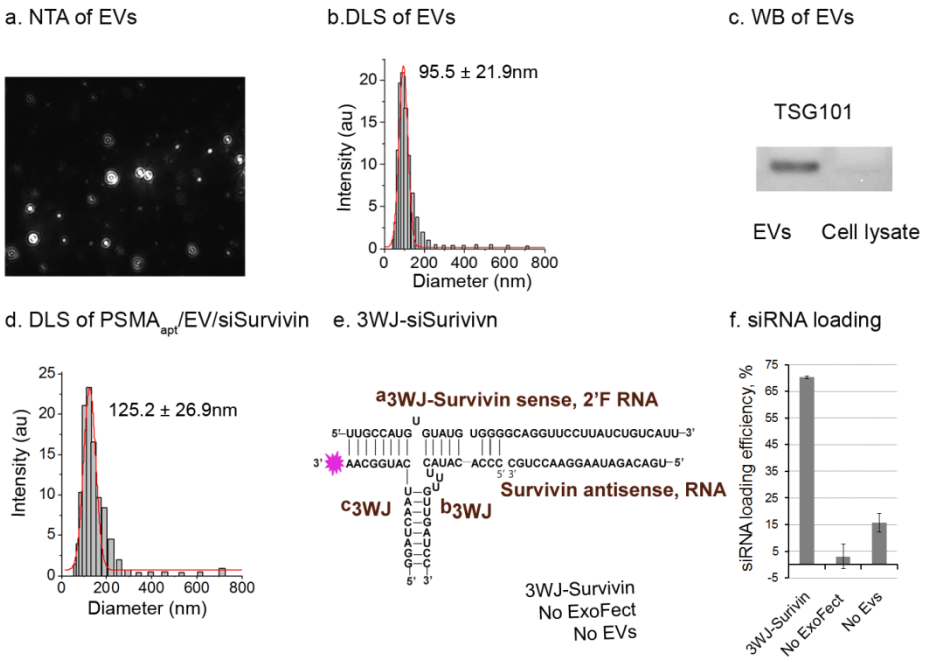

Figure 3.S1. Physopchemical characterization for EVs and RNA nanoparticles. a. A representative NTA image of EVs purified from HEK293T cell medium. b. Particle size distribution EVs from HEK293T cells measured by DLS. c. Western blot showed the presence of TSG101 on EVs from HEK293T cells. d. Particle size distribution of PSMA$_{apt}$/EV/siSurvivin measured by DLS. e. Sequence and structure of pRNA-3WJ fused with survivin siRNA. f. siRNA loading efficiency to EVs using ExoFect, the controls without EVs or without ExoFect were tested.

3.2. Arrow head or arrow tail cholesterol labeling of the RNA nanoparticles resulted in EV loading or membrane display, respectively.

a. Differentiation between entry or surface display on EVs using serum digestion.

The orientation and angle of the arrow shaped pRNA-3WJ nanostructure was used to control the RNA loading or surface display to EVs. We performed serum digestion experiment to confirm the localization of 2'F-RNA nanoparticles with EVs. Although the 3WJ 2'F-RNA nanoparticles are relatively resistant to RNaseA, it can be digested in 67 % fetal bovine serum (FBS) after incubation at 37 °C for 2 h (**Figure. 3S2c**). $Alexa_{647}$-2'F-RNA nanoparticle-displaying EVs were purified from free RNA nanoparticles by ultracentrifugation, then subjected to serum digestion experiment. It turned out the $Alex_{647}$-2'F-RNA with cholesterol on arrow tail decorated EVs were degraded more than arrow head cholesterol decorated counterparts after 37 °C FBS incubation (**Figure 3.2a-d**). The result can be explained by the protection of RNA nanoparticles by EVs against serum digestion. Cholesterol to the arrow tail promoted displaying onto exosomes surface thus being degraded; while cholesterol to the arrow head promoted RNA nanoparticles entering EVs, thus the EVs provided protection against serum digestion on the $Alexa_{647}$-2'F- RNA nanoparticles.

The displaying of ligand on the outer surface of EVs might be caused by pRNA-3WJ nanoparticles anchoring on the membrane without trafficking into the exosomes. The arm which forms a 60° angle with its adjacent arm of the RNA nanoparticles can act as a hook to lock the RNA nanoparticle in place, thereby preventing it from passing through the membrane (**Figure 3.2a**). This locking on the membrane displayed the ligand of either folate or PSMA RNA aptamer onto the EV surface.

The concentration of FBS used in the serum digestion experiment was chosen extremely high to purposely degrade the externally displayed RNA on EVs. The decorative $PSMA_{apt}$-3WJ 2'F RNA nanoparticles have been shown to remain stable and intact under physiological conditions.

b. Differentiation between entry into or surface display on EV by competition assay using ligands to cancer cells.

As described above, when cholesterol was attached to arrow tail of pRNA-3WJ , the RNA nanoparticles were anchored on EVs membrane and the incorporated ligands were displaced at the outer surface of the EVs (**Figure 3.2a**). An increase in uptake of EVs to folate receptor overexpressing KB cell was detected through displaying folate on EV surface by arrow tail cholesterol RNA nanoparticles (**Figure 3.2 e, f**). When incubating with folate receptor low expressing MDA-MB-231 cells, arrow tail shaped FA-3WJ/EV did not enhance its cellular uptake comparing to arrow tail 3WJ/EV (**Figure 3.2g**). The surface display of folate was further confirmed by free folate competition binding assay, in which a base line of uptake by the FA-3WJ/EVs to KB cells was established. A decrease in cellular uptake to KB cells was detected after adding 10uM of free folate to compete with the cholesterol-arrow tail RNA nanoparticles decorated FA-3WJ/ EV for folate receptor binding (**Figure 3.2f**). However, competition in uptaking of arrow head FA-3WJ/EV (**Figure 3.2h**) to KB cells by free folate was much lower (24.8 ± 0.6 %) (**Figure 3.2i**), possibly due to partial internalization of the arrow head shaped nanoparticle into the EVs, caused a lower displaying intensity of folate on the EVs surface.

EVs can mediate intercellular communications through transporting mRNA, siRNA, microRNA or proteins between cells. They internalize into recipient cells through multiple different pathways, including micropinocytosis, receptor-mediated endocytosis, or lipid raft mediated endocytosis as reported (132). Although the natural process for EVs uptake is not ligand dependent, the arrow tail cholesterol RNA 3WJ conferred successful ligand dependent uptake by cancer cells, thus displaying cancer targeting property.

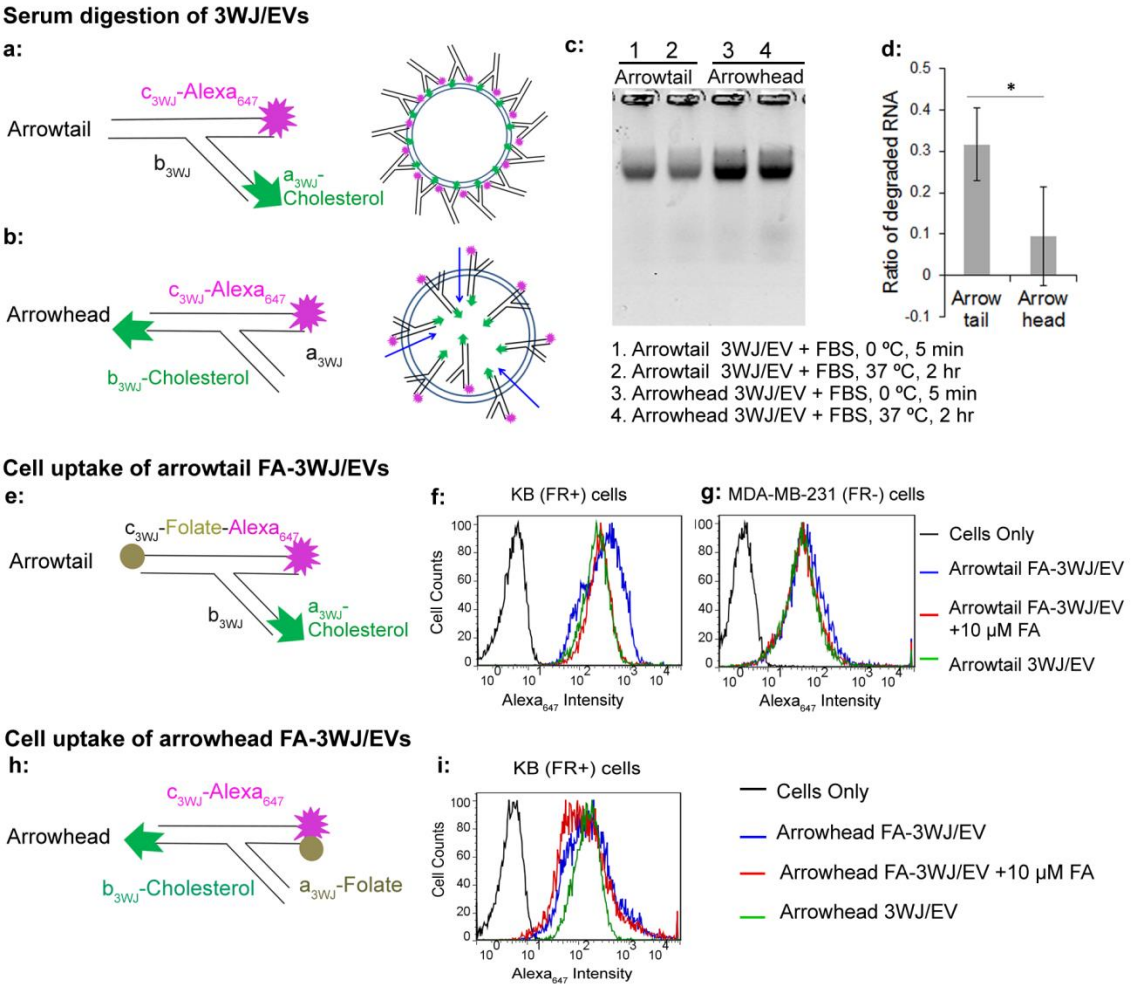

Figure 3.2: Comparison of the role between arrow head and arrow tail 3WJ. (a-b) Illustration showing the difference between arrow-head and arrow-tail display. **(c)** Syner gel to test arrow head and arrow tail $Alexa_{647}$-3WJ/EV degradation by RNase in FBS. The gel was imaged at $Alexa_{647}$ channel **(d)** and the bands were quantified by Image J. **(e-i)** Assay to compare cell uptake of folate-3WJ arrow tail (**e-g**) and arrow head (**h-i**) on folate receptor positive and negative cells.

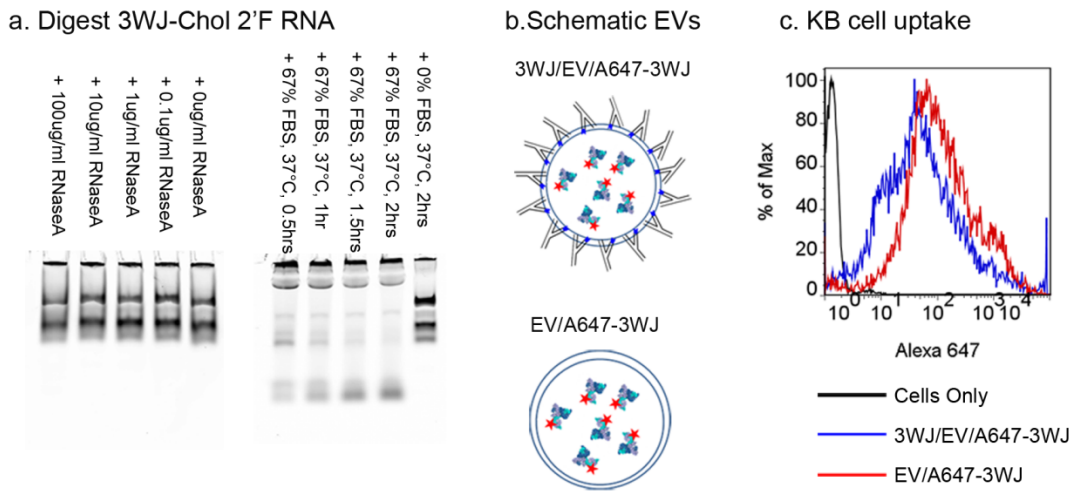

Figure 3.S2: RNA nanoparticles can be displayed on EVs outer surface by cholesterol anchoring. a. 2'F RNA nanoparticles cannot be digested by RNaseA, but can be digested in 67 % FBS after incubation for 2 h. To compare whether decorating EVs with RNA nanoparticles can reduce its nonspecific cell entry, b. shows the schematic drawing of EVs with or without RNA decoration, the EVs were labeled by loaded $Alexa_{647}$-3WJ nanoparticles. c. Flow cytometry tests the uptake of EVs by KB cells, 3WJ 2'F-RNA decorated EVs showed less cell entry comparing to undecorated EVs.

3.3. Specific cancer targeting and gene silencing of the RNA-displaying EV demonstrated *in vitro*.

Specific cancer cell targeting is one important prerequisite for applying nano-vesicles to cancer therapy. To generate cancer cell targeting EVs, approaches to express cancer cell specific ligand on EVs has been explored. One way to increase the specificity of EV to target cell is to overexpress peptide ligands on the EV membrane proteins (139). Neuron specific peptide RVG has been fused to EV membrane protein Lamp2b and overexpressed on dendritic cells(139). GE11 peptide, which is a ligand to EGFR was fused to the transmembrane domain of platelet-derived growth factor receptor (141). RGD peptide was fused to EV protein Lamp2b, thus generated EVs can delivery chemical drug doxorubicin specifically to tumor cells(194). One problem for using fusion peptide for targeted exosomal delivery is that the displayed peptide can be degraded during EV biogenesis. We explored here the method of displaying ligands onto EVs surface post biogenesis to enhance its specificity. The specific targeting, delivery and gene silence efficiency of the ligand displaying EVs were examined in cell culture. To ensure RNase resistance, 2'-F modifications were made to the RNA nanoparticles placed on the surface of EVs(43), while the thermodynamic stability of pRNA 3WJ provided a rigid structure to ensure the correct folding of RNA aptamers.(43,44) PSMA aptamer displaying EVs showed significantly enhanced binding and uptake to LNCaP cells compared to EVs without PSMA aptamer, but not to the PC3 cells, which is a PSMA receptor low expression cell line (**Figure 3.3a**). PSMA positive LNCaP prostate cancer cells were used as a model to evaluate whether the siRNA were delivered to cancer cells through ligand displaying EVs. Upon incubation with LNCaP cells,

$PSMA_{apt}$/EV/siSurvivin (PSMA aptamer/EV/Survivin siRNA) were able to knockdown survivin expression at the mRNA level as demonstrated by real-time PCR (**Figure 3.3b**), and protein level shown by western blot **(Figure 3.S3**). Cell viability and apoptosis was detected by MTT assays (**Figure 3.3c**), indicating that LNCaP cells were undergoing apoptosis as a result of survivin siRNA delivery.

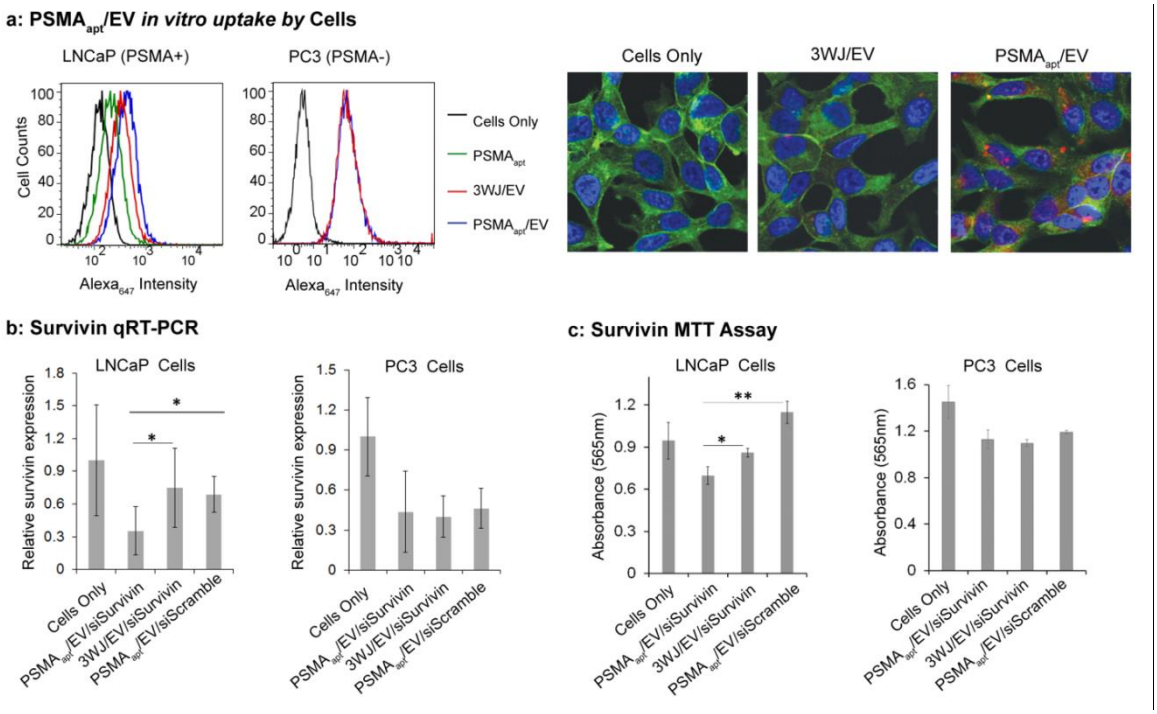

Figure 3.3: Specific binding and siRNA delivery to cells *in vitro* with PSMA aptamer displaying EVs. **(a)** Flow cytometry (left) and confocal images (right) showing the entry of PSMA$_{apt}$/EV to PSMA(+) prostate cancer LNCaP cells. The confocal images are overlap of Nucleus (Blue); Cytoskelton (Green); and EVs displaying with RNA (Red). **(b)** PSMA aptamer mediated delivery of survivin siRNA by EV to PSMA(+) prostate cancer cells assayed by RT-PCR. N = 3, experiment was run in three biological replicates and three technical repeats, statistics were calculated using a two sided t-test with center values presented as averages and errors as s.d. p = 0.016 for PSMA$_{apt}$/EV/siSurvivin vs. 3WJ/EV/siSurvivin, p=0.013 for PSMA$_{apt}$/EV/siSurivivn vs. PSMA$_{apt}$/EV/siScramble. **(c)** MTT assay showing reduced cellular proliferation. N = 3, experiment was run in three biological replicates, and statistics were calculated using a two sided t-test with center values presented as averages and errors as s.d. p = 6.8e-3. *p < 0.05, **p < 0.01.

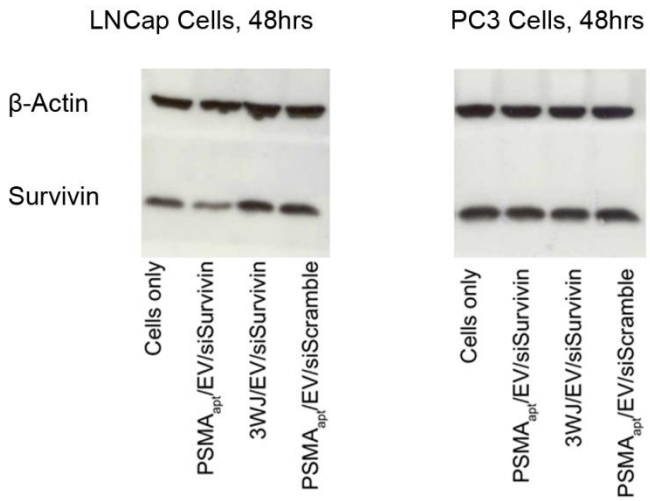

Figure 3.S3. Western blot detect the knockdown of survivin protein by EVs. Survivin protein knocked down was detected in PSMA$_{apt}$/EV/siSurvuvin PSMA positive LNCaP cells, but not PSMA negative PC3 cells. The same construct loaded with scramble siRNA or decorated without pRNA-3WJ were tested as negative controls.

3.4. The ligand displaying EVs target tumors

The tumor targeting and biodistribution properties of ligand-displaying EVs were evaluated. FA-3WJ/EVs were systemically administered *via* the tail vein into KB subcutaneous xenograft mice model. *Ex vivo* images of mice healthy organ and tumors taken after 8 hr showed that the FA-3WJ/EVs mainly accumulated in tumors, with low accumulation in vital organs in comparison with PBS control mice (**Figure 3.4a**). The results supports the assumption that displaying targeting RNAs on the EVs surface reduces their accumulation in normal organs (141), and the ideal nano-scale size of RNA displaying EVs facilitates tumor targeting *via* Enhance Permeability and Retention (EPR) effects, thereby avoiding toxicity and side effects.

3.5. Complete inhibition of tumor growth by ligand-3WJ-displaying EV as demonstrated in animal trials.

The therapeutic value of PSMA aptamer displaying EVs delivering survivin siRNA for prostate cancer was further evaluated *in vivo* using LNCaP-LN3 tumor xenografts generated in nude mice(195,196). Treatment with $PSMA_{apt}$/EV/siSurvivin (1 does every 3 days, totally 6 doses were given) completely suppressed *in vivo* tumor growth, compared to control groups (**Figure 3.4b**). EVs are biocompatible and well tolerated *in vivo* as we did not observe any toxicity as indicated by body weights of the mice, assessed 40 days after treatment (**Figure 3.4c**). The specific knockdown of survivin was validated by real time PCR (24.3 ± 8.1 %, $P < 0.05$) (**Figure 3.4d**), Taken together, the data showed that $PSMA_{apt}$/EV/siSurvivin could deliver survivin siRNA specifically into cancer cells upon systemic injection and achieve high therapeutic efficacy without significant toxicity to the mice.

The *in vivo* cancer growth inhibition effect was more significant than *in vitro* MTT assays. The favorable effect and parameters of biodistribution, EPR effect of the decoration by the negatively charged RNA motif explaining the difference *in vitro* and *in vivo*, as found in the course of the study of RNA nanoparticles decorated EVs.

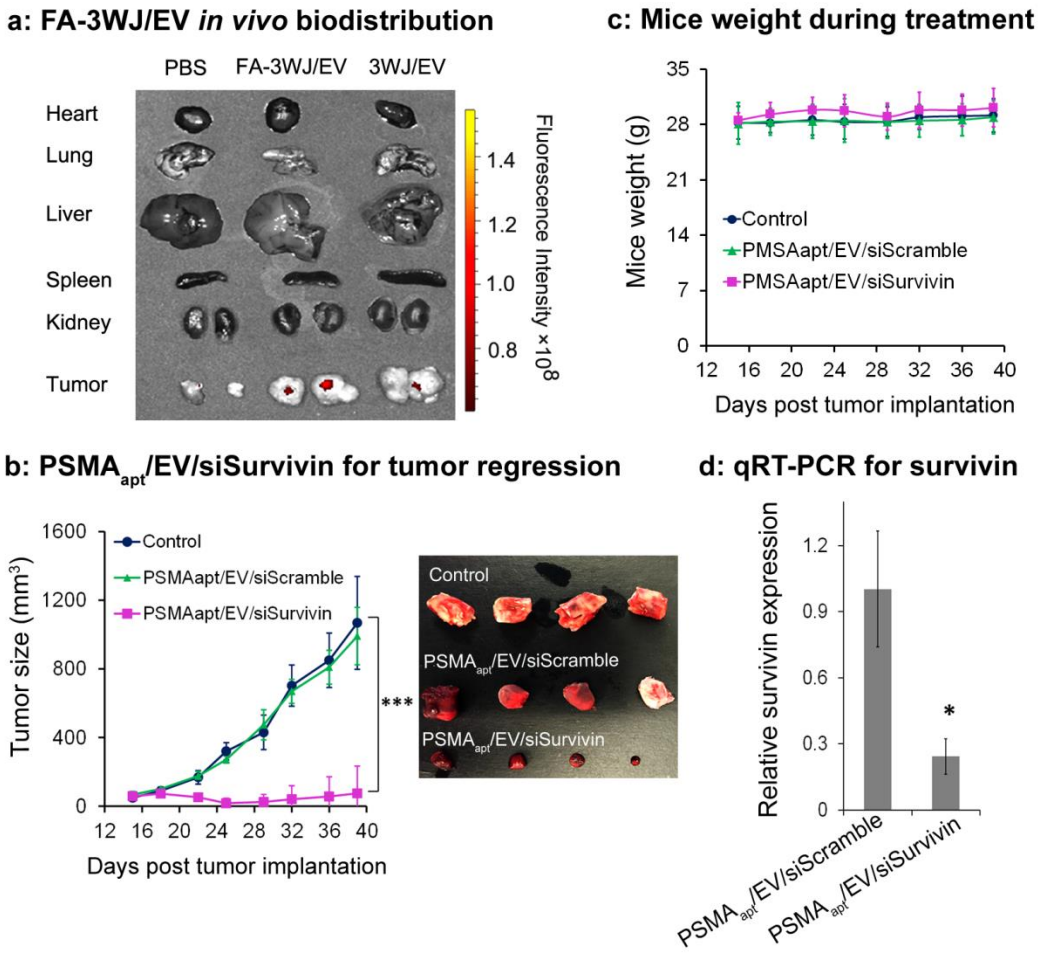

Figure 3.4: A*nimal* trials using ligands displaying EV for tumor inhibition. **(a)** Organ images showing specific tumor targeting 8 hr after systemic injection of folate displaying EVs to mice with subcutaneous KB cell xenografts. n = 2, two independent experiments. **(b)** Intravenous treatment of nude mice bearing LNCaP-LN3 subcutaneous xenografts with $PSMA_{apt}$/EV/siSurvivin (0.6 mg/kg, siRNA/mice body weight), $PSMA_{apt}$/EV/siScramble (0.6 mg/kg, siRNA/mice body weight), and PBS, injected twice per week for three weeks. n = 10 biological replicates, 2 independent experiments, and statistics were calculated using a two sided t-test with center values presented as averages and errors as s.d. p = 0.347, 0.6e-2, 1.5e-6, 8.2e-8, 2.1e-7, 1.0e-7, 1.9e-7, 1.8e-6 for days 15, 18, 22, 25, 29, 32, 36, 39, respectively for $PSMA_{apt}$/EV/siSurvivin compared to

control. **(c)** Body weight of mice during the time course of exosome treatment. **(d)** RT-PCR showing specific knockdown of survivin mRNA expression in prostate tumors after EV treatment. n = 4 biological replicates, experiment was run three times, and statistics were calculated using a two sided t-test with center values presented as averages and errors as standard deviation.

CONCLUSION

The use of RNA interference technology, such as siRNA, to knockdown gene expression has been of great interest (197). The discovery of EVs, which are cell-derived membranous vesicles that are universally released by many cell types (124) and play important roles in intercellular signaling (136) advanced the field of siRNA delivery study. EVs (124,136,198,199) are naturally capable of intracellular delivery of biomolecules; and have nanoscale size and deformable shape with intrinsic ability to cross biological barriers. EVs can directly fuse with the cell membrane through tetraspanin domains or back-fuse with endosomal compartment membranes following receptor-mediated endocytosis to release encapsulated cargo to cytosol. Therapeutic payloads, such as siRNA can be fully functional after delivery to cells (124,136,198,199). However, EVs lack selectivity and randomly fuse to healthy cells as well. To generate specific cell targeting EVs, approaches to express cell specific peptide ligands on EVs surface have been explored.(139,141) However, *in vivo* expression of protein ligands is limited to the availability of ligands and depends on EV and ligand producing cell types.(124,199) In addition, the use of protein ligands will result in larger sized particles that can get trapped in liver, lung and other organs, and can stimulate the production of host antibodies.(200) To date, there are no studies reporting the display of nucleic acid based or chemical targeting ligands on EVs.

Herein, we applied RNA nanotechnology (26) to reprogram natural EVs for specific delivery of siRNA to cancer models *in vitro* and *in vivo* (**Figure 3.1a-c**). Taking advantage of the thermodynamically stable properties of pRNA-3WJ(43,44,72), we generated multifunctional RNA nanoparticles harboring membrane anchoring lipid

domain, imaging, and targeting modules. The natural arrow shape of the pRNA-3WJ allowed for controlled entry or decoration on the surface of the EVs. With cholesterol placed on the arrow tail of the 3WJ, the RNA-ligand was prevented from trafficking into EVs, ensuring oriented surface display for cancer receptor binding. This was explicitly shown in the cell decoration and folate competition assays (**Figure 3.2b**) and further shown through the enhanced binding to LNCaP cells with the display of the PSMA aptamer (**Figure 3.3a**). Additionally, the placement of cholesterol on the arrowhead allowed for partial internalization of the RNA nanoparticle within the EVs (**Figure 3.2a, c**). The addition of RNA nanoparticles to the surface of the EVs not only provided a targeting ligand to the EV, they further added to the negative charge of the EV, thus reducing the non-specific binding of RNA displaying EVs to untargeted tissues. The cholesterol-TEG modified RNA nanoparticles should preferably anchor into the raft forming domains of lipid bilayer of EVs (186), further studies will be necessary to illustrate this process. Our *in vitro* decoration approach retained the favorable endogenous composition of EVs as delivery vectors, thus eliminated the need of building artificial endosome-escape strategies into the EV vectors comparing to using other synthetic nanovectors for siRNA delivery.

Building on the confirmed RNA decorated EVs, we were able to specifically target PSMA expressing prostate cancer cells and tumors *in vitro* and *in vivo*, respectively. Furthermore, the EVs can deliver survivin siRNA to targeted prostate cancer cells with a level that was able to completely inhibit the growth of LNCaP prostate cancer xenograft. The $PSMA_{apt}$ nanoparticles provided a specific delivery of the EVs to

the tumor while reducing accumulation in healthy organs which is normally seen in EV delivery (141).

EVs are heterogeneous; their compositions differ depending on their parental cells types. The interactions between EVs and immune system are also complex (201). Leukocytes and dendritic cells derived exosomes are proposed to be potential candidates for clinical therapeutics delivery vectors (202). But the exosome production scalability and reproducibility still need further studies.

In summary, we demonstrated that we can effectively reprogram native EVs using RNA nanotechnology. Nanoparticles orientation controls RNA loading or surface display on EV for efficient cell targeting, siRNA delivery and cancer regression. The reprogrammed EVs displayed robust physiochemical properties, adequate tumor site localization, minimal healthy organ accumulation, high cancer cell specific uptake, and efficient intracellular release of siRNA to suppress tumor growth in animal models with unusually high efficiency.

ACKNOWLEDGMENT:

We thank Zhefeng Li for assistance in EV purification. The research was supported by NIH grants UH3TR000875 (Huang-Ge Zhang and PG), R01CA186100 (BG), and P30CA177558 (BME). Peixuan Guo's Sylvan G. Frank Endowed Chair position in Pharmaceutics and Drug Delivery is funded by the CM Chen Foundation. PG is a consultant of Oxford Nnaopore, Nanobio Delivery Pharmaceutical Co., Ltd. and NanoBio RNA Technology Co. Ltd. His inventions at the University of Kentucky have been licensed to Matt Holding and Nanobio Delivery Pharmaceutical Co. Ltd.

Copyright © Fengmei Pi 2016

Chapter 4: RNA Nanoparticles Harboring Annexin A2 Aptamer Can Target Ovarian Cancer for Tumor Specific Doxorubicin Delivery

This chapter (with some modification) is in submission at *Molecular Therapy*. Special thanks to Dr. Thiviyanathan Varatharasa for help in preparation of 3WJc-endo28-3WJa DNA strand for the experiments.

ABSTRACT:

Utilizing the state-of-art RNA nanotechnology platform, we report here the design and construction of RNA nanoparticles harboring annexin A2 aptamer for ovarian cancer cell targeting, and a GC rich sequence for doxorubicin loading that can deliver drugs to ovarian cancer cells in a targeted manner. The system utilizes a highly stable three way junction (3WJ) derived from packaging RNA of the phi29 bacteriophage as a core of the nanoparticle. Annexin A2 aptamer was conjugated to one arm of the 3WJ. The highly stable pRNA-3WJ structural motif provides a rigid core to the RNA architecture and disfavors misfolding of aptamers when conjugated to other oligonucleotides, keeping affinity and functions of all functionalities intact, and thus is of significance utility for aptamer mediated targeted delivery. Nanoscale RNase-resistant RNA nanoparticles remained intact after systemic injection in mice and strongly bound to tumors with little or no accumulation in healthy organs 6 h post-injection, and the RNA nanoparticle/doxorubicin conjugates showed enhanced toxicity to ovarian cancer cells, but reduced toxicity to annexin A2 negative cells in cell toxicity assay. These results suggest that the constructed nanoparticle doxorubicin can potentially enhance ovarian

cancer targeted doxorubicin delivery for cancer treatment at lower doses with enhanced efficiency.

INTRODUCTION:

Ovarian cancer is a highly metastatic and lethal disease with the highest mortality rate of all cancers of the female reproductive system, although it is treatable when detected early. Most patients have high-grade disease with metastasis at the time of diagnosis due to vague clinical symptoms at early stages. The 5-year survival rate for patients with advanced disease is very low despite cytoreductive surgery and chemotherapy combination regimens. Furthermore, successful treatment is limited by the high rate of chemo-resistance and emergence of undesirable toxicities. Therefore, vehicles capable of targeted delivery of therapeutics to cancer cells with little collateral damage to healthy cells and tissues are needed. Annexin A2 is a calcium-binding cytoskeletal protein which is localized at the extracellular surface of endothelial cells and multiple types of tumor cells (203). Annexin A2 plays an important role in the angiogenesis and tumor progressing(204), targeting annexin A2 might be a strategy to develop effective therapeutics for cancer treatment. Using Cell-SELEX (Systematic Evolution of Ligands by Exponential Enrichment), a phosphorothiate modified DNA (thio-DNA) aptamers Endo28 against annexin A2 expressed in the vasculature and ovarian tumors obtained from human patients has been selected (205,206).

Doxorubicin is an anthracycline chemotherapy drug. It can slow or stop the growth of multiple cancer cells and is an important component of ovarian cancer treatment (207). Long circulating PEGylated liposomal doxorubicin is a FDA approved drug for the treatment of recurrent ovarian cancer(208). Given that the promise of the

delivery system could benefit the therapeutic effect of doxorubicin on ovarian cancers; we explored the possibility of using RNA nanoparticles with targeting ligand for ovarian cancer targeted drug delivery.

We recently discovered a phi29 pRNA three-way junction (3WJ) motif with unusually robust thermostable properties that can be used as an RNA nanotechnology platform to construct a new generation of therapeutic nanoparticles (43,53). The core structure of pRNA-3WJ can be assembled from three pieces of short RNA oligonucleotides, named 3WJa, 3WJb and 3WJc, with high efficiency forming a rigid scaffold. The rigid pRNA-3WJ scaffold can ensure the correct folding of its connected nucleic acid aptamers and other functionalities. We have demonstrated that RNA nanoparticles built with the 3WJ scaffold while harboring different functional modules retained their folding and independent functionalities for specific cell binding, cell entry, gene silencing, catalytic function and cancer targeting, both *in vitro* and in animal trials. The pRNA-3WJ nanoparticles are non-toxic and non-immunogenic (169). They are also capable of penetrating across heterogeneous biological barriers to selectively target cancer cells in mice and delivering therapeutics after systemic injection with little accumulation in healthy organs and tissues.

The sequences for the thio-DNA aptamer will be incorporated into the pRNA-3WJ 2'F-RNA scaffold to retain its authentic folding and functionality and in addition will harbor the fluorescent imaging probe $Alexa_{647}$. We hypothesize that this DNA/RNA hybrid nanoparticle will retain the anenxin A2 targeting property *in vitro* and *in vivo*. With addition of a fluorescent imaging probe $Alexa_{647}$ and the chemotherapeutic drug doxorubicin to the pRNA-3WJ scaffold, the nanoparticle can function as a drug carrier to

enhance the accumulation of doxorubicin in ovarian cancer cells, thus reducing the distribution of cargoes to other health organs. Load doxorubicin into the DNA/RNA hybrid nanoparticles also changed the pathway of doxorubicin entering cells. Without nanoparticles, doxorubicin enters cells mainly through passive diffusion; when doxorubicin is intercalated into nanoparticles, it selectively enters annexin A2 positive cells through receptor mediated endocytosis. Thus, the therapeutic effect can be enhanced by changing the drug internalization pathway on cancer cells. An ovarian cancer xenografts mouse model was utilized to evaluate the biodistribution of nanoparticles *in vivo*.

MATERIALS AND METHODS

Construction of pRNA-3WJnanoparticles harboring Annexin A2 binding aptamer.

DNA/RNA hybrid nanoparticles were constructed using a bottom-up approach, as previously described. Briefly, DNA oligo 3WJc-endo28-3WJa was synthesized by DNA synthesizer, and $Alexa_{647}$-3WJb 2'F-RNA, 3WJb-sph1 2'F RNA, Sph1-2'F-RNA were prepared by RNA synthesizer using solid phase synthesis. The sequences are described as below (_* represents a phosphorothioated bond, lower case letter represents a 2'-fluorine modified base):

3WJc-endo28-3WJa DNA: 5'-GGA TCA ATC ATG GCA ACG CTC GGA TCG ATA AGC TTC GCT CGT CCC CC*A GGC* AT*A G*AT* ACT CCG CCC CGT C*AC GG*A TCC TCT* AG*A GC*A CTG TTG CCA TGT GTA TGT GGG-3'

$Alexa_{647}$-3WJb 2'F-RNA: 5'-(Alexa 647) (C6-NH) ccc AcA uAc uuu Guu GAu cc-3'

3WJb-Sph1 2’F-RNA: 5’- ccc AcA uAc uuu Guu GAu ccA Auc ccG cGG ccA uGG cGG ccG GGA G-3’

Sph1-2’F- RNA: 5’-cuc ccG Gcc Gcc AuG Gcc GcG GGA uu-3’

3WJa 2’F- RNA: 5’-uuG ccA uGu GuA uGu GGG-3’

3WJc-2’F RNA: 5’-GGA ucA Auc AuG GcA A-3’

The RNA nanoparticle carrying a scramble aptamer sequnce was prepared by *in vitro* transcription with Y639F T7 polymerase. The DNA template was prepared by two step PCR using primer1 and 2 for first step, and primer 3 and 4 for second step PCR. 2’fluorine (2’-F) modified cytosine and uracil were used in the transcription reaction. The transcribed RNA strand was purified by 8 M Urea, 8 % polyacrylamide gel ran in TBE buffer (89 mmol/L tris-borate, 2 mmol/L EDTA). RNA bands of interest was excised from the gel visualized by UV shadow on thin layer chromatography plates, and eluted from gel with elution buffer (0.5 M Ammonium Acetate, 0.1 mol/L EDTA, 0.1 % SDS), followed by ethanol precipitation.

Primer1: 5’-TAA TAC GAC TCA CTA TAC CGG ATC AAT CAT GGC AAG TTC GGT TGT GTC GGC GAG TAT AG-3’

Primer 2: 5’- GGA TCA ACA AAG TAT GTG GGA TCG GCA TTA TAC GTA TAG CA-3’

Primer3: 5’-GTA TAA TAC GAC TCA CTA TAG GGC CGG ATC AAT CAT GGC AA-3

Primer4: 5’-CTC CCG GCC ATG GCC GCG GGA TTG GAT CAA CAA AGT ATG TGG-3’

Scramble template: 5’-GTC GGC GAG TAT AGG TGA AGT TGC CAT GTG TAT GTG GGG TGA TGG ATT GCT ATA CGT AT-3’

Nanoparticles were assembled by mixing strands at equal molar concentrations in PBS(w/Ca^{2+} Mg^{2+}) buffer(0.1 g/L $CaCl_2$, 0.2 g/L KCl, 0.2 g/L KH_2PO_4, 0.1 g/L $MgCl_2$-$6H_2O$, 8.0 g/L NaCl, 1.15 g/L Na_2HPO_4), the mixture was heated to 90 °C for 5 minutes and snap cooled down on ice.

Load doxorubicin to Endo28-3WJ-Sph1 nanoparticles.

Doxorubicin (Sigma) solution (20 μM) was incubated with extended Endo28-3WJ-Sph1 or Scr-3WJ-Sph1 RNA nanoparticles (2 μM) in intercalation buffer (0.1 M CH_3COONa, 0.05 M NaCl, 0.01 M $MgCl_2$) for 1h at room temperature. Then the free doxorubicin was removed by passing through Sephadex G50 spin column (NucAway^{TM}, Ambion). The loading efficiency of doxorubicin was monitored through measuring the fluorescence intensity of doxorubicin with fluorometer (Horiba Jobin Rivin) at excitation wavelength 480nm, emission 500-720 nm.

To measure the intercalation constant of Endo28-3WJ nanoparticle with doxorubicin, increasing concentration of nanoparticles were incubated with 1.4μM of doxorubicin, the fluorescence intensity of doxorubicin was measured. The fluorescence quenching as a function of increasing aptamer concentration was plot and fitted into a Hill equation with Origin to calculate the K_D.

Release of doxorubicin from the nanoparticle –doxorubicin conjugates

Drug release from the nanoparticle /doxorubicin conjugates was monitored using dialysis bag with 3.5 kDa cutoff under sink condition(209). About 400 μL of Endo28-3WJ-Sph1/doxorubicin conjugate which contains 1 μM doxorubicin was dialyzed in intercalation buffer at 37°C. 100 μL of releasing medium was collected at time point of 0, 0.7, 2.5, 4, 6, 8, 20, 24 h. Free doxorubicin was also dialyzed to test its release profile as a control. The concentration of doxorubicin in release buffer was tested with fluorometer (Horiba Jobin Rivin) at excitation wavelength 480nm, emission 500 to720 nm.

Serum stability assay

400 ng of $Alexa_{647}$ labeled Endo28-3WJ nanoparticle were incubated in PBS buffer containing fetal bovine serum (FBS) at final concentration of 10%. Samples were taken at multiple time points, including 0, 0.5, 1, 2, 4, 8, 9, and 24 h after incubation at 37 °C. 8 % Native TBM polyacrylamide gel electrophoresis was applied to visualize RNA. The gel was imaged at $Alexa_{647}$ channel with Typhoon FLA 7000 (GE Healthcare; Pittsburgh, Pennsylvania).

Nanoparticle size and zeta potential measurement by DLS

Apparent hydrodynamic sizes and zeta potential of assembled Endo28-3WJ nanoparticles were measured by a Zetasizer Nano-ZS (Malvern Instruments; Malvern, United Kingdom). RNA nanoparticles were measured at 1 μM in Diethylpyrocarbonate (DEPC) treated water at 25 °C.

Cell culture

Human ovarian cancer cell line SKOV3 (American Type Culture Collection; Manassas, Massachusetts) was cultured in McCoy's 5A medium (Life technologies)

containing 10% FBS, IGROV-1 cells were culture in RPMI 1640 medium (Invitrogen; Grand Island, New York) containing 10 % FBS and 1 % gentamicin sulfate (Gibco), HEK293T cells were cultured in DMEM medium (Life technologies) containing 10% FBS, HMVECad cells were cultured in flask where its surface coated with attachment factor (Gibco) with Medium 131(Gibco). All cells were cultured in a 37 °C incubator with a 5 % CO_2 and a humidified atmosphere.

Flow cytometry assay

Cells were trypsinized and rinsed with cell culture medium. $Alexa_{647}$-labeled Endo28-3WJ and the control 3WJ nanoparticles were each incubated with 2×10^5 SKOV3, IGROV-1 or HEK293T cells at 37 °C for 1 h, at the final RNA concentration of 100 nM. After washing with PBS (137 mmol/L NaCl, 2.7 mmol/L KCl, 100 mmol/LNa_2HPO_4, 2 mmol/L KH_2PO_4, pH 7.4), the cells were re-suspended in PBS buffer and subjected to flow cytometry assay. Flow cytometry assay was performed by the UK Flow Cytometry & Cell Sorting Core Facility.

Confocal microscopy imaging

SKOV3, IGROV-1 and HEK293T cells were grown on glass cover slides in their complete medium overnight. $Alexa_{647}$-labeled Endo28-3WJ and the control 3WJ nanoparticles were each incubated with the cells at 37 °C for 2 h at final concentration of 100 nM. After washing with PBS, the cells were fixed by 4% paraformaldehyde and stained by Alexa Fluor® 488 phalloidin (Invitrogen; Grand Island, New York) for actin and Prolong® Gold Antifade Reagent with DAPI (Life Technologies) for nucleus. For visualize intracellular doxorubicin delivery, the nanoparticles were incubated with cells at

final doxorubicin concentration of 1μM in PBS (with Mg^{2+}, Ca^{2+}) buffer for 6 h, then stained with DAPI for image. Doxorubicin was visualized through a channel with excitation at 480 nm, emission ranged from 530-650 nm. An Olympus FV1000 confocal microscope (Olympus Corporation) was used for these assays.

Cytotoxicity assay

The cytotoxicity of RNA nanoparticles were evaluated with an MTT assay (Promega, Madison, WI) following manufacture's instruction. Briefly, SKOV-3 and HEK293T cells were plated in a 96-well plate and cultured at 37 °C in humidified air containing 5% CO_2 overnight. The Endo28-3WJ-Sph1/Dox 2'F-RNA nanoparticle conjugates and control nanoparticles, free doxorubicin were incubated with cells at 37 °C, while keeping the final doxorubicin concentration to be 3 μM. After 48 h, 15 μL of dye solution was added to each well and incubated at 37 °C for 4 h; 100 μL of solubilization /stop solution was added to each well and incubated at room temperature for 2 h to develop color. The absorbance at 570 nm was recorded using a microplate reader (Synergy 4, Bio Tek Instruments, Inc, USA). The cell viability was calculated relative to the absorbance of cells only control.

In vivo biodistribution and tumor targeting of RNA nanoparticles

SKOV-3 cells were cultured *in vitro* and subcutaneously injected under the skin of 8-week-old female nude mice. A total of 2×10^6 cells were injected in solution. Tumors were grown for 4 weeks until tumors reached a volume of 200 mm^3. Mice were then administered PBS, Endo28-3WJ, or 3WJ each with $Alexa_{647}$ labels at a dose of 80 μg /mice through the tail vein. Mice were imaged for whole body fluorescence at time

points of 0, 1, 2, 4, and 6 h with an In Vivo Imaging System (IVIS) imager (Caliper Life Sciences; Waltham, Massachusetts). Upon the completion of the study, mice were sacrificed, and tumors, hearts, kidneys, livers, and brains were collected and imaged by the whole body imager for $Alexa_{647}$ signal. Furthermore, tumors were fixed in 4% paraformaldehyde with 10 % sucrose in PBS buffer at 4 °C overnight. Tumor samples were then placed in Tissue-Tek Optimum Cutting Temperature compound (Sakura Finetek USA; Torrance, California) for frozen sectioning (10 μm thick). Sectioned tissue were then stained with DAPI and mounted with ProLong Gold Anti-fade Reagent (Life Technologies; Carlsbad, California) overnight. Slides were then fluorescently imaged by Olympus FV1000 Confocal Microscope System (Olympus; Pittsburgh, Pennsylvania).

RESULTS AND DISCUSSION

Construction of pRNA-3WJ nanoparticles harboring Annexin A2 binding aptamer

The phosphorothioate modified DNA (thio-DNA) aptamer targeting Annexin A2, Endo28, was placed onto one end of the pRNA-3WJ 2'F-RNA, creating DNA/RNA hybrid nanoparticles suitable for ovarian cancer targeted dug delivery. The DNA/RNA hybrid nanoparticle with a two-piece design was found to have the highest assembly efficiency, in which the sequence of thio-DNA aptamer Endo28 was connected to the 3'end of 3WJc and 5'end of 3WJa DNA, forming one DNA strand. The DNA oligo was then assembled with 2'F modified $Alexa_{647}$-3WJb 2'F-RNA to form a 2'F-RNA/thio-DNA hybrid nanoparticle with 3WJ core structure, named Endo28-3WJ (**Figure 4.1a**). The formation of hybrid nanoparticle was confirmed by native PAGE analysis (**Figure 4.1b**). The hybrid nucleic acid nanoparticles have a mean particle size around 8 nm (**Figure 4.1c**), and negative charge with zeta potential around -20 mV (**Figure 4.1d**) as

measured by Dynamic Light Scattering (DLS). They are stable in serum with a half-life time of 4 h in 10 % FBS (**Figure 4.1e**).

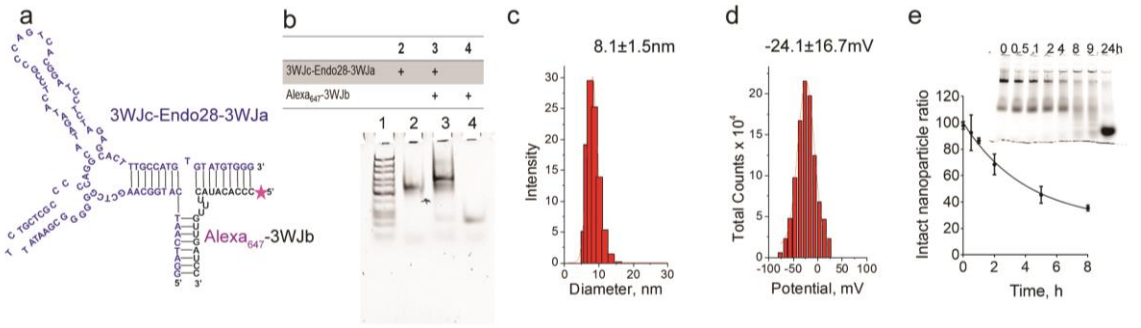

Figure 4.1. Characterization of endo28-3WJ DNA/RNA hybrid nanoparticles. (a). Primary sequence and secondary structure of Endo28-3WJ nanoparticle predicted by M Fold. (b). Native PAGE test the assembly of Endo28-3WJ nanoparticles. (c). Particle size of Endo28-3WJ as determined by DLS. (d). Zeta potential of Endo28-3WJ nanoparticles measured by DLS. (e). Serum stability assay showed the half-life of Endo28-3WJ in 10 % FBS is around 4 h, which was calculated by quantify the bands at Ethidium bromide channel. The gel image scanned at ethidium bromide channel is shown as insert.

Loading Doxorubicin into Endo28-3WJ Nanoparticles and in vitro release

Doxorubicin can physically intercalate to nucleic acid nanoparticles by preferentially binding to double stranded 5'-GC-3' or 5'-CG-3' sequences(210-212). To increase loading ratio of doxorubicin per nanoparticle, we extended the arm of Endo28-3WJ at the 3'end of 3WJb with adding a 26 bp GC rich sequence named Sph1. The extended Endo28-3WJ-Sph1 nanoparticle named Endo28-3WJ-Sph1 was assembled through three single strands of nucleic acid (**Figure.4.2a)** with high efficiency as detected by native PAGE (**Figure.4.2b**).

Doxorubicin (Dox), an anthracycline class drug, has fluorescence property that can be quenched after being interacted with nucleic acid (213).The incorportation of doxorubicin with extended nanoparticle, Endo28-3WJ-Sph1, was tested by fluorometer. A decrease in fluorescence intensity was detected when incubate a fixed amount of doxorubicin with an increasing concentration of Endo28-3WJ-Sph1 RNA nanoparticles (**Figure 4.2c**). Evaluation of the predicted secondary structure of Endo28-3WJ-Sph1 nanoparticle reveals eleven possible sites for doxorubicin intercalation, as marked by red asterisk in **Figure 4.2a**. The dissociation constant (K_D = 140 nM) of the Endo28-3WJ-Sph1/Dox physical conjugates was derived from the Hill plot in Figure 4.2c insert; while the doxorubicin concentration was kept 1.4 μM. It suggests that Doxorubicin and RNA nanoparticles spontaneously formed stable physical conjugates, and the molar binding ratio of equilibrium doxorubicin per RNA nanoparticle is around 10 : 1. The number is consistent with the predicted number of doxorubicin to be intercalated in each Endo28-3WJ-Sph1 RNA nanoparticles (**Figure 4.2a)**.

A study of Doxorubicin release from the nanoparticle–Doxorubicin physical conjugates over time was conducted using dialysis tube with membrane cutoff of 3 kDa. Upon dialysis, more than 80 % doxorubicin release was observed in 6 h with first order kinetics (**Figure 4.2d**). A significant slower drug release rate at the initial stage suggests this system is advantageous for *in vivo* systemically targeted delivery of doxorubicin. Free doxorubicin showed a much faster release profile with more than 80 % release in first hour (**Figure 4.2d**).

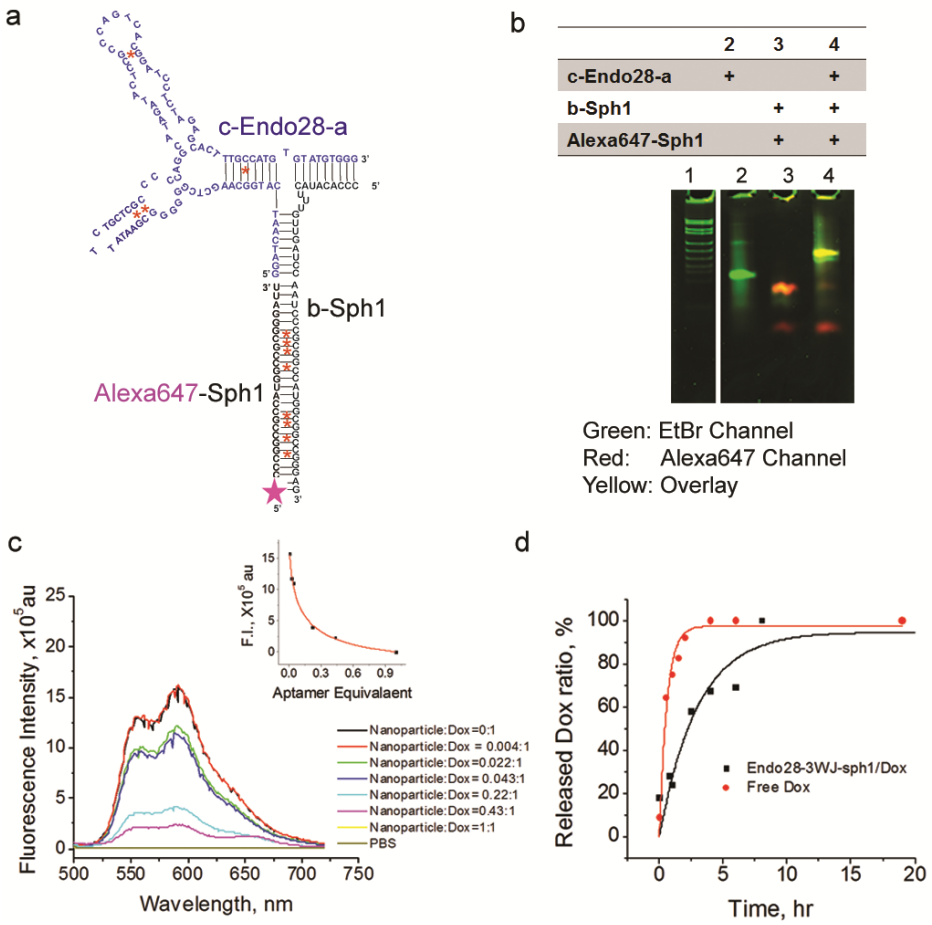

Figure 4.2. Loading doxorubicin into Endo28-3WJ nanoparticles and its *in vitro* release. (a). Secondary structure of Endo28-3WJ-Sph1 nanoparticles forming complex with doxorubicin. Doxorubicin which is shown as red star intercalates into the nanoparticles. (b). Native PAGE test the assembly of Endo28-3WJ-Sph1 nanoparticles, the gel image at EtBr channel is shown as green, at Cy5 channel is shown as red. (c). Fluorescence spectrum showing the intercalation of doxorubicin with Endo28-3WJ-Sph1 nanoparticles, the dissociation constant is calculated from the hill plot as insert. (d). *In vitro* release profile of doxorubicin from the nanoparticle doxorubicin intercalates.

Targeting of Endo28-3WJ nanoparticles to cancer cells in vitro

To test the targeting property of annexin A2 aptamer harboring pRNA-3WJ nanoparticles in cell culture, the fluorescent $Alexa_{647}$ labeled 3WJb 2'F-RNA strand was assembled to Endo28-3WJ nanoparticles allow for tracking of the RNA nanoparticles. The Endo28-3WJ nanoparticles were incubated with several cell lines, which have different level of annexin A2 expression. IGROV-1(214), SKOV-3(215), human microvascular endothelial cells (HMVECad) are tested as annexin A2 positive cells lines, while HEK293T cells are annexin A2 negative and used as a negative control. Following the RNA incubation and washing steps cells were analyzed by flow cytometry to confirm the binding of the Endo28-3WJ nanoparticles. Flow cytometry analysis data showed that Endo28-3WJ has stronger binding to IGROV-1 (71.2 %) than SKOV-3 (51.7 %), while HEK293T showed a very low binding (17.3 %) similar to the non-binding 3WJ RNA controls (**Figure 4.3a**). The result agrees with the annexin A2 expression level in cells as reported (215). The flow cytometry data indicated that after fusing Endo28 aptamer to the 3WJ core structure, the annexin A2 aptamer retained its binding property to annexin A2 on cells after being incorporated into the pRNA-3WJ, which provides a scaffold for building multifunctional nanoparticles, such as include additional sequences for loading drugs.

RNA nanoparticles suitable for targeted therapeutics delivery need to be internalized into their target cells for proper release of therapeutic agents. The entry of the Endo28-3WJ nanoparticles into annexin A2 positive cells including IGROV-1 and SKOV-3 was examined by confocal microscopy, and the annexin A2 low expression HEK293T cells were used as negative controls. After incubating $Alexa_{647}$ labeled

Endo28-3WJ nanoparticles with cells, Endo28-3WJ showed clear internalization to IGROV-1 and SKOV-3 cells; but very little signal was seen on HEK293T cells (**Figure 4.3b**). Additionally, low $Alexa_{647}$ signal was seen around cells for the 3WJ nanoparticles without annexin A2 aptamers (**Figure 4.3b**). These results suggest that Endo28-3WJ nanoparticles enter the cells in an annexin A2 dependent fashion.

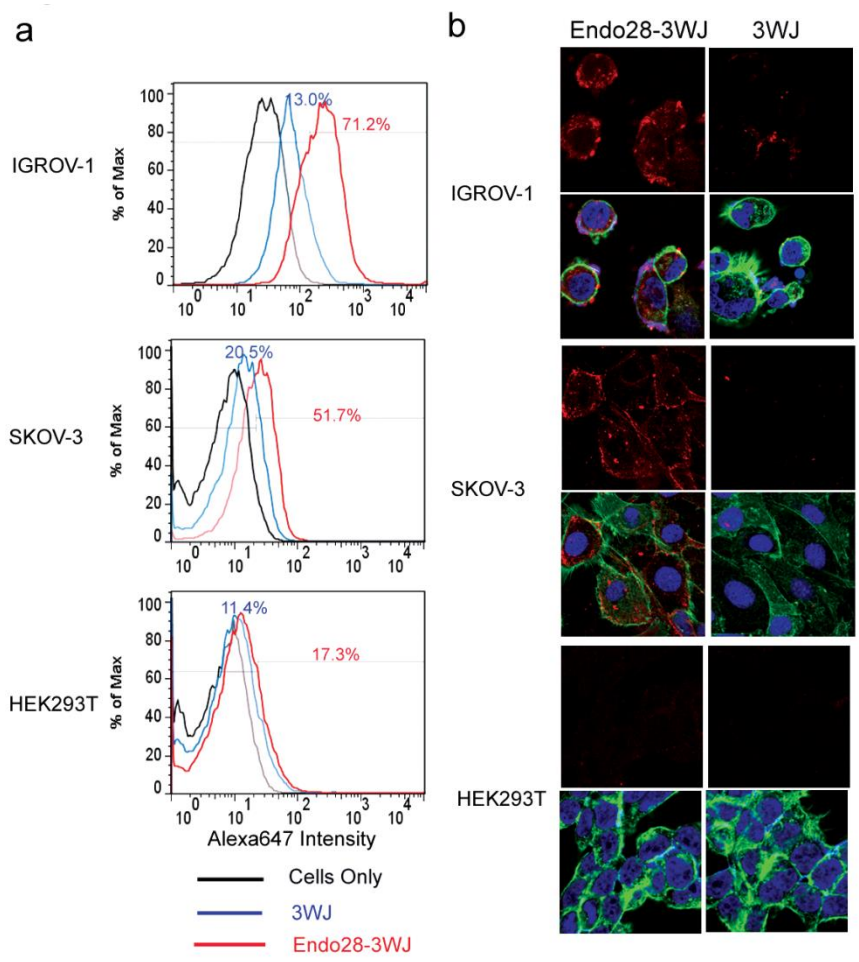

Figure 4.3 The binding and internalization of Endo28-3WJ to annexin A2 positive cells. (a) Flow cytometry test the binding of $Alexa_{647}$ labeled Endo28-3WJ nanoparticles with annexin A2 positive cells (IGROV-1 and SKOV-3), and annexin A2 negative cells (HEK293T). (b) Confocal microscopy test the internalization of $Alexa_{647}$ labeled Endo28-3WJ to annexin A2 positive cells (IGROV-1 and SKOV-3) and annexin A2 negative cells (HEK293T).

Intracellular delivery of doxorubicin to ovarian cancer cells in vitro

To determine if the extended DNA/RNA hybrid nanoparticles Endo28-3WJ-sph1 could deliver doxorubicin to annexin A2 overexpression ovarian cancer cell, confocal microscopy imaging was performed. Both SKOV3 (annexin A2 positive) and HEK293T (annexin A2 negative) cells were incubated with free doxorubicin, Endo28-3WJ-Sph1/Dox or Scr-3WJ-Sph1/Dox RNA nanoparticle conjugates for 8hrs and then analyzed by confocal microscopy. Scr-3WJ-sph1RNA nanoparticle with the similar doxorubicin loading efficiency and also with a pRNA-3WJ core structure was used as negative control. The SKOV-3 cells treated with Endo28-3WJ-Sph1/Dox exhibited strong doxorubicin fluorescence signal similar to free doxorubicin in the confocal microscopy assay. However, when treated with the scramble-3WJ-sph1/Dox intercalates, the cells showed much weaker cellular uptake of doxorubicin (**Figure 4.4d**). The doxorubicin after being released from Endo28-3WJ-sph1/Dox complex was found mostly located in cytoplasm; in contrast, free doxorubicin was located in cell nuclei after the same treatment (**Figure 4.4b**). When incubated with annexin A2 negative HEK293T cells(**Figure 4.4c**), both Endo28-3WJ-sph1/Dox and Scramble-3WJ-sph1/Dox intercalates showed weak uptake (**Figure 4.4g,h**). These results suggest that Endo28-3WJ-sph1/Dox physical conjugates can specifically deliver doxorubicin into annexinA2 positive cell lines.

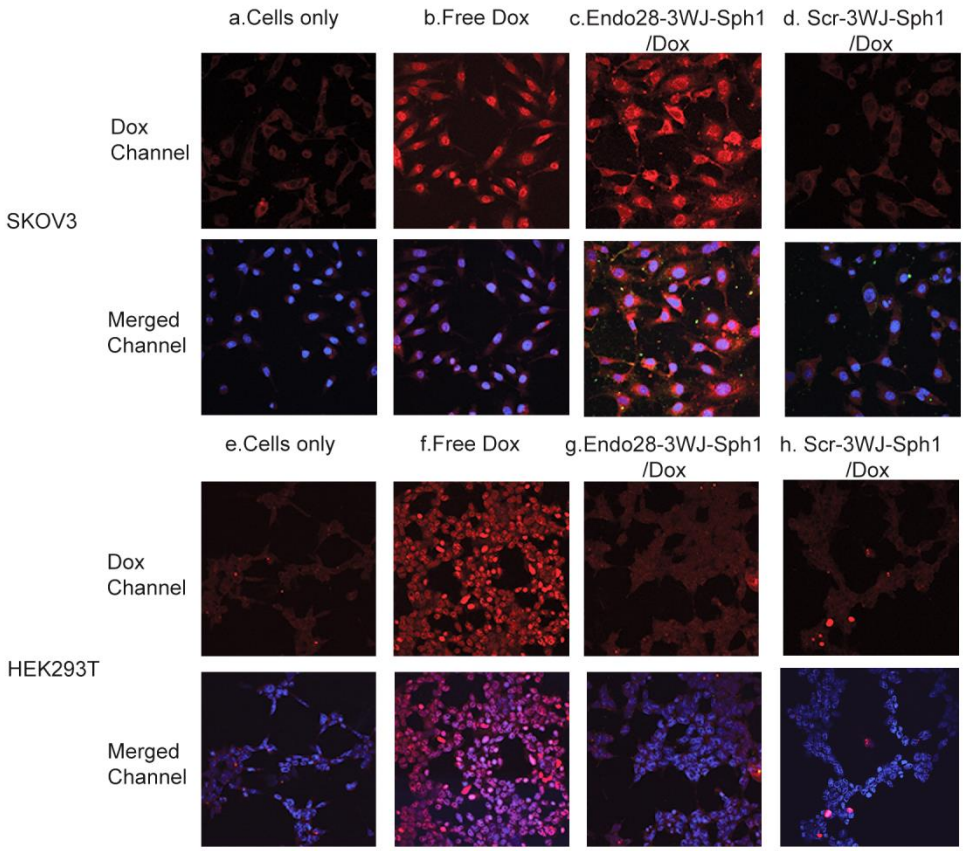

Figure 4.4 *In vitro* delivery of doxorubicin by Endo28-3WJ-Sph1 nanoparticles to cells. Both annexin A2 psotivie SKOV-3 (a-d) and annexin A2 negative HEK293T cells (e-h) were tested. Nanoparticles harboring doxorubicin conjugated with scramble aptamer was tested as negative control (d, h). The cells were treated with nanoparticles for 6hrs and imaged. The doxorubicin channel is shown as red, cell nuclei stained with DAPI is shown as blue. Endo28-3WJ-Sph1 nanoparticles are shown as green.

Effects of Endo28-3WJ-Sph1/Dox conjugate on cell cytotoxicity

Cell cytotoxicity was evaluated with an MTT assay, which monitors cell metabolic activity. The cytotoxicity effect of Endo28-3WJ-Sph1/Dox conjugates was tested with both annexin A2 positive SKOV3 cells and annexin A2 negative HEK293T cells. An equal concentration (3 μM) of doxorubicin from Endo28-3WJ-Sph1/Dox, and controls including Scr-3WJ-Sph1/Dox and free doxorubicin were incubated with cells. Endo28-3WJ-Sph1/Dox showed significantly higher toxicity on SKOV-3 cells than the controls including free doxorubicin and Scr-3WJ-Sph1/Dox conjugates (**Figure 4.5a**). Such a difference in cytotoxicity was not detected with HEK293T cells (**Figure 4.5b**). The results suggest that the Endo28-3WJ-Sph1 nanoparticles are able to deliver doxorubicin selectively to annexin A2 positive cells, and exert its cytotoxicity effect on the targeted cells.

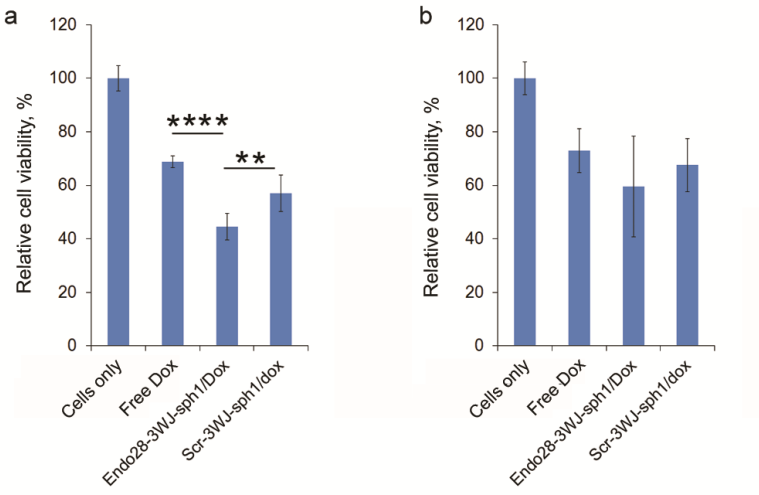

Figure 4.5. Cell cytotoxicity assay for Endo28-3WJ-Sph1/Dox intercalates *in vitro*. (a). Endo28-3WJ-Sph1/Dox showed significantly higher toxicity than the control groups including free doxorubicin and Scr-3WJ-Sph1/Dox on anenxin A2 positive SKOV3 cells. n=3 biological replicates, statistics were calculated using a two sided t-test with center values presented as averages and errors as s.d. p = 1e-4 and 1.5e-3comparing Endo28-3WJ-Sph1/Dox to free doxorubicin and Scr-3WJ-Sph1/Dox respectively. (b) Endo28-3WJ-Sph1/Dox did not show significant difference on toxicity with the control groups including free doxorubicin and Scr-3WJ-Sph1/Dox on anenxin A2 negative HEK293T cells. n = 3 biological replicates, statistics were calculated using a two sided t-test with center values presented as averages and errors as s.d. p = 7.8e-2 and 2.6e-1comparing Endo28-3WJ-Sph1/Dox to free doxorubicin and Scr-3WJ-Sph1/Dox respectively.

Targeting of Endo28-3WJ nanoparticles to cancer cells in vivo

Ovarian cancer xenograft mice model were developed through subcutaneous injection of SKOV-3 cells to female nude mice. Tumors were fully developed after 4 weeks. 100 μL of 10 μmol/L solution of $Alexa_{647}$ labeled Endo28-3WJ nanoparticles were administered to the mice through tail-vein injection. Mice were whole body imaged to monitor the biodistribution of nanoparticles *in vivo* at designed time points. The mice were sacrificed after 6 hours and nanoparticle accumulation in the organs was tested by imaging. $Alexa_{647}$ was detected throughout the whole body of the mice after 30 min of injection indicating nanoparticles successfully circulated through the mice. At early time points, $Alexa_{647}$ signal was detected in the tumor, liver, and bladder of the mice. After 6 hours, fluorescence signal was remained in xenograft tumor, while undetectable in all healthy organs (**Figure 4.6a**). Confocal microscopy imaging of the tumor sections shows specific targeting and accumulation of the Endo28-3WJ nanoparticles to the SKOV3 xenograft tumor, while the control group including 3WJ nanoparticles and PBS showed much lower fluorescent intensity in tumor cells (**Figure4.6b**). The results demonstrated that the 3WJ RNA nanoparticles harboring Annexin A2 aptamer are suitable for targeted *in vivo* drug delivery to cancer cell.

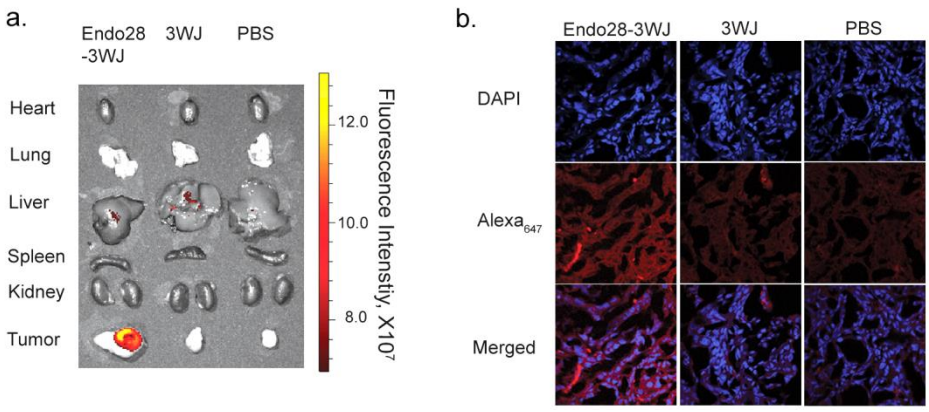

Figure 4.6. *In vivo* targeting of Endo28-3WJ to ovarian cancer xenograft in mice model. (a). Organ image of mice to test the accumulation of $Alexa_{647}$ labeled nanoparticles *in vivo* 6 hr post systemic injection. (b) Confocal microscopy to test the cellular distribution of $Alexa_{647}$-Endo28-3WJ inside the tumor tissue.

CONCLUSION:

Annexin A2, a calcium phospholipid binding protein, has been characterized in many cancer cell activity including cell invasion and metastasis. It is well known that annexin A2 is overexpressed in ovarian cancer cells (203). A DNA aptamer using phosphorothioate-modified DNA nucleotides was generated through SELEX for specific targeting of annexin A2 by Mangana et al. (206). The selected thio-DNA aptamer was placed onto the ultrastable pRNA-3WJ motif, creating a DNA/RNA hybrid nanoparticle that can specifically target and enter ovarian cancer cells. The polyvalence of the pRNA-3WJ scaffold also allowed for harboring of imaging probes for tracking and therapeutics for treatment. By incorporating a GC rich sequence specifically designed for the binding of a chemotherapy drug, doxorubicin, efficient loading of the drug was achieved at around 10 molecules per nanoparticle.

The nanoparticles showed a sustained release profile of doxorubicin, with the drug release reaching 80 % in 6 hours, as compared to naked doxorubicin that reached more than 80 % releasing within only 1 hour. Such sustained release will ensure that majority of the loaded drug will be released after the carrier nanoparticle reaches the targeted tumor site, thus reducing the distribution of toxic chemical drugs to the healthy organs and minimizing the side effect.

Upon confirmation of annexin A2 targeting nanoparticles entering into ovarian cancer cells, and proper loading/releasing profiling of doxorubicin, experiments were expanded to test the delivery of doxorubicin to cancer cells *in vitro*. SKOV-3 cells are known to overexpress annexin A2, and it is also resistant to multiple drugs including doxorubicin. The Endo28-3WJ-Sph1/Dox complex showed significantly higher toxicity

towards SKOV-3 cells than the scramble control and the free doxorubicin. This is possibly caused by changing the drug intracellular trafficking pathway, as confocal image showed that doxorubicin released from Endo28-3WJ-sph1/Dox nanoparticles mainly accumulated in cell cytoplasm, different from the free doxorubicin which was located in cell nuclei.

The *in vivo* biodistribution study showed a promising profiling with accumulation of nanoparticles in tumors, but not healthy organs. Thus using the Endo28-3WJ nanoparticle for cancer cell targeted drug delivery will benefit ovarian cancer patients with reducing the side effect of cancer chemotherapeutics, and increasing its local concentration in tumor microenvironment after systemic administration. Overall, the results demonstrated that stable RNA nanoparticles can be constructed for the specific targeting and treatment of ovarian cancers, expanding the application of RNA nanoparticles for including chemotherapeutic delivery.

RNA nanoparticles were constructed using the pRNA-3WJ core from the phi29 packaging motor to harbor annexin A2 aptamer for delivery of doxorubicin to ovarian cancer cells. The DNA/RNA hybrid nanoparticles were proven to remain chemically and thermodynamically stable for *in vivo* application. The annexin A2-specific nanoparticles produces good binding profiles with ovarian cancer cells at 50 nmol/L RNA and provided specific delivery of doxorubicin to SKOV-3 ovarian cacner cells, with significant higher toxicity than scramble nanoparticle controls. The annexin A2 aptamer harboring nanoparticles also showed specific targeting to ovarian cancer after systemic administration in mouse xenograft, therefor demonstrated great potential as vehicle for targeted drug delivery to treat ovarian cancer.

AKNOWLEDGEMENTS:

This research was supported by NIH grants R01EB003730 and U01CA151648 to P.G. The UK Flow Cytometry & Cell Sorting core facility is supported in part by the Office of the Vice President for Research, the Markey Cancer Center and an NCI Center Core Support Grant (P30 CA177558) to the University of Kentucky Markey Cancer Center. Funding to Peixuan Guo's Sylvan G. Frank Endowed Chair position in Pharmaceutics and Drug Delivery is funded by the C. M. Chen Fundation. PG is a consultant of Oxford Nanopore. His inventions at the University of Kentucky have been licensed to the Matt Holding and RNA Nanobio, Ltd.

copyright © Fengmei Pi 2016

Chapter 5: Discovery of a New Method for Potent Drugs Development Using Power Function of Stoichiometry of Homomeric Biocomplexes or Biological Nanomotors

This chapter was reproduced (with some modification) with permission from Pi F, Vieweger M, Zhao Z, Wang S, and Guo P. "Discovery of a new method for potent drug development using power function of stoichiometry of homomeric biocomplexes or biological nanomotors." Expert Opinion on Drug Delivery, 2016. 13 (1), 23-36. DOI: 10.1517/17425247.2015.1082544. Copyright 2016 Taylor and Francis. Special thanks to Zhengyi Zhao for help in preparation of data for Figures 5.1 and 5.4.

ABSTRACT:

Multi-drug resistance and the appearance of incurable diseases inspire the quest for potent therapeutics. We reviewed a new methodology in designing potent drugs by targeting multi-subunit homomeric biological motors, machines, or complexes with $Z > 1$ and $K = 1$, where Z is the stoichiometry of the target, and K is the number of drugged subunits required to block the function of the complex. The discussed rational behaves similarly to Christmas decorations, where a number of light bulbs are connected in series in an electrical circuit; failure of one bulb results in turn off of the entire lighting system. In most multisubunit homomeric biological systems, a sequential coordination or cooperative action mechanism is utilized, thus K equals 1. Drug inhibition depends on the ratio of drugged to non-drugged complexes. When $K = 1$, and $Z > 1$, the inhibition effect follows a power law with respect to Z, leading to enhanced drug potency. The hypothesis that the potency of drug inhibition depends on the stoichiometry of the targeted biological

complexes has been proved recently using a highly sensitive *in vitro* phi29 viral DNA packaging system. Examples of targeting homomeric bio-complexes with high stoichiometry for drug discovery are discussed. Biomotors with multiple subunits are widespread in viruses, bacteria, and cells, making this approach generally applicable in drug development.

INTRODUCTION :

The continuous escalation of drug resistance has been threatening human health and life, i.e., many microorganisms including bacteria, viruses, and even cancer cells are developing resistance to current chemotherapies. Drug resistance in cancer has partially contributed to ~600,000 deaths in the USA in 2012(216). To combat the on-rising drug resistance, different approaches for developing new drugs have been explored. One method is to develop drugs that target novel mechanisms. Components highly important for cancer cell growth have been explored as drug targets for the treatment of multidrug resistant cancer(217,218). The first FDA-approved drug to treat multidrug-resistant tuberculosis, bedaquiline, follows a novel mechanism of inhibiting the bacterial ATP synthase of M. tuberculosis and other mycobacterial species(219). Another approach is to use nano-drug carriers to enhance the binding efficiency of drugs to cancer cells(220-223). A third approach is to develop new combinational drugs acting on multiple targets to enhance its efficacy (224,225), including cocktail therapy(226). This involves identifying multiple targets that when treated simultaneously lead to a synergetic therapeutic effect and optimizing the design of multi-target ligands(227). Still, there is unmet need for treating multi-drug resistant disease. Thus, new approaches for drug development are needed to combat drug resistance.

A new hypothesis that potent drugs can be developed by targeting proteins or RNA complexes with high subunit stoichiometry was reported recently(228). The major challenge for testing this hypothesis is to evaluate the significance of the target stoichiometry and the binding affinity of the drug molecule with respect to its efficacy. In order to quantitatively correlate the drug inhibitory efficacy to the stoichiometry of the target biocomplexes, a well-studied multicomponent system is required, which allows an empirical comparison of functional inhibition efficiency of individual components with different numbers of subunits.

The DNA packaging motor of bacteriophage phi29 was an ideal model for testing this theory. The morphology and stoichiometry of the individual components in the phi29 DNA packaging motor have been well studied. The Phi29 biomotor (**Figure 5.1a**) is composed of three essential, co-axially stacked rings(34,229-231): a dodecameric connector ring located at the vertex of the viral procapsid; a hexameric packaging RNA (pRNA) ring bound to the N-terminus of the connector(34,232), and a hexameric ring of ATPase gp16 attached to the helical region of pRNA(233-235). The stoichiometry of pRNA was first determined using Yang Hui's Triangle (or binomial distribution) in 1997(236), and similar mathematical methods were applied to determine the stoichiometries of the protein subunits (229). Furthermore, dsDNA packaging utilizes a revolution mechanism without rotation to translocate its genomic DNA powered through the hydrolysis of ATP(234,235,237-242). The copy number of ATP molecules required to package one full Phi29 genomic dsDNA has been predicted to be 10,000(234,235,237-241,243). Phi29 DNA packaging, thus, offers an ideal platform to test the novel concept

described above: the dependence of the inhibitory drug efficiency on the stoichiometry of its targeted biocomplex.

Although the theory of targeting multisubunit complexes for developing potent drugs was reported and validated recently(228), real cases of targeting multisubunit complex for new drug development have been practiced(244-246). Since multicomponent biomotors are widely spread in nature(240,241,247,248), the approach of targeting multisubunit complexes for potent drug development discussed here is generally applicable, especially in developing new generations of drugs for combating the rising acquired drug resistance in viruses, bacteria, and cancers (249-251).

5.1 Rationale for selection of multi-subunit biocomplexes as efficient drug targets

Inhibitory drugs are typically designed to bind selectively to a target site, thereby blocking the site from interaction with other biomolecules leads to the loss of essential activity of the biological target. This target can be a single element, composed of only one subunit, or a complex consisted of multiple subunits, such as the biomotors of the hexameric ASCE (Additional Strand Catalytic E) superfamily(234,252). Conventional drugs are designed to inhibit pathogenesis through targeting of a single subunit molecule, such as an enzyme or a structural protein of a virus. As discussed below, the key in designing potent drugs lies in targeting multisubunit biological motors, machines, or complexes as drug targets that follow a sequential coordination or cooperative mechanism. The stoichiometry of the complex, Z, is larger than 1 and the number of drugged subunits that are required to block the activity of the target complex, K, equals 1 ($Z > 1$ and $K = 1$). Similar to in-series connected decorative Christmas lights, where one broken light bulb will turn off the entire chain, one drugged subunit will inhibit the entire

complex and therefore biological activity. Sequential action or cooperativity in multisubunit complexes has been widely reported in biological systems(253-257); inhibiting any subunit leads to inhibition of the entire complex, or in other words K equals 1.

For a conventional drug that inhibits its single subunit target (Z = 1) with efficiency p, the fraction of undrugged target molecules q will be 1-p; and those undrugged target molecules will remain active to maintain their biological function. In this situation, the inhibition efficiency is proportional to the substrate targeting efficiency p(253-255). When targeting a dimeric complex (Z = 2), for example, inactivating any subunit results in inhibition of the whole complex. For a drug targeting a dimeric complex with substrate targeting efficiency p = 0.9 (90 %), only 10 % of the first subunit and 10 % of the second subunit remain active after drug targeting. Thus, the fraction of undrugged complexes will be effectively reduced to 0.01, leaving 1 % of complexes active. Since drug inhibition depends on the ratio of drugged to undrugged complexes, the efficiency of the inhibition is proportional to the product of the inhibition of the individual subunits, in other words, it follows a power law with respect to Z.

Consequently, a complex composed of Z subunits with the smallest number of blocked subunits (K) to inhibit activity of the complex is 1, when *p* percent of subunits are interacting with the drugs, the fraction of uninhibited biocomplexes will be q^z and the proportion of inhibition equals $1 - q^Z$.

5.1.1 Drug inhibition efficiency predicted by binomial distribution model

The scenario outlined above follows a binomial distribution which can hence be used to outline the relation between drug inhibition efficiency and target stoichiometry in

general. When the target element is a monomer, the inhibition efficiency can be calculated using *Equation 1*, where *p* and *q* are the fractions of drugged (substrate targeting efficiency) and undrugged (normal active elements) subunits, respectively (p + q = 1).

$$X = (p + q)^1 \quad (1)$$

However, when the target element contains multiple subunits, a higher order binomial distribution (Equation 2) is required to calculate the ratio of active complexes, where Z represents the total number of subunits (the stoichiometry) and M the number of drugged subunits in one biocomplex.

$$X = (p+q)^Z = \sum_{M=0}^{Z} \binom{Z}{M} p^{Z-M} q^M = \sum_{M=0}^{Z} \left(\frac{Z!}{M!(Z-M)!} \right) p^{Z-M} q^M \quad (2)$$

The probability of drugged subunits (M) and undrugged subunits (N; M + N = Z) in any given biocomplex can be determined by the expansion of Equation 2. When Z = 3, The expanded form of Equation 2, $(p+q)^3 = p^3 + 3p^2q + 2pq^2 + q^3 = 1$, displays the probabilities of all possible combinations of drugged and undrugged subunits of a homoternary complex composed of three (p^3), two (p^2q), one (pq^2), or no (q^3) drugged subunits; the sum equals 1. Assuming that 70 % (p = 0.7) of subunits are inactivated by bound drugs leaving 30 % (q = 0.3) unaffected, then the percentage of complexes possessing at least two copies of normal subunits would be the sum of those possessing one copy of drugged and two copies of undrugged *wild-type* subunits, $3pq^2$, and those possessing three copies of native subunits is q^3, i.e., $3pq^2 + q^3 = 3(0.7)(0.3)^2 + (0.3)^3 = 0.216$. In another example, if a complex contains 6 subunits, and biological activity requires 5 out of the 6 subunits to remain uninhibited, the fraction of active complexes in

the total population equals the sum of probabilities of obtaining: 1) 5 and 2) 6 undrugged subunits.

Using the binomial distribution, the probabilities that a population contains any combination of undrugged *versus* drugged subunits can be predicted. The effect of the targeting efficiency p on the probability of obtaining a given complex with M drugged and N undrugged subunits is displayed in Table 1. The probabilities are calculated using equation 2, $\frac{Z!}{M!N!}p^M q^N$, with the coefficients $\frac{Z!}{M!N!}$ obtained from Yang Hui's Triangle, which is also called Pascal's Triangle, or binomial distribution (**Figure 5.1b**)(258). The use of Yang Hui's Triangle and binomial distribution to determine the stoichiometry of biological motor was published in Guo Lab in 1997(236,259) for RNA component and restated in 2014 for protein component(229) in phi29 DNA packaging motor.

5.1.2 Cooperativity in multisubunit biocomplexes leads to high inhibition efficiency

The cooperativity of multisubunit biocomplexes is the key to high drug inhibition efficiency. Cooperativity means that multiple subunits work sequentially or processively to accomplish one essential biological reaction (237,254-256,260-264). Blocking any subunit of the complex inhibits the activity of the whole complex. Many reactions involving multiple subunits work cooperatively, e.g. assembly pathways in viral assembly systems (253,265). An analogy to such a biological reaction mechanism is given by the difference between parallel and series circuits. When a chain of light bulbs is arranged in a parallel circuit, burning out one light bulb will not affect others, while in a series circuit, breaking any one light bulb turns off the entire lighting system. The *K* value, the smallest number of subunits that needs to be inhibited in order to inhibit function of the light chain is therefore, $K = 1$. Thus, the *K* value is a key factor in

estimating the probability of obtaining inactive nanomachines or biocomplexes by combination and permutation of all subunits.

$K = 1$ is critical for obtaining ultrahigh inhibition. The foundation of the approach in this report is the difference in inhibition probability for biocomplexes with the same ratio of drugged target subunits but different K values. Biological systems display complicated reactions that involve several steps and multiple components interacting in series or parallel. Based on the binomial math model and cooperative nature of biological reactions, we suggest that targeting of multi-subunit biocomplexes can serve as a tool to develop highly potent drugs. In a conventional six-component system, when one drug is designed to target only the component #3 to stop the entire system, such a condition resembles the model in equation 2 with $Z = 1$ and $K = 1$. Thus, the inhibition efficiency is linear to the substrate targeting efficiency (p) of the drug. However, in a homohexameric component system, the entire complex is blocked when a drug targets any subunit of the hexamer, which resembles $Z = 6$ and $K = 1$. Thus, the probability of active target complexes equals q^6 ($q = 1 - p$). In other words, the drug inhibition efficiency is equal to $1-q^6$, which scales with the 6^{th} power of q compared to linearly with q as for conventional mono-subunit approaches (see Table 2).

Targeting a biological complex that exhibits a higher stoichiometry substantially reduces the fraction of non-inhibited complexes. K=1 implies that drug binding to one subunit inactivates the subunit, in which one drugged subunit is sufficient to inhibit the function of the entire complex. As an example, a probability calculation for $Z = 6$ and $K = 1$ is given below. As all 6 ($Z = 6$) copies of the subunits are required for function, while one drugged subunit ($K = 1$) is sufficient to block the activity, all elements possessing 1

through 5 copies of drugged subunits are non-functional (**Figure 5.1c**). Only those complexes possessing 6 copies of undrugged subunits are functional. The probability that a complex contains 6 copies of unaffected subunits is q^6 and therefore the inhibition efficiency is $1-q^6$ (227,237,253,260,265,266).

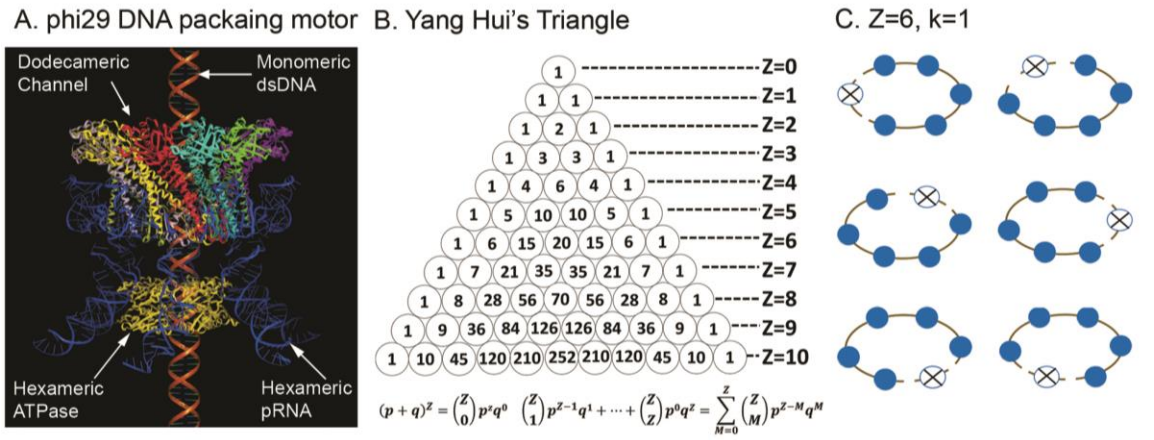

Figure 5.1. The morphology and stoichiometry of Phi29 DNA packaging motor. (a) Illustration of Phi29 DNA packaging motor composed of 1 copy of genomic DNA through a channel composed of three coaxil rings, a 12 subunit connector, 6 subunit pRNA, 6 subunit ATPase gp16. (b) Bionomial distribution equation with its coefficient displayed by Yang Hui Triangle. (c) Illustration of Z = 6 and K = 1, drug targeting any subunit of a hexameric complex would block its function. Adapted from ref.(228) with permission.

Table 2. Probability of obtaining complexes containing M copies of drugged and N copies of undrugged subunits

Inhibited Subunits (*p*)	Z=1		Z=6						
	M=0, N=1	M=1, N=0	M=0, N=6	M=1, N=5	M=2, N=4	M=3, N=3	M=4, N=2	M=5, N=1	M=6, N=0
0%	100%	0%	100%	0%	0%	0%	0%	0%	0%
10%	90%	9%	53%	35%	10%	1%	0%	0%	0%
20%	80%	16%	26%	39%	25%	8%	2%	0%	0%
30%	70%	21%	12%	30%	32%	19%	6%	1%	0%
40%	60%	24%	5%	19%	31%	28%	14%	4%	0%
50%	50%	25%	2%	9%	23%	31%	23%	9%	2%
60%	40%	24%	0%	4%	14%	28%	31%	19%	5%
70%	30%	21%	0%	1%	6%	19%	32%	30%	12%
80%	20%	16%	0%	0%	2%	8%	25%	39%	26%
90%	10%	9%	0%	0%	0%	1%	10%	35%	53%
100%	0%	0%	0%	0%	0%	0%	0%	0%	100%

Consequently, for a drug with binding efficiency p, a larger stoichiometry of the target complex substantially increases the inhibition efficiency. To illustrate, we compare the fraction of non-inhibited complexes for $Z = 6$ and $Z = 1$, while keeping $q = 0.4$ and $K=1$ fixed for both target systems. The fraction of non-inhibited complexes for Z = 1 amounts to $q^Z = 0.4^1 = 0.4$, resulting in 1-0.4 = 60 % of inhibited complexes. In contrast, for $Z=6$, the fraction of non-inhibited complexes is $q^Z = 0.4^6 = 0.0041$ and therefore 1-0.0041 = 99.59 % of complexes are inhibited. The ratio of the remaining non-inhibited complexes (0.4/0.0041 = 98) shows a 98-fold decrease in non-inhibited complexes for $Z = 6$ compared to $Z=1$. At a targeting efficiency of $p=0.9$, the inhibition efficiency for $Z = 6$ is $1-q^Z = 1-0.1^6 = 0.999999$ resulting in a 10,000-fold increased inhibition efficiency compared to Z = 1 ($0.1/0.1^6 = 10^5$, see Table 1). The binomial distribution indicates that the inhibitory effect follows a power law with respect to the stoichiometry of the target. Thus, for $K = 1$, the fraction of uninhibited biocomplexes equals q^z; the larger Z, the smaller q^z, (as $0 < q < 1$). That is to say when developing drugs with the same binding affinity to their targets, the higher the stoichiometry of its multimeric target, the fewer uninhibited targets will remain and the more efficient the drug will be.

5.1.3 IC_{50} decreases as the stoichiometry of target complexes increases

The half maximal inhibitory concentration (IC_{50}) is one parameter used to evaluate drug efficacy. It quantitatively indicates how much of a particular drug is required to reduce the activity of a given biological process by half. It is universally used as a measurement of drug potency in pharmacological research. The median lethal dose LD_{50}, also known as 50 % of lethal concentration, is an important parameter to evaluate the safety profile, i.e., acute toxicity of a drug. Most importantly, a larger ratio of LD_{50} to $IC_{50,}$ results in a safer drug. By increasing the inhibition efficiency through targeting components with high stoichiometry, the effective drug dosage is greatly decreased, thus decreasing the IC_{50}. As a result, the ratio of LD_{50} to IC_{50} increases, resulting in an enlarged therapeutic window of the drug.

If we denote P_{IC50} as the percentage of drugged subunits needed to reach 50% inhibition, then $1-(1-p_{IC50})^{Z}=50\%$ Solving this equation, $p_{IC50}=1-0.5^{1/Z}$. **Figure 5.2** shows the relationship between stoichiometry (Z) and drug targeting level *p* to reach the inhibition effect (IC), where *p* is a combined result of drug binding efficacy and drug concentration (dosage). When the stoichiometry *Z* of the multimeric drug target increases, the dosage of drug to reach IC_{50}, IC_{20}, or IC_{80} decreases, presented by the percentage of drugged subunits. This clearly shows that as *Z* increases, p_{IC50} decreases, and hence the drug is more potent.

Focusing on the stoichiometry of the target complex for drug development differs from conventional approaches. Conventional drug molecules are sought to have a high binding affinity to the target, which means we expect more drug molecules to bind to one

target molecule. Here stoichiometry refers to the copy number of subunits within a biocomplex or nanomachine that serves as the drug target. This idea agrees with a newer model for predicting clinical drug efficacy, the receptor occupancy. Receptor occupancy acts as a predictor for human pharmacodynamics and antihistamine potency and takes into account both the affinity of the drug for its receptor and its free plasma concentration (267).

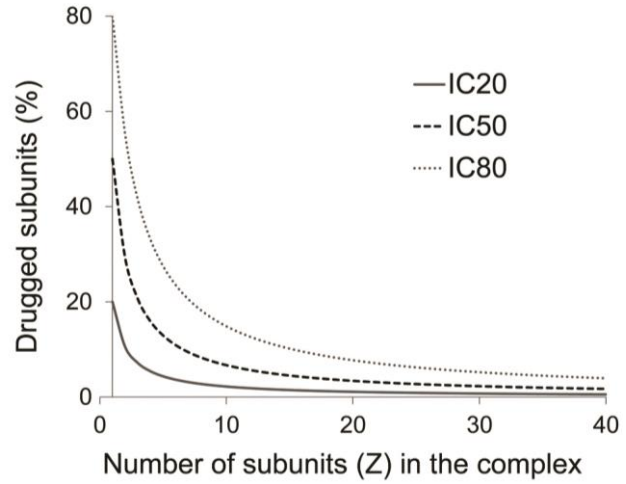

Figure 5.2. The relationship between the stoichiometry of homomeric target complex (Z) and target complex inhibition effect (IC). Adapted from ref.(228) with permission .

5.2 Inhibition efficiency as a power function of target stoichiometry proved by Phi29 viral assembly system

The hypothesis that drug inhibition efficiency follows a power function with respect to the target stoichiometry has been proved using the Phi29 viral assembly system (268). This well-defined *in vitro* assembly system is composed of four components, each of which is comprised of different subunits that can act as the nano-machine target. Inhibition of viral assembly is achieved using mutant components that represent drugged target components. The inhibition efficiencies were analyzed with Yang Hui's triangle for targeting each of the Phi29 DNA packaging motor components. Binomial distribution analysis of these viral assembly competition assays confirmed the concept that drug targeting biological complexes with higher stoichiometry results in a higher efficiency than drugs acting on a single subunit target.

The highly sensitive *in vitro* Phi29 assembly system was used to determine the inhibition efficiency of drugs targeting multi-subunit complexes (236,253,259,269), thus validating a new method for developing potent drugs. The bacteriophage Phi29 DNA packaging motor contains one copy of genomic dsDNA, 6 copies of packaging RNA, 6 copies of ATPase protein gp16, and consumes more than 10,000 copies of ATP during genome packaging. The hexameric stoichiometry of Phi29 pRNA has been extensively shown using single-molecule techniques(268), AFM imaging(47,48), pRNA crystal structure determination(184), and statistical evaluations(236). The hexameric stoichiometry of Phi29 gp16 has been proved by native gel binding, capillary electrophoresis assays, Hill constant determination, and by titration of mutant subunits using binomial distribution(234,237). The copy number of ATP molecules was calculated

based on the fact that 6 ATP molecules are required to package one pitch of dsDNA containing 10.5 base pairs (270), thus one ATP is used to package 1.7 base pairs of dsDNA. The entire Phi29 genome is composed of 19,400 base pairs, thus, it is expected that more than 10,000 ATP molecules are required to package an entire Phi29 genome. The availability of a motor system with multiple well-defined and characterized components makes an ideal disease model for the analysis of drug inhibition efficiency versus the subunit stoichiometry of individual subcomponents within the same assay.

Inhibition efficiencies were determined for ATP, pRNA, ATPase gp16, and DNA as drug targets with stoichiometries of 10,000, 6, 6, and 1, respectively. Among these components, targeting of ATP showed the strongest inhibition, while drugged mutant pRNA and mutant gp16 still showed stronger inhibitory effects than mutant DNA (**Figure 5.3)**. For example, adding 20 % mutant DNA caused 20 % inhibition of viral assembly, while 20 % of drugged mutant pRNA exerted 74 % of inhibition on viral assembly and 20 % of γ-S-ATP almost completely inhibited the viral assembly, indicating that higher stoichiometry results in stronger inhibition efficacy.

The target with ten-thousand-subunits showed higher inhibition than those with six subunits, which in turn showed higher inhibition than the single subunit target. In conclusion, these results show that inhibition efficiency displays a power function with respect to the stoichiometry of the target biocomplexes. Drug inhibition potency depends on the stoichiometry of the targeted components of the biocomplex or nano-machine. Since bio-motors share certain common structural and operational mechanisms across viruses, bacteria, and other cells, this approach has general application in drug development.

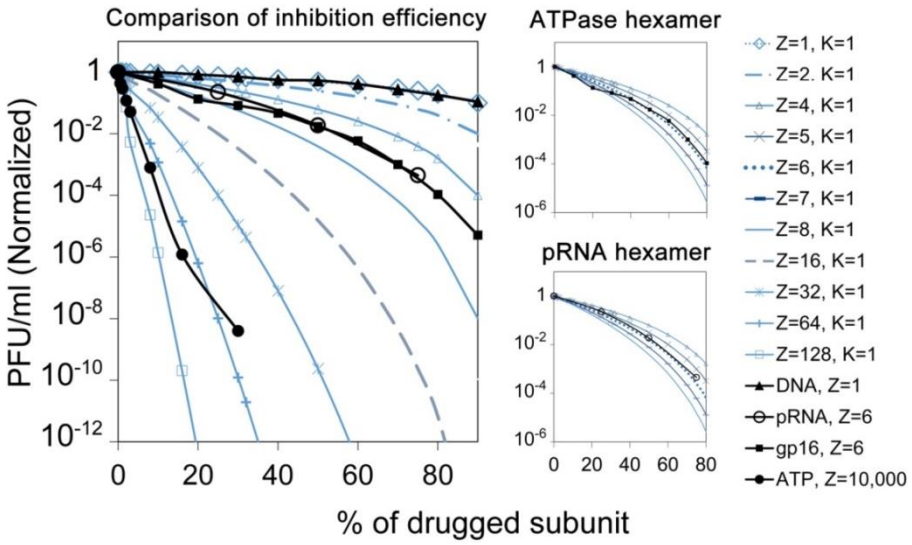

Figure 5.3. Comparing Phi29 viral assembly inhibition efficiency by targeting components with different stoichiometry. Components in the system with different stoichiometries were tested as drug targets (left pannel): DNA with stoichiometry of 1, ATPase gp16 with stoichiometry of 6 (right upper pannel), pRNA with stoichiometry of 6 (right lower pannel), and ATP with stoichiometry of 10,000. Adapted from ref.(228) with permission.

5.3 Wide-spread distribution of biomotors with multiple subunits or high order stoichiometry

Biological systems contain a wide variety of nanomachines with highly ordered stoichiometry that are essential for DNA replication, DNA repair(271), homologous recombination, cell mitosis, bacterial binary fission, Holliday junction resolution(272), viral genome packaging(273), RNA transcription, nuclear pore transport, as well as motion, trafficking, and exportation of cellular components. Here we use biological motors as an example to elucidate the rationale of $Z > 1$ and $K = 1$. These biological motors can generally be classified into three categories according to their DNA transportation mechanism: linear motors, rotation motors and the newly discovered revolution motors(237,241,248). High order stoichiometries are wildly observed among biomotors, especially in rotation and revolution motors. Thus, biomotors are feasible targets for the development of potent inhibitory drugs that exploit the power law behavior of the subunit stoichiometry.

5.3.1 Rotation nanomachines

FoF1 ATP synthase and helicases are representatives of rotary motors (274,275). FoF1 ATP synthase is a ubiquitous membrane enzyme that plays a key role in biological energy metabolism (276,277). It consists of two linked rotary motors, F1 and Fo, which are distinct in structure and function. F1 ATPase, forming the catalytic core, shows strong ATP hydrolysis activity. It is composed of 5 subunits ($\alpha_3\beta_3\gamma_1\delta_1\varepsilon_1$), with three α and three β subunits forming a hexameric ring with part of a long coiled coil γ subunit. Fo is the proton pore that is embedded in the membrane, it consists of at least 3 subunits ($a_1b_1c_{8\text{-}15}$) whereby subunit c differs among species.

Helicase DnaB is a hexameric nanomachine (**Figure 5.4a**) that unwinds dsDNA in front of the replication fork during DNA replication(278,279). Recently, a hand-over-hand translocation mechanism was proposed for DnaB based on the crystal structure of the DnaB hexamer complexed with ssDNA and GDP-AIF4 (280). In this mechanism, the 5'-3' translocation of the subunits at a stepsize of two nucleotides is coupled with the sequential hydrolysis of NTP (281). The sequential hand-by-hand migration of the individual subunits results in DNA translocation.

RecA, a family of ATP-dependent recombinases, plays an important role in dsDNA repair and genetic recombination in Archaea, Bacteria, and Eukaryota. It can interact with ssDNA forming right-handed helical filaments as a complex with approximately six monomers of RecA per turn (**Figure 5.4b**)(282,283). Electron microscopy studies have demonstrated that ATP binding induces a re-orientation between the RecA ATPase domains, resulting in the relative rotation of the protein on DNA substrate during DNA translocation powered by ATP hydrolysis.

5.3.2 Revolution nanomachines

All the dsDNA viruses known to date utilize similar mechanisms to transport their genome into preformed protein shells during replication. For example, Bacteriophage phi29, HK97, SPP1, P22, and T7 all share a common revolution mechanism for dsDNA packaging that employ a hexameric ATPase and predominantly dodecameric connector channels for packaging dsDNA. The phi29 DNA packaging motor is composed of three coaxial rings: a dodecameric channel ring and an ASCE hexameric ATPase linked by a hexameric ring of pRNA (**Figure 5.4c**)(184,234,268). During genome packaging, more

than 10,000 ATP molecules are consumed by the hexameric ATPase as energy source to drive the translocation of one copy of the dsDNA genome(270).

The ASCE superfamily, including FtsK-HerA superfamilies and the AAA+ (ATPases associated with diverse cellular Activities), is a clade of nanomachines that display a hexameric arrangement(284-287) of subunits. Their biological function is to convert chemical energy from ATP into mechanical motion(234,243,288,289), typically associated with conformational changes of the ATPase enzyme (234,290,291).

FtsK belongs to the ASCE superfamily. It is a multi-domain protein composed of a C-terminal ATPase domain FtsK(C) containing α, β and γ sub-domains, an N-terminal membrane-spanning domain FtsK(N) and a 600-amino acid linker(292-294). It is responsible for conjugation between bacterial cells and dsDNA bidirectional translocation(295,296). It has been proposed that FtsK subunits acts in a sequential manner employing a revolution mechanism to translocate dsDNA(297,298). The crystal structure and electron microscopy of FtsK(C) demonstrates formation of a ring-like hexamer with DNA passing through the hexameric ring (**Figure 5.4d**)(298,299).

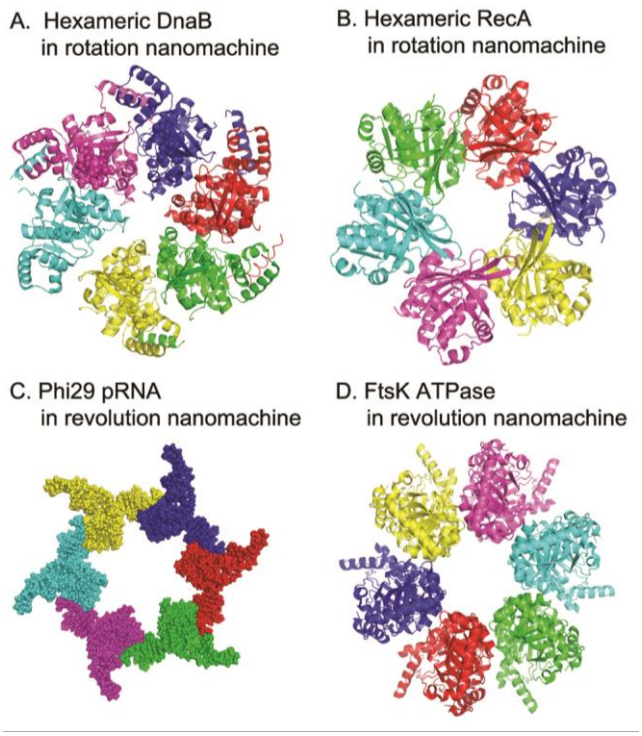

Figure 5.4. Widespread biomotors or nanomachines are composed of multisubunit complex. (A) Rotation nanomachine DnaB helicase is a hexamer (280) (PDB ID: 4ESV), (B) rotation nanomachine RecA motor protein is a hexamer (283) (PDB ID: 1N03), (C) revolution Phi29 DNA packaging motor contains a hexameric pRNA (184), (D) revolution DNA motor protein FtsK is a hexamer (298) (PDB ID: 2IUU).

5.4 Targeting biocomplexes for developing potent drugs

As illustrated above, drug efficiency follows a power function of the stoichiometry of the subunits of the multimeric target biocomplex. Targeting biocomplexes with higher stoichiometry therefore can lead to the development of more potent drugs. Experimentally, approaches targeting receptor dimers, hetero- and homo-oligomers for drug screening open exciting possibilities for drug discovery and development(300).

5.4.1 Targeting homomeric channel proteins for drug development

In the history of drug development, one important property of most channel protein receptors has been overlooked, their stoichiometry. As a matter of fact, many channel proteins are expressed as dimers or oligomers on cell membrane, including most G-Protein-Coupled Receptors (GPCR) proteins (300). Targeting of GPCR hetero- and homo- oligomers is generally starting to be considered for drug development. Therefore, new models for multisubunit protein binding are being developed(300). Cooperative binding affinity between ligand and multisubunit targets has been reported and cooperativity factors were calculated by fitting to the Hill equation(237,300).

The ATP-sensitive homotrimeric P2X7 receptor (P2X7R) acts as a ligand-gated ion channel. It forms a chalice-like channel with three ATP binding sites localized at the interface of the three subunits. Occupancy of at least two of the three sites is necessary for activation of the receptors which results in opening of the channel pore allowing passage of small cations (Na^+, Ca^{2+}, and K^+). P2X7R has received particular attention as a potential drug target for its widespread involvement in inflammatory diseases and pivotal roles in central nervous system (CNS) pathology (244). These concepts will

broaden the therapeutic potential of drugs that target multi-subunit channel proteins, including receptor heteromer-selective drugs with a lower incidence of side effects. They will also help to identify novel pharmacological profiles using cell models that express heteromeric receptors.

5.4.2 Targeting homomeric enzyme for antibiotics development

Targeting of key enzymes in essential biosynthesis pathways is an important approach for antibiotics development. Many key proteins in the fatty acid synthesis pathway and nucleotide synthesis pathway are found to be multivalent. The highly ordered oligomeric enzymes in biosynthesis pathways could be promising targets for developing more potent antibacterial drugs. Some examples of developing potent drugs by targeting multisubunit biocompelxes are discussed below.

Fatty acid synthesis is an essential lipogenesis process in both Gram-positive and Gram-negative bacteria. A key enzyme in the fatty acid biosynthesis pathway is fatty acid biosynthesis 1 (FabI), which is a homotetramer complex acting as the major enoyl-ACP reductase present in burkholderia pseudomallei (Bpm). A recent X-ray structure study revealed the binding mode of the inhibitor PT155 with the homo-tetrameric BpmFabI (245) (**Figure 5.5a**). The substrate BpmFabI is a homo-tetramer, one PT155 molecule bound to each monomeric subunit has shown significant promise for antibacterial drug development(245). Another example of targeting multisubunit biocomplex as drug target is found in the guanine nucleotide biosynthesis pathway to control parasitic infection. Inosine 5'-monophosphate dehydrogenase (IMPDH) is a homo-tetramer enzyme(246)(**Figure 5.5b**), which plays an important role by catalyzing the oxidation of IMP to XMP in guanosine monophosphate(GMP) biosynthesis(246).Structural

characterization of IMPDH with chemical inhibitor drugs indicates that binding to the repeating units shows a more potent inhibition effect(301).

These examples of successfully targeted homotetramer enzymes for potent drug development further proved the importance of the stoichiometry of target homo-meric complexes. When applying this method to search enzymes as drug targets, it is critical to test whether the stoichiometry of the complexes (Z) is > 1, and the number of subunits needed to inhibit to block biological function (K) equals 1.

5.4.3 Targeting homomeric drug transporters for drug development

The mechanism of drug transporter, very similar to that of the revolution motor, involves entropy induced transitions by ATP. High stoichiometry of the target complex is a key consideration in drug efficiency. Targeting multidrug efflux transporters with high stoichiometry has a better chance to develop drugs for treating multi-drug resistant disease. The structure of bacterial multidrug efflux transporter AcrB is composed of three alpha-helix subunits, that connect to form a funnel around a central cavity (**Figure 5.5c**)(302). The multidrug exporter MexB from Pseudomonas aeruginosa also forms a homotrimer (**Figure 5.5d**)(303). Pyridopyrimidine derivatives have been reported to be promising drugs to treat multidrug resistant pathogens by specific inhibition of the homotrimeric AcrB and MexB transporters[117]. The structural architecture of ABC transporters consists minimally of two TMDs and two NBDs. These four individual polypeptide chains combine to form a full transporter such as in the E. coli BtuCD(304). Although the stoichiometry of the heterodimer is not very high, the stoichiometry of ATP per transporter is high. It is involved in the uptake of vitamin B12.

The TMDs of ModBC-A and MalFGK2-E have six helices per subunit. These unique structural features can be used in target considerations.

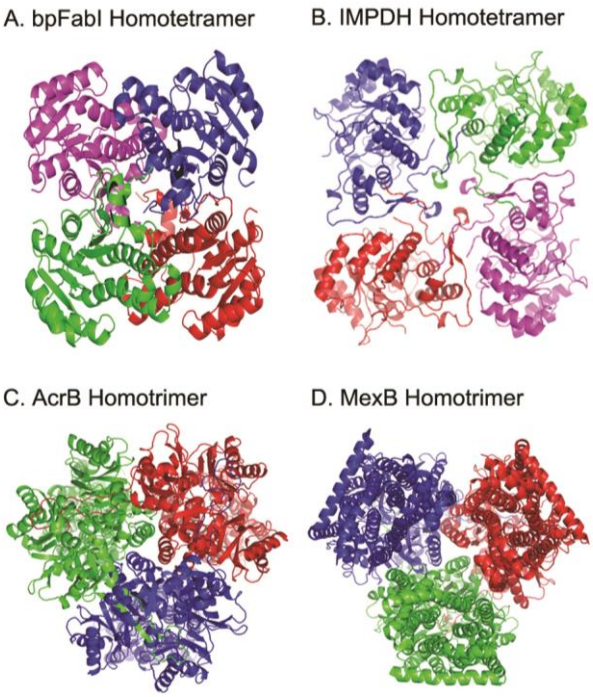

Figure 5.5. Examples of homomeric multisubunit complex as drug target for developing potent drugs. (A) Tetrameric bpFabI is a key enzyme in fatty acid synthesis in bacterial, inhibitor PT155 forms a tetrameric complex with BpmFabI (245) (PDB ID: 4BKU). (B) Inosine monophosphate dehydrogenase (IMPDH) (246) (PDB ID: 1AK5) is a key enzyme in guanine nucleotide biosynthesis pathway, inhibitors have been developed targeting the tetrameric IMPDH. (C) Bacterial multidrug efflux transporter AcrB forms a homotrimer(302)(PDB ID: 1IWG). (D) Multidrug exporter MexB from Pseudomonas aeruginosa forms a homotrimer(303)(PDB ID: 2V50).

CONCLUSION AND FUTURE PERSPECTIVE

Targeting functional biological units with higher stoichiometries allows for higher inhibition efficiencies. The inhibition efficacy follows a power law with respect to the subunit copy number when targeting multimeric biocomplex, compared to a linear effect of the drug-target binding affinity when targeting a single-subunit substrate. This new concept outlined herein suggests that potent drugs can be developed by targeting biocomplexes with high stoichiometries with the potential of complete inhibition of the targets activity. Possibly, this method can further be applied to guide development of dominant negative proteins for potent gene therapy, which can be incorporated into a multimeric protein nanomachine and results in a change of its activity (305). Since bio-motors share certain common structural and operational mechanisms across viruses, bacteria, and cells, this approach has general applicability in drug development.

Living systems contain many elegant arrays, motors and nanomachines that are composed of multiple identical subunits. As reported here, these homomeric biocomplexes can serve as potent drug targets. For example, most members of the ASCE family are hexamers(234,306-310). As these machines are common among living systems, specificity and toxicity need to be considered. In the development of anti-bacterial and anti-viral drugs, specificity and toxicity is not problematic since the target biocomplexes differ from those found in human cells and thus all targets are intended to be killed nonexclusively. In the development of anti-cancer drugs, mutations in multiple-subunit biocomplexes of cancer cell will present ideal targets for potent drug development.

Drug discovery is a multidisciplinary science including the fields of medicine, biotechnology and pharmacology. Aiming to find a method for developing drugs with ultra-high potency, much effort has been placed in the screening of new drug compounds, uncovering of new drug targets, and illumination of functional pathways, but little attention has been paid to the exploration of new methods for the design and development of more efficient drugs. Here we propose that the inhibition efficiency of a given drug depends on the stoichiometry of the biocomplex or bio-machine that serves as drug target. Here the notion of "stoichiometry" differs from the conventional concept in drug development. Conventionally, stoichiometry refers to the number of drug molecules bound to each substrate or cell membrane. In the current study stoichiometry refers to the number of identical subunits that the target biocomplex is composed of. Phi29 viral components with a series of variable but known stoichiometries were evaluated as mock drug targets to test the hypothesis. Both *in vitro* and *in vivo* virion assembly assays were employed to compare inhibition efficiencies for targets with differing subunit stoichiometries. Viral inhibition efficiency was analyzed with Yang Hui's (Pascal's) Triangle (also known as binomial distribution) (**Figure 5.1**), as shown in equation 2.

It was observed that inhibition efficiency of virus replication correlates with the stoichiometry of the drug target. The inhibition efficacy follows a power law behavior where the percentage of uninhibited biocomplexes equals q^Z (see equation 2). For a system with fixed q and K values, the inhibition efficiency thus depends on Z, the number of subunits within the target biocomplex or bio-machine. This hypothesis is supported by empirical data that a target with ten-thousand-subunits shows higher inhibition effect than a target with six subunits, which in turn shows higher inhibition than a single-subunit

target (**Figure 5.3**). The unconventional hypothesis described in this article for the development of potent drugs with power function behavior with respect to the target stoichiometry can be foreign or even outlandish to the main force of the pharmaceutical field. The approach of developing highly potent drugs through targeting of protein, RNA or other macromolecule complexes with high stoichiometry has never been reported due to challenges to prove the concept.

Traditionally, it is almost impossible to prove this concept by comparing efficacies of two drugs where one of them targets a biocomplex with multiple subunits. When reporting the efficiency of this new approach, it is very difficult to distinguish essentiality of the two targets in biological function; it is also very challenging to compare the binding affinity of two different drugs to two different targets. For instance, if two drugs target two stoichiometrically different complexes, it becomes extremely difficult to prove whether the difference in drug efficiency is due to differences in their target binding affinity or essential level of the target in the biological organism.

The mechanism of drug inhibition mainly relies on blocking an essential biological target element from functioning. The target elements can be monomers or a complex of multiple homosubunits; such as the biomotors of the hexameric ASCE superfamily(234,252). Conventional drugs are designed to target a single subunit molecule to inhibit pathogenesis, such as an enzyme or a structural protein of a virus. The key in designing potent drugs is to target multi-subunit biological motors, machines, or complexes with $Z > 1$ and $K = 1$, where Z is the stoichiometry of the complex and K is the number of drugged subunit that are required in order to block the function of the

entire complex. Similarly, in a series circuit Christmas decorative light chain, one broken light bulb will turn off the entire lighting system.

In most, if not all, multi-subunit biological systems, sequential coordination or cooperative action mechanisms are utilized, thus, *K* equals 1. Drug inhibition depends on the ratio of drugged to the non-drugged complex. For $K = 1$, and $Z > 1$, inhibition efficacy follows a power function with respect to *Z*, leading to an increased potency of the drug since inhibition of any subunit results in complete inhibition of activity. For a drug designed to target a single-subunit molecule at targeting efficiency *p*, the fraction of undrugged target molecules q that will remain active is *1- p*. In this situation, the inhibition efficiency is proportional to the substrate targeting efficiency *p* and the inhibition efficacy is of the first order of *p*. Sequential action or cooperativity in multi-subunit complexes has widely been reported in biological systems(253-255). Drugs targeting a complex with multiple subunits can inhibit the complex activity if any homosubunit of the target is inactivated. Thus, if the copy number of this cooperative complex is $Z > 1$, and the least number of blocked subunit to inhibit complex activity (K) is 1, the fraction of uninhibited biocomplexes is q^Z, and the inhibition efficiency is $1 - q^Z$, where 1- q is the portion of drugged subunits.

The binomial distribution analysis allows prediction of the inhibition efficiencies. For example, in targeting a six-subunit biocomplex with K = 1, the inhibition efficiency is determined by drug binding to any one of the six homosubunits. Therefore, the probability of inhibiting any subunit at random position is $\frac{1-q^6}{1-q}$ times higher than inhibiting a monomer substrate. With this new elucidation and understanding of the

concepts behind targeting of cooperative multi-homosubunit complexes, a new generation of potent drugs may emerge in the near future.

Our discovery is an approach, not a drug. This approach will have general impact in the development of drugs for many diseases such as cancer, viral or bacterial infections. In living systems, biological machines or complexes with high stoichiometry and operated by sequential cooperative action or coordination with $Z > 1$ and $K = 1$ are ubiquitous. This class of biological machines is involved in many aspects of crucial cellular processes to the survival of viruses, bacteria, and eukaryotic cells. For example, multi-subunit biomotors are involved in chaperon, ATPase, ATP synthase, cell mitosis, bacterial binary fission, DNA replication, DNA repair, homologous recombination, Holliday junction resolution, nuclear pore transportation, RNA transcription, drug transporters, muscle contraction, viral genome packaging, as well as motion, trafficking, and exportation of cellular components. These systems use a sequential mechanism similar to the serial circuit of the Christmas decoration lighting chain. Thus, our approach will have broad application in drug development in many biological systems. Drugs targeting to these motors will be highly efficient.

Biomotors belonging to the multi-subunit ATPase are widely spread in organisms, including bacteria, viruses and cancer cells. Successful implementation of this new methodology will lead to the development of the next generation of potent drugs. In fact the first drug approved to treat multidrug-resistant tuberculosis, bedaquiline (219), is acting on the ATP synthase which is a multisubunit biomotor (311-322). Treating multidrug-resistant tuberculosis had been very challenging previously. Although this drug's inventors were not aware of the concept of targeting multisubunit complexes for

potent drug development, the success in this drug conquering the tough Mycobacterium tuberculosis organism supports the concept of using the multisubunit complex as a potent drug target. Cancer or bacterial mutant multi-subunit ATPase can be used as target. The drug developers can simply check the published literature and identify a multi-subunit machine as the drug target. For cancer treatment, it is to find a multi-subunit machine with mutation.

The concept of K = 1 for high efficiency inhibition may be impactful in gene or protein therapy. By introducing the dominant negative protein(305) or inactive mutant protein into the cell, either by intracellular expression or direct introduction of proteins, which resembles the above illustrated approach and mechanism used for phi29 DNA packaging motor systems (228,229,259,323)(**Figure 5.3**). This involves the incorporation of mutant proteins, either intracellularly expressed or directly introduced, into a highly multimeric complex that is identified as the target unit. For purposes of serving as a small molecule drug target, a multimeric complex might be identified, such that binding of one drug molecule to any one binding site on the complex will inactivate the whole complex. The fact that the complex composed of Z subunits holding one drugged subunit will only come into play as the drug concentration is at the high end. However, if the strategy was to express a dominant negative protein, as has been done in recent cardiac gene therapy with dominant negative phospholamban(305), a high inhibition efficacy will achieve. The greater the value of Z the more the effect of the dominant negative protein subunit or mutant subunit will be achieved.

Another possibility is the use of homomeric drug transporters (324,325) as drug targets (see section 5.3). The mechanism of drug transporters is very similar to that of the

revolution motor featuring an entropy transition induced by ATP. High stoichiometry of target complex is a key consideration for achieving high drug efficiency. Targeting multidrug efflux transporters with high stoichiometry has a better chance to develop drugs for treating multi-drug resistant disease.

While the hypothesis behind this method might theoretically seem challenging, elucidation of the mechanism should greatly facilitate application of this approach. Two factors are essential for drugs development: efficiency and specificity. The strategy described herein focuses on drug efficiency, while specificity is similar to the general consideration in the development of chemicals and drugs. Nevertheless, design of potent drugs to common machines or general targets is still possible. For example, if an oncogenic mutant hexameric ATPase is found in one specific type of cancer cells, drugs targeting to this mutation of the altered ATPase will not only be highly efficient but also specific.

ACKNOWLEDGEMENT

P Guo was supported by NIH grants NIH/R01 EB012135 and NIH/U01 CA151648. P Guo's Endowed Chair in Nanobiotechnology position is funded by the William Fairish Endowment Fund. P Guo is a co-founder of Biomotor and RNA Nanotech Development Co. Ltd. The authors have no other relevant affiliations or financial involvement with any organization or entity with a financial interest in or financial conflict with the subject matter or materials discussed in the manuscript apart from those disclosed.

Chapter 6: Future Direction and Current State of the Field

CONCLUSIONS AND FUTURE DIRECTION:

In this thesis work is described for the advancement of the RNA nanotechnology towards therapeutically application. The main advantage of using RNA nanoparticles for drug delivery remains in: 1. RNA nanoparticles functioned with nucleic acid based aptamers can exert active targeting effect; 2. nucleic acid based therapeutics can be easily conjugated to RNA nanoparticles and processed by dicer *in vivo* for siRNA and miRNA release. Here in Chapter 2 of this dissertation, the development of bivalent 2'F-RNA aptamer against cancer stem cell marker EpCAM was explored. By using previously developed stable pRNA-3WJ motif as the core structure for constructing the divalent RNA antibody library, and 2'-fluoro modifications on RNAs, a highly stable 2'F-RNA aptamer against EpCAM was selected. The selected aptamer mimics antibody can specifically deliver LNA based anti-miR21 to EpCAM positive cancer cells and knock down miR21 levels in cancer cells. In Chapter 3 I explored utilizing the special orientation of pRNA-3WJ to display RNA aptamers on the membrane surface of extracellular vesicles. Taking the advantage that EVs are natural carrier for small RNAs, and that RNA aptamers can recognize cancer cell marker and specifically target cancers, the PSMA aptamer displaying EVs were tested as carrier for delivery therapeutic siRNA to treat cancer. Results showed that the PSMA aptamer displaying EVs can deliver survivin siRNA into prostate cancer cells *in vitro* and *in vivo*, and achieve very significant effect in inhibiting xenograft prostate cancer growth in mice after multi-dose treatment. In chapter 4 I explored the possibility of utilizing nanoparticle functionalized

with aptamer against Annexin A2 to deliver doxorubicin to ovarian cancer cells. The nanoparticles are optimized by elongating with GC rich dsRNA sequences to enhance the doxorubicin loading efficiency. The nanoparticle doxorubicin intercalates have uniform particle size around 8nm, and showed sustained release profile for doxorubicin *in vitro*. They can deliver doxorubicin specifically to annexin A2 positive ovarian cancer cells cytoplasm *in vitro*, and also showed targeting effect to subcutaneous xenograft ovarian tumor in mice after systemic injection *in vivo*. All these results suggest the nanoparticles harboring an aptamer are promising candidates for targeted delivery of chemical drugs to treat cancer disease.

However, in order to fully prove the potential of the selected bivalent EpCAM RNA aptamer for cancer treatment, future work is need. While it is proven that the bivalent EpCAM aptamer A9-8 can bind to cancer cells and deliver anti-miR21 to cancer cells *in vitro, in vivo* experiments should also be conducted to better evaluate the functionality of this aptamer. Bio-distribution of fluorescent labeled EpCAM aptamer, as well as the treatment effect of EpCAM aptamer harboring anti-miR21 on proper mice model with subcutaneous tumor xenografts should be tested. For the newly developed platform of utilizing orientation of pRNA-3WJ to control the display of RNA aptamers on exosome surface, further experiments including exploring more advanced RNA nanoparticle structures with lipid chemical modification to display ligands on exosomes should be performed, the possibility of using aptamer displaying EVs for chemical drug, miRNA, and mRNA delivery should also be explored. In order to fully prove the potential of annexin A2 aptamer harboring nanoparticles for cancer specific doxorubicin

delivery, *in vivo* treatment experiment should also be conducted with proper mice model. Further development of RNA nanoparticles into clinical trials should be considered.

CURRENT STATE OF THE FIELD:

Since the development of RNA nanotechnology in 1998 (34), the field has been making great progress towards clinical application. The discovery of pRNA-3WJ provided a platform to build thermodynamically stable multifunctional RNA nanoparticles for therapeutics delivery. 2'F pyrimidine modification on RNA nanoparticles make them resistant to nuclease. RNA nanoparticles functionalized with aptamers or chemical ligand(49,66) can recognize their specific target; and the nanometer scaled size of RNA nanoparticles further enhanced their tumor targeting efficiency through EPR effect. Recently, RNA nanoparticles have been developed into vehicles for delivering anti-microRNA(52,66), siRNAs(50,51) to cancer cells. Doxorubicin, the anthracycline chemical drug can be easily loaded into the RNA nanoparticle through intercalating into GC pairs. In the future, more sophisticated RNA nanoparticles will be designed for controlled gene therapy and chemotherapy delivery. Multifunctional RNA nanoparticles may also help to avoid the on rising multidrug resistance problem as they can change the drug cell entry pathways (173).

The design of antibody shaped RNA library opened a new field for RNA antibody development. Previously libraries for aptamer selection are designed to have a single random region with 20 to 50 nucleotides; while this Y shaped RNA library containing two random regions to enhance its binding affinity and specificity. The selected aptamers can be directly fused with siRNA or miRNA sequences on the third arm for various *in vitro* and *in vivo* applications. Except for drug delivery, RNA antibodies can be

developed as new drugs for therapeutically application. The advantage of developing RNA nanoparticle based therapeutics include: they can be developed *in vitro*, can be designed to control its immunogenicity (54), can be batch produced as chemical drugs and quality controlled.

Current popular EV engineering method is to co-express peptide or protein ligand onto EV membranes during its biogenesis. This method faces the challenge of the integrity of expressed ligand after EV secretion(326). Decorating EVs with cholesterol modified RNA nanoparticles provides a new method to engineer EVs for targeted drug delivery. This system takes the advantages of both extracellular vesicles for RNAi delivery and also RNA nanoparticles for specific cancer cell targeting. More research on this topic includes how to stabilize the association of RNA-cholesterol with EVs membranes, how to use EVs for other gene therapeutics delivery such as miRNA, mRNA and protein, as well as large scale production of high quality EVs.

After around two decades of growth, the field of RNA nanotechnology has conquered lots of hurdles. With the continuous researching on this area, we wish this field can grow forward towards industrial and clinical application.

Copyright © Fengmei Pi 2016

REFERENCE

1. Bharali DJ & Mousa SA (2010) Emerging Nanomedicines for Early Cancer Detection and Improved Treatment: Current Perspective and Future Promise. *Pharmacol. Ther.* 128: 324-335

2. Park K (2007) Nanotechnology: What It Can Do for Drug Delivery. *J Control Release* 120: 1-3

3. Park HH, Jamison AC, & Lee TR (2007) Rise of the Nanomachine: the Evolution of a Revolution in Medicine. *Nanomedicine. (Lond)* 2: 425-439

4. Shu Y, Pi F, Sharma A, Rajabi M, Haque F, Shu D, Leggas M, Evers BM, & Guo P (2014) Stable RNA Nanoparticles As Potential New Generation Drugs for Cancer Therapy. *Adv. Drug Deliv. Rev.* 66C: 74-89

5. Lukyanov AN, Gao Z, & Torchilin VP (2003) Micelles From Polyethylene Glycol/Phosphatidylethanolamine Conjugates for Tumor Drug Delivery. *J Control Release* 91: 97-102

6. Kabanov AV, Batrakova EV, & Alakhov VY (2002) Pluronic Block Copolymers As Novel Polymer Therapeutics for Drug and Gene Delivery. *J Control Release* 82: 189-212

7. Danilo D.Lasic (1997) *Liposomes in gene delivery*, CRC Press LLC.

8. Bianco A, Kostarelos K, & Prato M (2005) Applications of Carbon Nanotubes in Drug Delivery. *Curr. Opin. Chem Biol* 9: 674-679

9. Smith AM, Duan H, Mohs AM, & Nie S (2008) Bioconjugated Quantum Dots for in Vivo Molecular and Cellular Imaging. *Adv. Drug Deliv. Rev.* 60: 1226-1240

10. Lee T, Yagati AK, Pi F, Sharma A, Choi J-W, & Guo P (2015) Construction of RNA-Quantum Dot Chimera for Nanoscale Resistive Biomemory Application. *ACS Nano* 9: 6675-6682

11. Boisselier E & Astruc D (2009) Gold Nanoparticles in Nanomedicine: Preparations, Imaging, Diagnostics, Therapies and Toxicity. *Chem Soc Rev.* 38: 1759-1782

12. Gadde S & Rayner KJ (2016) Nanomedicine Meets MicroRNA: Current Advances in RNA-Based Nanotherapies for Atherosclerosis. *Arterioscler. Thromb. Vasc. Biol* 36: e73-e79

13. Peer D (2014) Harnessing RNAi Nanomedicine for Precision Therapy. *Mol Cell Ther.* 2: 5

14. Tam YY, Chen S, & Cullis PR (2013) Advances in Lipid Nanoparticles for SiRNA Delivery. *Pharmaceutics* 5: 498-507

15. Lv H, Zhang S, Wang B, Cui S, & Yan J (2006) Toxicity of Cationic Lipids and Cationic Polymers in Gene Delivery. *J. Control Release* 114: 100-109

16. Villares GJ, Zigler M, Wang H, Melnikova VO, Wu H, Friedman R, Leslie MC, Vivas-Mejia PE, Lopez-Berestein G, Sood AK, & Bar-Eli M (2008) Targeting Melanoma Growth and Metastasis With Systemic Delivery of Liposome-Incorporated Protease-Activated Receptor-1 Small Interfering RNA. *Cancer Res* 68: 9078-9086

17. Weinstein S & Peer D (2010) RNAi Nanomedicines: Challenges and Opportunities Within the Immune System. *nanotechnology* 21: 232001

18. Peer D (2010) Induction of Therapeutic Gene Silencing in Leukocyte-Implicated Diseases by Targeted and Stabilized Nanoparticles: a Mini-Review. *J Control Release* 148: 63-68

19. Davis ME, Zuckerman JE, Choi CH, Seligson D, Tolcher A, Alabi CA, Yen Y, Heidel JD, & Ribas A (2010) Evidence of RNAi in Humans From Systemically Administered SiRNA Via Targeted Nanoparticles. *Nature* 464: 1067-1070

20. Song E, Zhu P, Lee SK, Chowdhury D, Kussman S, Dykxhoorn DM, Feng Y, Palliser D, Weiner DB, Shankar P, Marasco WA, & Lieberman J (2005) Antibody Mediated in Vivo Delivery of Small Interfering RNAs Via Cell-Surface Receptors. *Nat Biotechnol.* 23: 709-717

21. McNamara JO, Andrechek ER, Wang Y, Viles KD, Rempel RE, Gilboa E, Sullenger BA, & Giangrande PH (2006) Cell Type-Specific Delivery of SiRNAs With Aptamer-SiRNA Chimeras. *Nat Biotech* 24: 1005-1015

22. Nakamura Y, Mochida A, Choyke PL, & Kobayashi H (2016) Nanodrug Delivery: Is the Enhanced Permeability and Retention Effect Sufficient for Curing Cancer? *Bioconjug. Chem*

23. Danquah MK, Zhang XA, & Mahato RI (2011) Extravasation of Polymeric Nanomedicines Across Tumor Vasculature. *Adv. Drug Deliv. Rev.* 63: 623-639

24. Marcucci F & Corti A (2012) How to Improve Exposure of Tumor Cells to Drugs: Promoter Drugs Increase Tumor Uptake and Penetration of Effector Drugs. *Adv. Drug Deliv. Rev.* 64: 53-68

25. Sato K, Watanabe R, Hanaoka H, Harada T, Nakajima T, Kim I, Paik CH, Choyke PL, & Kobayashi H (2014) Photoimmunotherapy: Comparative Effectiveness of Two Monoclonal Antibodies Targeting the Epidermal Growth Factor Receptor. *Mol Oncol.* 8: 620-632

26. Guo P (2010) The Emerging Field of RNA Nanotechnology. *Nature Nanotechnology* 5: 833-842

27. Duckett DR & Lilley DM (1990) The Three-Way DNA Junction Is a Y-Shaped Molecule in Which There Is No Helix-Helix Stacking. *EMBO J* 9: 1659-1664

28. Eckardt LH, Naumann K, Pankau WM, Rein M, Schweitzer M, Windhab N, & von KG (2002) DNA Nanotechnology: Chemical Copying of Connectivity. *Nature* 420: 286

29. Rothemund PWK (2006) Folding DNA to Create Nanoscale Shapes and Patterns. *Nature* 440: 297-302

30. Li J, Pei H, Zhu B, Liang L, Wei M, He Y, Chen N, Li D, Huang Q, & Fan CH (2011) Self-Assembled Multivalent DNA Nanostructures for Noninvasive Intracellular Delivery of Immunostimulatory CpG Oligonucleotides. *ACS Nano* 5: 8783-8789

31. Hamblin GD, Carneiro KM, Fakhoury JF, Bujold KE, & Sleiman HF (2012) Rolling Circle Amplification-Templated DNA Nanotubes Show Increased Stability and Cell Penetration Ability. *J Am. Chem Soc* 134: 2888-2891

32. Mei Q, Wei X, Su F, Liu Y, Youngbull C, Johnson R, Lindsay S, Yan H, & Meldrum D (2011) Stability of DNA Origami Nanoarrays in Cell Lysate. *Nano Lett* 11: 1477-1482

33. Hahn J, Wickham SF, Shih WM, & Perrault SD (2014) Addressing the Instability of DNA Nanostructures in Tissue Culture. *ACS Nano* 8: 8765-8775

34. Guo P, Zhang C, Chen C, Trottier M, & Garver K (1998) Inter-RNA Interaction of Phage Phi29 PRNA to Form a Hexameric Complex for Viral DNA Transportation. *Mol. Cell.* 2: 149-155

35. Hendrix RW (1998) Bacteriophage DNA Packaging: RNA Gears in a DNA Transport Machine (Minireview). *Cell* 94: 147-150

36. Smith JB, Miesbauer LR, Leeds J, Smith DL, Loo JA, Smith RD, & Edmonds CG (1991) Mass Spectrometric Analysis of Lens B-Crystallins. *Int J Mass Spectrom.* 111: 229-245

37. Shaw BR, Moussa L, Sharaf M, Cheek M, & Dobrikov M (2008) Boranophosphate SiRNA-Aptamer Chimeras for Tumor-Specific Downregulation of Cancer Receptors and Modulators 3. *Nucleic Acids Symp. Ser. (Oxf)* 655-656

38. Liu J, Guo S, Cinier M, Shlyakhtenko LS, Shu Y, Chen C, Shen G, & Guo P (2011) Fabrication of Stable and RNase-Resistant RNA Nanoparticles Active in Gearing the Nanomotors for Viral DNA Packaging. *ACS Nano* 5: 237-246

39. Helmling S, Moyroud E, Schroeder W, Roehl I, Kleinjung F, Stark S, Bahrenberg G, Gillen C, Klussmann S, & Vonhoff S (2003) A New Class of Spiegelmers Containing 2'-Fluoro-Nucleotides. *Nucleosides Nucleotides Nucleic Acids* 22: 1035-1038

40. Luy B & Marino JP (2001) Measurement and Application of 1H-19F Dipolar Couplings in the Structure Determination of 2'-Fluorolabeled RNA. *J. Biomol. NMR* 20: 39-47

41. Reif B, Wittmann V, Schwalbe H, Griesinger C, Worner K, JahnHofmann K, Engels JW, & Bermel W (1997) Structural Comparison of Oligoribonucleotides and Their 2'-Deoxy-2'-Fluoro Analogs by Heteronuclear NMR Spectroscopy. *Helvetica Chimica Acta* 80: 1952-1971

42. Boulme F, Freund F, Moreau S, Nielsen P, Gryaznov S, Toulme JJ, & Litvak S (2003) Modified (PNA, 2'-O-Methyl and Phosphoramidate) Anti-TAR Antisense Oligonucleotides As Strong and Specific Inhibitors of in Vitro HIV-1 Reverse Transcription. *Nucelic Acids Research* 26: 5492-5500

43. Shu D, Shu Y, Haque F, Abdelmawla S, & Guo P (2011) Thermodynamically Stable RNA Three-Way Junctions for Constructing Multifuntional Nanoparticles for Delivery of Therapeutics. *Nature Nanotechnology* 6: 658-667

44. Binzel DW, Khisamutdinov EF, & Guo P (2014) Entropy-Driven One-Step Formation of Phi29 PRNA 3WJ From Three RNA Fragments. *Biochemistry* 53: 2221-2231

45. Chen C, Zhang C, & Guo P (1999) Sequence Requirement for Hand-in-Hand Interaction in Formation of PRNA Dimers and Hexamers to Gear Phi29 DNA Translocation Motor. *RNA* 5: 805-818

46. Shu Y, Cinier M, Fox SR, Ben-Johnathan N, & Guo P (2011) Assembly of Therapeutic PRNA-SiRNA Nanoparticles Using Bipartite Approach. *Molecular Therapy* 19: 1304-1311

47. Shu Y, Haque F, Shu D, Li W, Zhu Z, Kotb M, Lyubchenko Y, & Guo P (2013) Fabrication of 14 Different RNA Nanoparticles for Specific Tumor Targeting Without Accumulation in Normal Organs. *RNA* 19: 766-777

48. Shu Y, Shu D, Haque F, & Guo P (2013) Fabrication of PRNA Nanoparticles to Deliver Therapeutic RNAs and Bioactive Compounds into Tumor Cells. *Nat Protoc*. 8: 1635-1659

49. Rychahou P, Haque F, Shu Y, Zaytseva Y, Weiss HL, Lee EY, Mustain W, Valentino J, Guo P, & Evers BM (2015) Delivery of RNA Nanoparticles into Colorectal Cancer Metastases Following Systemic Administration. *ACS Nano* 9: 1108-1116

50. Cui D, Zhang C, Liu B, Shu Y, Du T, Shu D, Wang K, Dai F, Liu Y, Li C, Pan F, Yang Y, Ni J, Li H, Brand-Saberi B, & Guo P (2015) Regression of Gastric Cancer by Systemic Injection of RNA Nanoparticles Carrying Both Ligand and SiRNA. *Scientific reports* 5: 10726

51. Lee TJ, Haque F, Shu D, Yoo JY, Li H, Yokel RA, Horbinski C, Kim TH, Kim S-H, Nakano I, Kaur B, Croce CM, & Guo P (2015) RNA Nanoparticles As a Vector for Targeted SiRNA Delivery into Glioblastoma Mouse Model. *Oncotarget* 6: 14766-14776

52. Binzel D, Shu Y, Li H, Sun M, Zhang Q, Shu D, Guo B, & Guo P (2016) Specific Delivery of MiRNA for High Efficient Inhibition of Prostate Cancer by RNA Nanotechnology. *Molecular Therapy* 24: 7: 1267-1277

53. Haque F, Shu D, Shu Y, Shlyakhtenko L, Rychahou P, Evers M, & Guo P (2012) Ultrastable Synergistic Tetravalent RNA Nanoparticles for Targeting to Cancers. *Nano Today* 7: 245-257

54. Khisamutdinov E, Li H, Jasinski D, Chen J, Fu J, & Guo P (2014) Enhancing Immunomodulation on Innate Immunity by Shape Transition Among RNA Triangle, Square, and Pentagon Nanovehicles. *Nucleic Acids Res.* 42: 9996-10004

55. Jasinski D, Khisamutdinov EF, Lyubchenko YL, & Guo P (2014) Physicochemically Tunable Poly-Functionalized RNA Square Architecture With Fluorogenic and Ribozymatic Properties. *ACS Nano* 8: 7620-7629

56. Li H, Zhang K, Pi F, Guo S, Shlyakhtenko L, Chiu W, Shu D, & Guo P (2016) Controllable Self-Assembly of RNA Tetrahedrons With Precise Shape and Size for Cancer Targeting. *Adv. Mater.* In press. DOI: 10.1002/adma.201601976.

57. Khisamutdinov EF, Jasinski DL, Li H, Zhang K, Chiu W, & Guo P (2016) Fabrication of RNA 3D Nanoprism for Loading and Protection of Small RNAs and Model Drugs. *Advanced Materials* In press

58. Horiya S, Li X, Kawai G, Saito R, Katoh A, Kobayashi K, & Harada K (2003) RNA LEGO: Magnesium-Dependent Formation of Specific RNA Assemblies Through Kissing Interactions. *Chem Biol* 10: 645-654

59. Geary C, Rothemund PW, & Andersen ES (2014) A Single-Stranded Architecture for Cotranscriptional Folding of RNA Nanostructures. *Science* 345: 799-804

60. Nasalean L, Baudrey S, Leontis NB, & Jaeger L (2006) Controlling RNA Self-Assembly to Form Filaments. *Nucleic Acids Res.* 34: 1381-1392

61. Li H, Lee T, Dziubla T, Pi F, Guo S, Xu J, Li C, Haque F, Liang X, & Guo P (2015) RNA As a Stable Polymer to Build Controllable and Defined Nanostructures for Material and Biomedical Applications. *Nano Today* 10: 631-655

62. Afonin KA, Bindewald E, Yaghoubian AJ, Voss N, Jacovetty E, Shapiro BA, & Jaeger L (2010) In Vitro Assembly of Cubic RNA-Based Scaffolds Designed in Silico. *Nat. Nanotechnol.* 5: 676-682

63. Afonin KA, Grabow WW, Walker FM, Bindewald E, Dobrovolskaia MA, Shapiro BA, & Jaeger L (2011) Design and Self-Assembly of SiRNA-Functionalized RNA Nanoparticles for Use in Automated Nanomedicine. *Nat. Protoc.* 6: 2022-2034

64. Afonin KA, Viard M, Kagiampakis I, Case CL, Dobrovolskaia MA, Hofmann J, Vrzak A, Kireeva M, Kasprzak WK, & KewalRamani VN (2014) Triggering of RNA Interference With RNA–RNA, RNA–DNA, and DNA–RNA Nanoparticles. *ACS Nano* 9 (1): 251-259

65. Zhou J, Shu Y, Guo P, Smith D, & Rossi J (2011) Dual Functional RNA Nanoparticles Containing Phi29 Motor PRNA and Anti-Gp120 Aptamer for Cell-Type Specific Delivery and HIV-1 Inhibition. *Methods* 54: 284-294

66. Shu D, Li H, Shu Y, Xiong G, Carson WE, Haque F, Xu R, & Guo P (2015) Systemic Delivery of Anti-MiRNA for Suppression of Triple Negative Breast Cancer Utilizing RNA Nanotechnology. *ACS Nano* 9: 9731-9740

67. Davis S, Lollo B, Freier S, & Esau C (2006) Improved Targeting of MiRNA With Antisense Oligonucleotides. *Nucleic Acids Res* 34: 2294-2304

68. Gold L (1995) The SELEX Process: a Surprising Source of Therapeutic and Diagnostic Compounds. *Harvey Lect.* 91: 47-57

69. Kolpashchikov DM (2005) Binary Malachite Green Aptamer for Fluorescent Detection of Nucleic Acids. *J. Am. Chem. Soc.* 127: 12442-12443

70. Baugh C, Grate D, & Wilson C (2000) 2.8 A Crystal Structure of the Malachite Green Aptamer. *J. Mol. Biol.* 301: 117-128

71. Paige JS, Wu KY, & Jaffrey SR (2011) RNA Mimics of Green Fluorescent Protein. *Science* 333: 642-646

72. Shu D, Khisamutdinov E, Zhang L, & Guo P (2013) Programmable Folding of Fusion RNA Complex Driven by the 3WJ Motif of Phi29 Motor PRNA. *Nucleic Acids Res.* 42: e10

73. Tuerk C & Gold L (1990) Systematic Evolution of Ligands by Exponential Enrichment: RNA Ligands to Bacteriophage T4 DNA Ploymerase. *Science* 249: 505-510

74. quino-Jarquin G & Toscano-Garibay JD (2011) RNA Aptamer Evolution: Two Decades of SELEction. *Int. J. Mol Sci.* 12: 9155-9171

75. Lou X, Qian J, Xiao Y, Viel L, Gerdon AE, Lagally ET, Atzberger P, Tarasow TM, Heeger AJ, & Soh HT (2009) Micromagnetic Selection of Aptamers in Microfluidic Channels. *Proc. Natl. Acad. Sci. U. S. A* 106: 2989-2994

76. Guo KT, Ziemer G, Paul A, & Wendel HP (2008) CELL-SELEX: Novel Perspectives of Aptamer-Based Therapeutics. *Int. J. Mol. Sci.* 9: 668-678

77. Li S, Xu H, Ding H, Huang Y, Cao X, Yang G, Li J, Xie Z, Meng Y, Li X, Zhao Q, Shen B, & Shao N (2009) Identification of an Aptamer Targeting HnRNP A1 by Tissue Slide-Based SELEX. *J. Pathol.* 218: 327-336

78. Klug SJ, Huttenhofer A, & Famulok M (1999) In Vitro Selection of RNA Aptamers That Bind Special Elongation Factor SelB, a Protein With Multiple RNA-Binding Sites, Reveals One Major Interaction Domain at the Carboxyl Terminus. *RNA.* 5: 1180-1190

79. Kupakuwana GV, Crill JE, McPike MP, & Borer PN (2011) Acyclic Identification of Aptamers for Human Alpha-Thrombin Using Over-Represented Libraries and Deep Sequencing. *PLoS ONE* 6: e19395

80. Cho M, Xiao Y, Nie J, Stewart R, Csordas AT, Oh SS, Thomson JA, & Soh HT (2010) Quantitative Selection of DNA Aptamers Through Microfluidic Selection and High-Throughput Sequencing. *Proc. Natl. Acad. Sci. U. S. A* 107: 15373-15378

81. Zon G & Geiser TG (1991) Phosphorothioate Oligonucleotides: Chemistry, Purification, Analysis, Scale-Up and Future Directions. *Anticancer Drug Des* 6: 539-568

82. Veedu RN & Wengel J (2010) Locked Nucleic Acids: Promising Nucleic Acid Analogs for Therapeutic Applications. *Chem Biodivers.* 7: 536-542

83. Knudsen SM, Robertson MP, & Ellington AD (2002) In Vitro Selection Using Modified or Unnatural Nucleotides. *Curr. Protoc. Nucleic Acid Chem* Chapter 9: Unit

84. Green LS, Jellinek D, Bell C, Beebe LA, Feistner BD, Gill SC, Jucker FM, & Janjic N (1995) Nuclease-Resistant Nucleic Acid Ligands to Vascular Permeability Factor/Vascular Endothelial Growth Factor. *Chem. Biol.* 2: 683-695

85. Pagratis NC, Bell C, Chang YF, Jennings S, Fitzwater T, Jellinek D, & Dang C (1997) Potent 2'-Amino-, and 2'-Fluoro-2'-Deoxyribonucleotide RNA Inhibitors of Keratinocyte Growth Factor. *Nat Biotechnol* 15: 68-73

86. Lupold SE, Hicke BJ, Lin Y, & Coffey DS (2002) Identification and Characterization of Nuclease-Stabilized RNA Molecules That Bind Human Prostate Cancer Cells Via the Prostate-Specific Membrane Antigen. *Cancer Res.* 62: 4029-4033

87. Shigdar S, Lin J, Yu Y, Pastuovic M, Wei M, & Duan W (2011) RNA Aptamer Against a Cancer Stem Cell Marker Epithelial Cell Adhesion Molecule. *Cancer Sci.* 102: 991-998

88. Burmeister PE, Lewis SD, Silva RF, Preiss JR, Horwitz LR, Pendergrast PS, McCauley TG, Kurz JC, Epstein DM, Wilson C, & Keefe AD (2005) Direct in Vitro Selection of a 2'-O-Methyl Aptamer to VEGF. *Chem Biol* 12: 25-33

89. Kasahara Y, Irisawa Y, Ozaki H, Obika S, & Kuwahara M (2013) 2',4'-BNA/LNA Aptamers: CE-SELEX Using a DNA-Based Library of Full-Length 2'-O,4'-C-Methylene-Bridged/Linked Bicyclic Ribonucleotides. *Bioorg. Med. Chem. Lett.* 23: 1288-1292

90. Kato Y, Minakawa N, Komatsu Y, Kamiya H, Ogawa N, Harashima H, & Matsuda A (2005) New NTP Analogs: the Synthesis of 4'-ThioUTP and 4'-ThioCTP and Their Utility for SELEX. *Nucleic Acids Res* 33: 2942-2951

91. Burmeister PE, Wang C, Killough JR, Lewis SD, Horwitz LR, Ferguson A, Thompson KM, Pendergrast PS, McCauley TG, Kurz M, Diener J, Cload ST, Wilson C, & Keefe AD (2006) 2'-Deoxy Purine, 2'-O-Methyl Pyrimidine (DRmY) Aptamers As Candidate Therapeutics. *Oligonucleotides* 16: 337-351

92. Keefe AD & Cload ST (2008) SELEX With Modified Nucleotides. *Curr. Opin. Chem Biol* 12: 448-456

93. Battersby TR, Ang DN, Burgstaller P, Jurczyk SC, Bowser MT, Buchanan DD, Kennedy RT, & Benner SA (1999) Quantitative Analysis of Receptors for Adenosine Nucleotides Obtained Via in Vitro Selection From a Library Incorporating a Cationic Nucleotide Analog. *J Am. Chem Soc* 121: 9781-9789

94. Wiegand TW, Janssen RC, & Eaton BE (1997) Selection of RNA Amide Synthases. *Chem Biol* 4: 675-683

95. Teramoto N, Imanishi Y, & Ito Y (2000) In Vitro Selection of a Ligase Ribozyme Carrying Alkylamino Groups in the Side Chains. *Bioconjug. Chem* 11: 744-748

96. Meek KN, Rangel AE, & Heemstra JM (2016) Enhancing Aptamer Function and Stability Via in Vitro Selection Using Modified Nucleic Acids. *Methods* 106: 29-36

97. Kasahara Y, Kitadume S, Morihiro K, Kuwahara M, Ozaki H, Sawai H, Imanishi T, & Obika S (2010) Effect of 3'-End Capping of Aptamer With Various 2',4'-Bridged Nucleotides: Enzymatic Post-Modification Toward a Practical Use of Polyclonal Aptamers. *Bioorg. Med. Chem Lett* 20: 1626-1629

98. Kuwahara M, Obika S, Takeshima H, Hagiwara Y, Nagashima J, Ozaki H, Sawai H, & Imanishi T (2009) Smart Conferring of Nuclease Resistance to DNA by 3'-End Protection Using 2',4'-Bridged Nucleoside-5'-Triphosphates. *Bioorg. Med. Chem Lett* 19: 2941-2943

99. Ng EWM, Shima DT, Calias P, Cunningham ET, Guyer DR, & Adamis AP (2006) Pegaptanib, a Targeted Anti-VEGF Aptamer for Ocular Vascular Disease. *Nature Reviews Drug Discovery* 5: 123-132

100. Jellinek D, Green LS, Bell C, & Janjic N (1994) Inhibition of Receptor Binding by High-Affinity RNA Ligands to Vascular Endothelial Growth Factor. *Biochemistry* 33: 10450-10456

101. Ruckman J, Green LS, Beeson J, Waugh S, Gillette WL, Henninger DD, Claesson-Welsh L, & Janjic N (1998) 2 '-Fluoropyrimidine RNA-Based Aptamers to the 165-Amino Acid Form of Vascular Endothelial Growth Factor (VEGF(165)) - Inhibition of Receptor Binding and VEGF-Induced Vascular Permeability Through Interactions Requiring the Exon 7-Encoded Domain. *J Biol Chem* 273: 20556-20567

102. Bock LC, Griffin LC, Latham JA, Vermaas EH, & Toole JJ (1992) Selection of Single-Stranded-Dna Molecules That Bind and Inhibit Human Thrombin. *Nature* 355: 564-566

103. Ni X, Castanares M, Mukherjee A, & Lupold SE (2011) Nucleic Acid Aptamers: Clinical Applications and Promising New Horizons. *Curr. Med. Chem* 18: 4206-4214

104. Xiong X, Liu H, Zhao Z, Altman MB, Lopez-Colon D, Yang CJ, Chang LJ, Liu C, & Tan W (2013) DNA Aptamer-Mediated Cell Targeting. *Angew. Chem. Int. Ed Engl.* 52: 1472-1476

105. Liu X, Yan H, Liu Y, & Chang Y (2011) Targeted Cell-Cell Interactions by DNA Nanoscaffold-Templated Multivalent Bispecific Aptamers. *Small* 7: 1673-1682

106. Gilboa E, McNamara J, & Pastor F (2013) Use of Oligonucleotide Aptamer Ligands to Modulate the Function of Immune Receptors. *Clin. Cancer Res* 19: 1054-1062

107. Zhu H, Li J, Zhang XB, Ye M, & Tan W (2015) Nucleic Acid Aptamer-Mediated Drug Delivery for Targeted Cancer Therapy. *ChemMedChem* 10: 39-45

108. Huang YF, Chang HT, & Tan W (2008) Cancer Cell Targeting Using Multiple Aptamers Conjugated on Nanorods. *Anal. Chem.* 80: 567-572

109. Wang J, Sefah K, Altman MB, Chen T, You M, Zhao Z, Huang CZ, & Tan W (2013) Aptamer-Conjugated Nanorods for Targeted Photothermal Therapy of Prostate Cancer Stem Cells. *Chem Asian J* 8: 2417-2422

110. Chen T, Shukoor MI, Wang R, Zhao Z, Yuan Q, Bamrungsap S, Xiong X, & Tan W (2011) Smart Multifunctional Nanostructure for Targeted Cancer Chemotherapy and Magnetic Resonance Imaging. *ACS Nano* 5: 7866-7873

111. Zhang Q, Jiang Q, Li N, Dai L, Liu Q, Song L, Wang J, Li Y, Tian J, & Ding B (2014) DNA Origami As an In Vivo Drug Delivery Vehicle for Cancer Therapy. *ACS Nano* 8: 6633-6643

112. Keefe AD, Pai S, & Ellington A (2010) Aptamers As Therapeutics. *Nat Rev. Drug Discov.* 9: 537-550

113. Raposo G & Stoorvogel W (2013) Extracellular Vesicles: Exosomes, Microvesicles, and Friends. *J Cell Biol* 200: 373-383

114. Simpson RJ, Kalra H, & Mathivanan S (2012) ExoCarta As a Resource for Exosomal Research. *J Extracell. Vesicles.* 1:

115. Colombo M, Moita C, van NG, Kowal J, Vigneron J, Benaroch P, Manel N, Moita LF, Thery C, & Raposo G (2013) Analysis of ESCRT Functions in Exosome Biogenesis, Composition and Secretion Highlights the Heterogeneity of Extracellular Vesicles. *J Cell Sci.* 126: 5553-5565

116. van NG, Porto-Carreiro I, Simoes S, & Raposo G (2006) Exosomes: a Common Pathway for a Specialized Function. *J Biochem.* 140: 13-21

117. Savina A, Furlan M, Vidal M, & Colombo MI (2003) Exosome Release Is Regulated by a Calcium-Dependent Mechanism in K562 Cells. *J Biol Chem* 278: 20083-20090

118. Saunderson SC, Schuberth PC, Dunn AC, Miller L, Hock BD, MacKay PA, Koch N, Jack RW, & McLellan AD (2008) Induction of Exosome Release in Primary B Cells Stimulated Via CD40 and the IL-4 Receptor. *J Immunol.* 180: 8146-8152

119. King HW, Michael MZ, & Gleadle JM (2012) Hypoxic Enhancement of Exosome Release by Breast Cancer Cells. *BMC Cancer* 12: 421

120. Riches A, Campbell E, Borger E, & Powis S (2014) Regulation of Exosome Release From Mammary Epithelial and Breast Cancer Cells - a New Regulatory Pathway. *Eur. J Cancer* 50: 1025-1034

121. Mfunyi CM, Vaillancourt M, Vitry J, Nsimba Batomene TR, Posvandzic A, Lambert AA, & Gilbert C (2015) Exosome Release Following Activation of the Dendritic Cell Immunoreceptor: a Potential Role in HIV-1 Pathogenesis. *Virology* 484: 103-112

122. Pan BT & Johnstone RM (1983) Fate of the Transferrin Receptor During Maturation of Sheep Reticulocytes in Vitro: Selective Externalization of the Receptor. *Cell* 33: 967-978

123. Harding C, Heuser J, & Stahl P (1984) Endocytosis and Intracellular Processing of Transferrin and Colloidal Gold-Transferrin in Rat Reticulocytes: Demonstration of a Pathway for Receptor Shedding. *Eur. J Cell Biol* 35: 256-263

124. EL-Andaloussi S., Mager I, Breakefield XO, & Wood MJ (2013) Extracellular Vesicles: Biology and Emerging Therapeutic Opportunities. *Nat Rev. Drug Discov.* 12: 347-357

125. Raposo G, Nijman HW, Stoorvogel W, Liejendekker R, Harding CV, Melief CJ, & Geuze HJ (1996) B Lymphocytes Secrete Antigen-Presenting Vesicles. *J Exp. Med.* 183: 1161-1172

126. Ratajczak J, Miekus K, Kucia M, Zhang J, Reca R, Dvorak P, & Ratajczak MZ (2006) Embryonic Stem Cell-Derived Microvesicles Reprogram Hematopoietic Progenitors: Evidence for Horizontal Transfer of MRNA and Protein Delivery. *Leukemia* 20: 847-856

127. Gatti S, Bruno S, Deregibus MC, Sordi A, Cantaluppi V, Tetta C, & Camussi G (2011) Microvesicles Derived From Human Adult Mesenchymal Stem Cells Protect Against Ischaemia-Reperfusion-Induced Acute and Chronic Kidney Injury. *Nephrol. Dial. Transplant* 26: 1474-1483

128. Del C, I, Shrimpton CN, Thiagarajan P, & Lopez JA (2005) Tissue-Factor-Bearing Microvesicles Arise From Lipid Rafts and Fuse With Activated Platelets to Initiate Coagulation. *Blood* 106: 1604-1611

129. Camussi G, Deregibus MC, Bruno S, Grange C, Fonsato V, & Tetta C (2011) Exosome/Microvesicle-Mediated Epigenetic Reprogramming of Cells. *Am. J Cancer Res* 1: 98-110

130. Mack M, Kleinschmidt A, Bruhl H, Klier C, Nelson PJ, Cihak J, Plachy J, Stangassinger M, Erfle V, & Schlondorff D (2000) Transfer of the Chemokine Receptor CCR5 Between Cells by Membrane-Derived Microparticles: a Mechanism for Cellular Human Immunodeficiency Virus 1 Infection. *Nat Med.* 6: 769-775

131. Bellingham SA, Guo BB, Coleman BM, & Hill AF (2012) Exosomes: Vehicles for the Transfer of Toxic Proteins Associated With Neurodegenerative Diseases? *Front Physiol* 3: 124

132. Marcus ME & Leonard JN (2013) FedExosomes: Engineering Therapeutic Biological Nanoparticles That Truly Deliver. *Pharmaceuticals. (Basel)* 6: 659-680

133. Dreyer F & Baur A (2016) Biogenesis and Functions of Exosomes and Extracellular Vesicles. *Methods Mol Biol* 1448: 201-216

134. Melo SA, Sugimoto H, O'Connell JT, Kato N, Villanueva A, Vidal A, Qiu L, Vitkin E, Perelman LT, Melo CA, Lucci A, Ivan C, Calin GA, & Kalluri R (2014)

Cancer Exosomes Perform Cell-Independent MicroRNA Biogenesis and Promote Tumorigenesis. *Cancer Cell* 26: 707-721

135. Corrado C, Raimondo S, Chiesi A, Ciccia F, De LG, & Alessandro R (2013) Exosomes As Intercellular Signaling Organelles Involved in Health and Disease: Basic Science and Clinical Applications. *Int. J Mol Sci.* 14: 5338-5366

136. Valadi H, Ekstrom K, Bossios A, Sjostrand M, Lee JJ, & Lotvall JO (2007) Exosome-Mediated Transfer of MRNAs and MicroRNAs Is a Novel Mechanism of Genetic Exchange Between Cells. *Nat Cell Biol* 9: 654-659

137. Mittelbrunn M, Gutierrez-Vazquez C, Villarroya-Beltri C, Gonzalez S, Sanchez-Cabo F, Gonzalez MA, Bernad A, & Sanchez-Madrid F (2011) Unidirectional Transfer of MicroRNA-Loaded Exosomes From T Cells to Antigen-Presenting Cells. *Nat Commun.* 2: 282

138. Singer O, Marr RA, Rockenstein E, Crews L, Coufal NG, Gage FH, Verma IM, & Masliah E (2005) Targeting BACE1 With SiRNAs Ameliorates Alzheimer Disease Neuropathology in a Transgenic Model. *Nat Neurosci.* 8: 1343-1349

139. varez-Erviti L, Seow Y, Yin H, Betts C, Lakhal S, & Wood MJ (2011) Delivery of SiRNA to the Mouse Brain by Systemic Injection of Targeted Exosomes. *Nat Biotechnol.* 29: 341-345

140. Pegtel DM, Cosmopoulos K, Thorley-Lawson DA, van Eijndhoven MA, Hopmans ES, Lindenberg JL, de Gruijl TD, Wurdinger T, & Middeldorp JM

(2010) Functional Delivery of Viral MiRNAs Via Exosomes. *Proc. Natl. Acad. Sci. U. S. A* 107: 6328-6333

141. Ohno S, Takanashi M, Sudo K, Ueda S, Ishikawa A, Matsuyama N, Fujita K, Mizutani T, Ohgi T, Ochiya T, Gotoh N, & Kuroda M (2013) Systemically Injected Exosomes Targeted to EGFR Deliver Antitumor MicroRNA to Breast Cancer Cells. *Mol Ther.* 21: 185-191

142. Lener T, Gimona M, Aigner L, Borger V, Buzas E, Camussi G, Chaput N, Chatterjee D, Court FA, Del Portillo HA, O'Driscoll L, Fais S, Falcon-Perez JM, Felderhoff-Mueser U, Fraile L, Gho YS, Gorgens A, Gupta RC, Hendrix A, Hermann DM, Hill AF, Hochberg F, Horn PA, de KD, Kordelas L, Kramer BW, Kramer-Albers EM, Laner-Plamberger S, Laitinen S, Leonardi T, Lorenowicz MJ, Lim SK, Lotvall J, Maguire CA, Marcilla A, Nazarenko I, Ochiya T, Patel T, Pedersen S, Pocsfalvi G, Pluchino S, Quesenberry P, Reischl IG, Rivera FJ, Sanzenbacher R, Schallmoser K, Slaper-Cortenbach I, Strunk D, Tonn T, Vader P, van Balkom BW, Wauben M, Andaloussi SE, Thery C, Rohde E, & Giebel B (2015) Applying Extracellular Vesicles Based Therapeutics in Clinical Trials - an ISEV Position Paper. *J Extracell. Vesicles.* 4: 30087

143. Federici C, Petrucci F, Caimi S, Cesolini A, Logozzi M, Borghi M, D'Ilio S, Lugini L, Violante N, Azzarito T, Majorani C, Brambilla D, & Fais S (2014) Exosome Release and Low PH Belong to a Framework of Resistance of Human Melanoma Cells to Cisplatin. *PLoS ONE* 9: e88193

144. Parolini I, Federici C, Raggi C, Lugini L, Palleschi S, De MA, Coscia C, Iessi E, Logozzi M, Molinari A, Colone M, Tatti M, Sargiacomo M, & Fais S (2009) Microenvironmental PH Is a Key Factor for Exosome Traffic in Tumor Cells. *J Biol Chem* 284: 34211-34222

145. Pascucci L, Cocce V, Bonomi A, Ami D, Ceccarelli P, Ciusani E, Vigano L, Locatelli A, Sisto F, Doglia SM, Parati E, Bernardo ME, Muraca M, Alessandri G, Bondiolotti G, & Pessina A (2014) Paclitaxel Is Incorporated by Mesenchymal Stromal Cells and Released in Exosomes That Inhibit in Vitro Tumor Growth: a New Approach for Drug Delivery. *J Control Release* 192: 262-270

146. Kim MS, Haney MJ, Zhao Y, Mahajan V, Deygen I, Klyachko NL, Inskoe E, Piroyan A, Sokolsky M, Okolie O, Hingtgen SD, Kabanov AV, & Batrakova EV (2016) Development of Exosome-Encapsulated Paclitaxel to Overcome MDR in Cancer Cells. *Nanomedicine* 12: 655-664

147. Toffoli G, Hadla M, Corona G, Caligiuri I, Palazzolo S, Semeraro S, Gamini A, Canzonieri V, & Rizzolio F (2015) Exosomal Doxorubicin Reduces the Cardiac Toxicity of Doxorubicin. *Nanomedicine (Lond)*

148. Navabi H, Croston D, Hobot J, Clayton A, Zitvogel L, Jasani B, Bailey-Wood R, Wilson K, Tabi Z, Mason MD, & Adams M (2005) Preparation of Human Ovarian Cancer Ascites-Derived Exosomes for a Clinical Trial. *Blood Cells Mol Dis.* 35: 149-152

149. Wolfers J, Lozier A, Raposo G, Regnault A, Thery C, Masurier C, Flament C, Pouzieux S, Faure F, Tursz T, Angevin E, Amigorena S, & Zitvogel L (2001) Tumor-Derived Exosomes Are a Source of Shared Tumor Rejection Antigens for CTL Cross-Priming. *Nat Med.* 7: 297-303

150. Andre F, Chaput N, Schartz NE, Flament C, Aubert N, Bernard J, Lemonnier F, Raposo G, Escudier B, Hsu DH, Tursz T, Amigorena S, Angevin E, & Zitvogel L (2004) Exosomes As Potent Cell-Free Peptide-Based Vaccine. I. Dendritic Cell-Derived Exosomes Transfer Functional MHC Class I/Peptide Complexes to Dendritic Cells. *J Immunol.* 172: 2126-2136

151. Dai S, Wei D, Wu Z, Zhou X, Wei X, Huang H, & Li G (2008) Phase I Clinical Trial of Autologous Ascites-Derived Exosomes Combined With GM-CSF for Colorectal Cancer. *Mol Ther.* 16: 782-790

152. Escudier B, Dorval T, Chaput N, Andre F, Caby MP, Novault S, Flament C, Leboulaire C, Borg C, Amigorena S, Boccaccio C, Bonnerot C, Dhellin O, Movassagh M, Piperno S, Robert C, Serra V, Valente N, Le Pecq JB, Spatz A, Lantz O, Tursz T, Angevin E, & Zitvogel L (2005) Vaccination of Metastatic Melanoma Patients With Autologous Dendritic Cell (DC) Derived-Exosomes: Results of Thefirst Phase I Clinical Trial. *J Transl. Med.* 3: 10

153. Morse MA, Garst J, Osada T, Khan S, Hobeika A, Clay TM, Valente N, Shreeniwas R, Sutton MA, Delcayre A, Hsu DH, Le Pecq JB, & Lyerly HK (2005) A Phase I Study of Dexosome Immunotherapy in Patients With Advanced Non-Small Cell Lung Cancer. *J Transl. Med.* 3: 9

154. Dai S, Wei D, Wu Z, Zhou X, Wei X, Huang H, & Li G (2008) Phase I Clinical Trial of Autologous Ascites-Derived Exosomes Combined With GM-CSF for Colorectal Cancer. *Mol Ther.* 16: 782-790

155. Besse B, Charrier M, Lapierre V, Dansin E, Lantz O, Planchard D, Le CT, Livartoski A, Barlesi F, Laplanche A, Ploix S, Vimond N, Peguillet I, Thery C, Lacroix L, Zoernig I, Dhodapkar K, Dhodapkar M, Viaud S, Soria JC, Reiners KS, Pogge von SE, Vely F, Rusakiewicz S, Eggermont A, Pitt JM, Zitvogel L, & Chaput N (2016) Dendritic Cell-Derived Exosomes As Maintenance Immunotherapy After First Line Chemotherapy in NSCLC. *Oncoimmunology.* 5: e1071008

156. Khisamutdinov EF, Jasinski DL, & Guo P (2014) RNA As a Boiling-Resistant Anionic Polymer Material to Build Robust Structures With Defined Shape and Stoichiometry. *ACS Nano.* 8: 4771-4781

157. Guo S, Tschammer N, Mohammed S, & Guo P (2005) Specific Delivery of Therapeutic RNAs to Cancer Cells Via the Dimerization Mechanism of Phi29 Motor PRNA. *Hum Gene Ther.* 16: 1097-1109

158. Reif R, Haque F, & Guo P (2013) Fluorogenic RNA Nanoparticles for Monitoring RNA Folding and Degradation in Real Time in Living Cells. *Nucleic Acid Ther.* 22(6): 428-437

159. Larkin MA, Blackshields G, Brown NP, Chenna R, McGettigan PA, McWilliam H, Valentin F, Wallace IM, Wilm A, Lopez R, Thompson JD, Gibson TJ, &

Higgins DG (2007) Clustal W and Clustal X Version 2.0. *Bioinformatics* 23: 2947-2948

160. Corpet F (1988) Multiple Sequence Alignment With Hierarchical Clustering. *Nucleic Acids Res* 16: 10881-10890

161. Zuker M (2003) Mfold Web Server for Nucleic Acid Folding and Hybridization Prediction. *Nucleic Acids Res.* 31: 3406-3415

162. Obad S, dos Santos CO, Petri A, Heidenblad M, Broom O, Ruse C, Fu C, Lindow M, Stenvang J, Straarup EM, Hansen HF, Koch T, Pappin D, Hannon GJ, & Kauppinen S (2011) Silencing of MicroRNA Families by Seed-Targeting Tiny LNAs. *Nat. Genet.* 43: 371-378

163. Ellington AD (2009) Back to the Future of Nucleic Acid Self-Amplification. *Nature Chemical Biology* 5: 200-201

164. Sundaram P, Kurniawan H, Byrne ME, & Wower J (2013) Therapeutic RNA Aptamers in Clinical Trials. *Eur. J Pharm. Sci.* 48: 259-271

165. Moghimi SM, Hunter AC, & Andresen TL (2012) Factors Controlling Nanoparticle Pharmacokinetics: An Integrated Analysis and Perspective. *Annual Review of Pharmacology and Toxicology, Vol 52* 52: 481-503

166. Longmire M, Choyke PL, & Kobayashi H (2008) Clearance Properties of Nano-Sized Particles and Molecules As Imaging Agents: Considerations and Caveats. *Nanomedicine (Lond)* 3: 703-717

167. Shopsowitz KE, Roh YH, Deng ZJ, Morton SW, & Hammond PT (2014) RNAi-Microsponges Form Through Self-Assembly of the Organic and Inorganic Products of Transcription. *Small* 10: 1623-1633

168. Liang Z & Wang XJ (2013) Rising From Ashes: Non-Coding RNAs Come of Age. *J Genet. Genomics* 40: 141-142

169. Abdelmawla S, Guo S, Zhang L, Pulukuri S, Patankar P, Conley P, Trebley J, Guo P, & Li QX (2011) Pharmacological Characterization of Chemically Synthesized Monomeric PRNA Nanoparticles for Systemic Delivery. *Molecular Therapy* 19: 1312-1322

170. Gires O & Bauerle PA (2010) EpCAM As a Target in Cancer Therapy. *Journal of Clinical Oncology* 28: E239-E240

171. Lin CW, Liao MY, Lin WW, Wang YP, Lu TY, & Wu HC (2012) Epithelial Cell Adhesion Molecule Regulates Tumor Initiation and Tumorigenesis Via Activating Reprogramming Factors and Epithelial-Mesenchymal Transition Gene Expression in Colon Cancer. *J. Biol. Chem.* 287: 39449-39459

172. Munz M, Baeuerle PA, & Gires O (2009) The Emerging Role of EpCAM in Cancer and Stem Cell Signaling. *Cancer Res.* 69: 5627-5629

173. Subramanian N, Raghunathan V, Kanwar JR, Kanwar RK, Elchuri SV, Khetan V, & Krishnakumar S (2012) Target-Specific Delivery of Doxorubicin to Retinoblastoma Using Epithelial Cell Adhesion Molecule Aptamer. *Mol. Vis.* 18: 2783-2795

174. Mi ZY, Guo HT, Russell MB, Liu YM, Sullenger BA, & Kuo PC (2009) RNA Aptamer Blockade of Osteopontin Inhibits Growth and Metastasis of MDA-MB231 Breast Cancer Cells. *Molecular Therapy* 17: 153-161

175. Okada Y & Hirokawa N (1999) A Processive Single-Headed Motor: Kinesin Superfamily Protein KIF1A. *Science* 283: 1152-1157

176. Brischwein K, Schlereth B, Guller B, Steiger C, Wolf A, Lutterbuese R, Offner S, Locher M, Urbig T, Raum T, Kleindienst P, Wimberger P, Kimmig R, Fichtner I, Kufer P, Hofmeister R, da Silva AJ, & Baeuerle PA (2006) MT110: a Novel Bispecific Single-Chain Antibody Construct With High Efficacy in Eradicating Established Tumors. *Mol. Immunol.* 43: 1129-1143

177. Diez S, Reuther C, Dinu C, Seidel R, Mertig M, Pompe W, & Howard J (2003) Stretching and Transporting DNA Molecules Using Motor Proteins. *Nano Letters* 3: 1251-1254

178. Hess H, Matzke CM, Doot RK, Clemmens J, Bachand GD, Bunker BC, & Vogel V (2003) Molecular Shuttles Operating Undercover: A New Photolithographic Approach for the Fabrication of Structured Surfaces Supporting Directed Motility. *Nano Letters* 3: 1651-1655

179. Jia LL, Moorjani SG, Jackson TN, & Hancock WO (2004) Microscale Transport and Sorting by Kinesin Molecular Motors. *Biomedical Microdevices* 6: 67-74

180. Xiong B, Cheng Y, Ma L, & Zhang C (2013) MiR-21 Regulates Biological Behavior Through the PTEN/PI-3 K/Akt Signaling Pathway in Human Colorectal Cancer Cells. *Int. J Oncol.* 42: 219-228

181. Schramedei K, Morbt N, Pfeifer G, Lauter J, Rosolowski M, Tomm JM, von Bergen M, Horn F, & Brocke-Heidrich K (2011) MicroRNA-21 Targets Tumor Suppressor Genes ANP32A and SMARCA4. *Oncogene* 30: 2975-2985

182. Thery C, Amigorena S, Raposo G, & Clayton A (2006) Isolation and Characterization of Exosomes From Cell Culture Supernatants and Biological Fluids. *Curr. Protoc. Cell Biol* Chapter 3: Unit 3.22

183. Jasinski D, Schwartz C, Haque F, & Guo P (2015) Large Scale Purification of RNA Nanoparticles by Preparative Ultracentrifugation. *Methods in Molecular Biology* 1297: 67-82

184. Zhang H, Endrizzi JA, Shu Y, Haque F, Sauter C, Shlyakhtenko LS, Lyubchenko Y, Guo P, & Chi YI (2013) Crystal Structure of 3WJ Core Revealing Divalent Ion-Promoted Thermostability and Assembly of the Phi29 Hexameric Motor PRNA. *RNA* 19: 1226-1237

185. Lamichhane TN, Raiker RS, & Jay SM (2015) Exogenous DNA Loading into Extracellular Vesicles Via Electroporation Is Size-Dependent and Enables Limited Gene Delivery. *Mol. Pharm.* 12: 3650-3657

186. Bunge A, Loew M, Pescador P, Arbuzova A, Brodersen N, Kang J, Dahne L, Liebscher J, Herrmann A, Stengel G, & Huster D (2009) Lipid Membranes

Carrying Lipophilic Cholesterol-Based Oligonucleotides--Characterization and Application on Layer-by-Layer Coated Particles. *J Phys Chem. B* 113: 16425-16434

187. Pfeiffer I & Hook F (2004) Bivalent Cholesterol-Based Coupling of Oligonucletides to Lipid Membrane Assemblies. *J Am. Chem. Soc* 126: 10224-10225

188. Kumar D, Gupta D, Shankar S, & Srivastava RK (2015) Biomolecular Characterization of Exosomes Released From Cancer Stem Cells: Possible Implications for Biomarker and Treatment of Cancer. *Oncotarget* 6: 3280-3291

189. van Dongen HM, Masoumi N, Witwer KW, & Pegtel DM (2016) Extracellular Vesicles Exploit Viral Entry Routes for Cargo Delivery. *Microbiol. Mol. Biol. Rev.* 80: 369-386

190. Parker N, Turk MJ, Westrick E, Lewis JD, Low PS, & Leamon CP (2005) Folate Receptor Expression in Carcinomas and Normal Tissues Determined by a Quantitative Radioligand Binding Assay. *Anal. Biochem.* 338: 284-293

191. Dassie JP, Hernandez LI, Thomas GS, Long ME, Rockey WM, Howell CA, Chen Y, Hernandez FJ, Liu XY, Wilson ME, Allen LA, Vaena DA, Meyerholz DK, & Giangrande PH (2014) Targeted Inhibition of Prostate Cancer Metastases With an RNA Aptamer to Prostate-Specific Membrane Antigen. *Mol Ther.* 22: 1910-1922

192. Rockey WM, Hernandez FJ, Huang SY, Cao S, Howell CA, Thomas GS, Liu XY, Lapteva N, Spencer DM, McNamara JO, Zou X, Chen SJ, & Giangrande PH

(2011) Rational Truncation of an RNA Aptamer to Prostate-Specific Membrane Antigen Using Computational Structural Modeling. *Nucleic Acid Ther.* 21: 299-314

193. Paduano F, Villa R, Pennati M, Folini M, Binda M, Daidone MG, & Zaffaroni N (2006) Silencing of Survivin Gene by Small Interfering RNAs Produces Supra-Additive Growth Suppression in Combination With 17-Allylamino-17-Demethoxygeldanamycin in Human Prostate Cancer Cells. *Molecular Cancer Therapeutics* 5: 179-186

194. Tian Y, Li S, Song J, Ji T, Zhu M, Anderson GJ, Wei J, & Nie G (2014) A Doxorubicin Delivery Platform Using Engineered Natural Membrane Vesicle Exosomes for Targeted Tumor Therapy. *Biomaterials* 35: 2383-2390

195. Li Y, Tian Z, Rizvi SM, Bander NH, & Allen BJ (2002) In Vitro and Preclinical Targeted Alpha Therapy of Human Prostate Cancer With Bi-213 Labeled J591 Antibody Against the Prostate Specific Membrane Antigen. *Prostate Cancer Prostatic. Dis.* 5: 36-46

196. Pettaway CA, Pathak S, Greene G, Ramirez E, Wilson MR, Killion JJ, & Fidler IJ (1996) Selection of Highly Metastatic Variants of Different Human Prostatic Carcinomas Using Orthotopic Implantation in Nude Mice. *Clin. Cancer Res* 2: 1627-1636

197. Pecot CV, Calin GA, Coleman RL, Lopez-Berestein G, & Sood AK (2011) RNA Interference in the Clinic: Challenges and Future Directions. *Nat Rev. Cancer* 11: 59-67

198. El-Andaloussi S, Lakhal S, Mager I, & Wood MJ (2013) Exosomes for Targeted SiRNA Delivery Across Biological Barriers. *Adv. Drug Deliv. Rev.* 65: 391-397

199. van Dommelen SM, Vader P, Lakhal S, Kooijmans SA, van Solinge WW, Wood MJ, & Schiffelers RM (2012) Microvesicles and Exosomes: Opportunities for Cell-Derived Membrane Vesicles in Drug Delivery. *J Control Release* 161: 635-644

200. Wiklander OP, Nordin JZ, O'Loughlin A, Gustafsson Y, Corso G, Mager I, Vader P, Lee Y, Sork H, Seow Y, Heldring N, varez-Erviti L, Smith CE, Le BK, Macchiarini P, Jungebluth P, Wood MJ, & Andaloussi SE (2015) Extracellular Vesicle in Vivo Biodistribution Is Determined by Cell Source, Route of Administration and Targeting. *J Extracell. Vesicles.* 4: 26316

201. Kulshreshtha A, Ahmad T, Agrawal A, & Ghosh B (2013) Proinflammatory Role of Epithelial Cell-Derived Exosomes in Allergic Airway Inflammation. *J. Allergy Clin. Immunol.* 131: 1194-203, 1203

202. Batrakova EV & Kim MS (2015) Using Exosomes, Naturally-Equipped Nanocarriers, for Drug Delivery. *J. Control Release*

203. Lokman NA, Ween MP, Oehler MK, & Ricciardelli C (2011) The Role of Annexin A2 in Tumorigenesis and Cancer Progression. *Cancer Microenviron.* 4: 199-208

204. Sharma MC & Sharma M (2007) The Role of Annexin II in Angiogenesis and Tumor Progression: a Potential Therapeutic Target. *Curr. Pharm Des* 13: 3568-3575

205. Kang SA, Hasan N, Mann AP, Zheng W, Zhao L, Morris L, Zhu W, Zhao YD, Suh KS, Dooley WC, Volk D, Gorenstein DG, Cristofanilli M, Rui H, & Tanaka T (2015) Blocking the Adhesion Cascade at the Premetastatic Niche for Prevention of Breast Cancer Metastasis. *Mol. Ther.* 23: 1044-1054

206. Mangala L, Wang H, Jiang D, Wu S, Somasunderam A, VolK D, Lokesh G, Li X, Pradeep S, Yang X, Haemmerle M, Rodriguez-Aguayo C, Nagaraja A, Rupaimoole R, Bayraktar R, Li L, Hu W, Ivan C, Gharpure K, McGuire M, Thiviyanathan V, Maiti S, Cooper L, Bulayeva N, Choi H, Dorniak P, Rosenblatt K, Tanaka T, Lopez-Berestein G, Gorenstein D, & Sood A (2016) Improving Tumor Vascular Maturation Using Non-Coding RNAs Increases Anti-Tumor Effect of Chemotherapy. *J. Clin. Invest.* (In revision):

207. A'hern RP & Gore ME (1995) Impact of Doxorubicin on Survival in Advanced Ovarian Cancer. *J. Clin. Oncol.* 13: 726-732

208. Rose PG (2005) Pegylated Liposomal Doxorubicin: Optimizing the Dosing Schedule in Ovarian Cancer. *Oncologist* 10: 205-214

209. D'Souza SS & Deluca PP (2006) Methods to Assess in Vitro Drug Release From Injectable Polymeric Particulate Systems. *Pharm. Res.* 23: 460-474

210. Chaires JB, Herrera JE, & Waring MJ (1990) Preferential Binding of Daunomycin to 5'ATCG and 5'ATGC Sequences Revealed by Footprinting Titration Experiments. *Biochemistry* 29: 6145-6153

211. Frederick CA, Williams LD, Ughetto G, van der Marel GA, van Boom JH, Rich A, & Wang AH (1990) Structural Comparison of Anticancer Drug-DNA Complexes: Adriamycin and Daunomycin. *Biochemistry* 29: 2538-2549

212. Bagalkot V, Farokhzad OC, Langer R, & Jon S (2006) An Aptamer-Doxorubicin Physical Conjugate As a Novel Targeted Drug-Delivery Platform. *Angew. Chem. Int. Ed Engl.* 45: 8149-8152

213. Valentini L, Nicolella V, Vannini E, Menozzi M, Penco S, & Arcamone F (1985) Association of Anthracycline Derivatives With DNA: a Fluorescence Study. *Farmaco Sci.* 40: 377-390

214. Zhang N, Wu ZM, McGowan E, Shi J, Hong ZB, Ding CW, Xia P, & Di W (2009) Arsenic Trioxide and Cisplatin Synergism Increase Cytotoxicity in Human Ovarian Cancer Cells: Therapeutic Potential for Ovarian Cancer. *Cancer Sci.* 100: 2459-2464

215. Lokman NA, Elder AS, Ween MP, Pyragius CE, Hoffmann P, Oehler MK, & Ricciardelli C (2013) Annexin A2 Is Regulated by Ovarian Cancer-Peritoneal Cell Interactions and Promotes Metastasis. *Oncotarget.* 4: 1199-1211

216. Batra S, Adekola KUA, Rosen ST, & Shanmugam M (2013) Cancer Metabolism As a Therapeutic Target. *ONCOLOGY-NEW YORK* 27: 460-467

217. Aird KM, Ding XY, Baras A, Wei JP, Morse MA, Clay T, Lyerly HK, & Devi GR (2008) Trastuzumab Signaling in ErbB2-Overexpressing Inflammatory Breast Cancer Correlates With X-Linked Inhibitor of Apoptosis Protein Expression. *Molecular Cancer Therapeutics* 7: 38-47

218. Park SH, Kim H, & Song BJ (2002) Down Regulation of Bcl2 Expression in Invasive Ductal Carcinomas Is Both Estrogen- and Progesterone-Receptor Dependent and Associated With Poor Prognostic Factors. *Pathol. Oncol. Res.* 8: 26-30

219. Lakshmanan M & Xavier AS (2013) Bedaquiline - The First ATP Synthase Inhibitor Against Multi Drug Resistant Tuberculosis. *J. Young. Pharm.* 5: 112-115

220. Akinc A, Querbes W, De S, Qin J, Frank-Kamenetsky M, Jayaprakash KN, Jayaraman M, Rajeev KG, Cantley WL, Dorkin JR, Butler JS, Qin L, Racie T, Sprague A, Fava E, Zeigerer A, Hope MJ, Zerial M, Sah DW, Fitzgerald K, Tracy MA, Manoharan M, Koteliansky V, Fougerolles A, & Maier MA (2010) Targeted Delivery of RNAi Therapeutics With Endogenous and Exogenous Ligand-Based Mechanisms. *Mol. Ther.* 18: 1357-1364

221. Aronov O, Horowitz AT, Gabizon A, & Gibson D (2003) Folate-Targeted PEG As a Potential Carrier for Carboplatin Analogs. Synthesis and in Vitro Studies. *Bioconjugate Chem.* 14: 563-574

222. Bae YH & Park K (2011) Targeted Drug Delivery to Tumors: Myths, Reality and Possibility. *J. Control Release* 153: 198-205

223. Guo P, Haque F, Hallahan B, Reif R, & Li H (2012) Uniqueness, Advantages, Challenges, Solutions, and Perspectives in Therapeutics Applying RNA Nanotechnology. *Nucleic Acid Ther.* 22: 226-245

224. Chatterjee A, Chattopadhyay D, & Chakrabarti G (2014) MiR-17-5p Downregulation Contributes to Paclitaxel Resistance of Lung Cancer Cells Through Altering Beclin1 Expression. *PLoS ONE* 9: e95716

225. Sanchez C, Chan R, Bajgain P, Rambally S, Palapattu G, Mims M, Rooney CM, Leen AM, Brenner MK, & Vera JF (2013) Combining T-Cell Immunotherapy and Anti-Androgen Therapy for Prostate Cancer. *Prostate Cancer Prostatic. Dis.*

226. Lusky K (1999) HIV's Potent Cocktail. *Contemp. Longterm. Care* 22: 59

227. Ito M, Zhao N, Zeng Z, Chang CC, & Zu Y (2010) Synergistic Growth Inhibition of Anaplastic Large Cell Lymphoma Cells by Combining Cellular ALK Gene Silencing and a Low Dose of the Kinase Inhibitor U0126. *Cancer Gene Ther.*

228. Shu D, Pi F, Wang C, Zhang P, & Guo P (2015) New Approach to Develop Ultra-High Inhibitory Drug Using the Power-Function of the Stoichiometry of the Targeted Nanomachine or Biocomplex. *Nanomedicine* 10: 1881-1897

229. Fang H, Zhang P, Huang LP, Zhao Z, Pi F, Montemagno C, & Guo P (2014) Binomial Distribution for Quantification of Protein Subunits in Biological Nanoassemblies and Functional Nanomachines. *Nanomedicine.* 10: 1433-1440

230. Fang H, Jing P, Haque F, & Guo P (2012) Role of Channel Lysines and "Push Through a One-Way Valve" Mechanism of Viral DNA Packaging Motor. *Biophysical Journal* 102: 127-135

231. Hugel T, Michaelis J, Hetherington CL, Jardine PJ, Grimes S, Walter JM, Faik W, Anderson DL, & Bustamante C (2007) Experimental Test of Connector Rotation During DNA Packaging into Bacteriophage Phi29 Capsids. *Plos Biology* 5: 558-567

232. Xiao F, Moll D, Guo S, & Guo P (2005) Binding of PRNA to the N-Terminal 14 Amino Acids of Connector Protein of Bacterial Phage Phi29. *Nucleic Acids Res* 33: 2640-2649

233. Guo P, Peterson C, & Anderson D (1987) Prohead and DNA-Gp3-Dependent ATPase Activity of the DNA Packaging Protein Gp16 of Bacteriophage Phi29. *J Mol Biol* 197: 229-236

234. Schwartz C, De Donatis GM, Fang H, & Guo P (2013) The ATPase of the Phi29 DNA-Packaging Motor Is a Member of the Hexameric AAA+ Superfamily. *Virology* 443: 20-27

235. Zhang H, Schwartz C, De Donatis GM, & Guo P (2012) "Push Through One-Way Valve" Mechanism of Viral DNA Packaging. *Adv. Virus Res* 83: 415-465

236. Trottier M & Guo P (1997) Approaches to Determine Stoichiometry of Viral Assembly Components. *J. Virol.* 71: 487-494

237. Schwartz C, De Donatis GM, Zhang H, Fang H, & Guo P (2013) Revolution Rather Than Rotation of AAA+ Hexameric Phi29 Nanomotor for Viral DsDNA Packaging Without Coiling. *Virology* 443: 28-39

238. Zhao Z, Khisamutdinov E, Schwartz C, & Guo P (2013) Mechanism of One-Way Traffic of Hexameric Phi29 DNA Packaging Motor With Four Electropositive Relaying Layers Facilitating Anti-Parallel Revolution. *ACS Nano* 7: 4082-4092

239. Guo P, Schwartz C, Haak J, & Zhao Z (2013) Discovery of a New Motion Mechanism of Biomotors Similar to the Earth Revolving Around the Sun Without Rotation. *Virology* 446: 133-143

240. Guo P, Grainge I, Zhao Z, & Vieweger M (2014) Two Classes of Nucleic Acid Translocation Motors: Rotation and Revolution Without Rotation. *Cell Biosci.* 4: 54

241. De-Donatis G, Zhao Z, Wang S, Huang PL, Schwartz C, Tsodikov VO, Zhang H, Haque F, & Guo P (2014) Finding of Widespread Viral and Bacterial Revolution DsDNA Translocation Motors Distinct From Rotation Motors by Channel Chirality and Size. *Cell Biosci* 4: 30

242. Wolfe A, Phipps K, & Weitao T (2014) Viral and Cellular SOS-Regulated Motor Proteins: DsDNA Translocation Mechanisms With Divergent Functions. *Cell Biosci.* 4: 31

243. Guo P, Peterson C, & Anderson D (1987) Initiation Events in *in Vitro* Packaging of Bacteriophage Phi29 DNA-Gp3. *J Mol Biol* 197: 219-228

244. Sperlagh B & Illes P (2014) P2X7 Receptor: an Emerging Target in Central Nervous System Diseases. *Trends Pharmacol. Sci.* 35: 537-547

245. Schiebel J, Chang A, Shah S, Lu Y, Liu L, Pan P, Hirschbeck MW, Tareilus M, Eltschkner S, Yu WX, Cummings JE, Knudson SE, Bommineni GR, Walker SG, Slayden RA, Sotriffer CA, Tonge PJ, & Kisker C (2014) Rational Design of Broad Spectrum Antibacterial Activity Based on a Clinically Relevant Enoyl-Acyl Carrier Protein (ACP) Reductase Inhibitor. *J Biol Chem* 289: 15987-16005

246. Whitby FG, Luecke H, Kuhn P, Somoza JR, HuetePerez JA, Phillips JD, Hill CP, Fletterick RJ, & Wang CC (1997) Crystal Structure of Tritrichomonas Foetus Inosine-5'-Monophosphate Dehydrogenase and the Enzyme-Product Complex. *Biochemistry* 36: 10666-10674

247. Casjens SR (2011) The DNA-Packaging Nanomotor of Tailed Bacteriophages. *Nat Rev. Microbiol.* 9: 647-657

248. Guo P, Zhao Z, Haak J, Wang S, Wu D, Meng B, & Weitao T (2014) Common Mechanisms of DNA Translocation Motors in Bacteria and Viruses Using One-Way Revolution Mechanism Without Rotation. *Biotechnology Advances* 32: 853-872

249. Buskin SE, Zhang S, & Thibault CS (2012) Prevalence of and Viral Outcomes Associated With Primary HIV-1 Drug Resistance. *Open. AIDS J.* 6: 181-187

250. Boal AK, Ilhan F, DeRouchey JE, Thurn-Albrecht T, Russell TP, & Rotello VM (2000) Self-Assembly of Nanoparticles into Structured Spherical and Network Aggregates. *Nature* 404: 746-748

251. Holohan C, Van SS, Longley DB, & Johnston PG (2013) Cancer Drug Resistance: an Evolving Paradigm. *Nat. Rev. Cancer* 13: 714-726

252. Hanson PI & Whiteheart SW (2005) AAA+ Proteins: Have Engine, Will Work. *Nat. Rev. Mol Cell Biol.* 6: 519-529

253. Lee CS & Guo P (1995) Sequential Interactions of Structural Proteins in Phage Phi29 Procapsid Assembly. *J. Virol.* 69: 5024-5032

254. Stitt BL & Xu Y (1998) Sequential Hydrolysis of ATP Molecules Bound in Interacting Catalytic Sites of Escherichia Coli Transcription Termination Protein Rho. *J. Biol. Chem.* 273: 26477-26486

255. Persechini A & Hartshorne DJ (1982) Cooperative Behavior of Smooth Muscle Myosin. *Fed. Proc.* 41: 2868-2872

256. Lisal J & Tuma R (2005) Cooperative Mechanism of RNA Packaging Motor. *J Biol Chem* 280: 23157-23164

257. Andrews BT & Catalano CE (2013) Strong Subunit Coordination Drives a Powerful Viral DNA Packaging Motor. *Proc. Natl. Acad. Sci. U. S. A* 110: 5909-5914

258. Zhang H, Shu D, Huang F, & Guo P (2007) Instrumentation and Metrology for Single RNA Counting in Biological Complexes or Nanoparticles by a Single Molecule Dual-View System. *RNA* 13: 1793-1802

259. Chen C, Trottier M, & Guo P (1997) New Approaches to Stoichiometry Determination and Mechanism Investigation on RNA Involved in Intermediate Reactions. *Nucleic Acids Symposium Series* 36: 190-193

260. Chen C & Guo P (1997) Sequential Action of Six Virus-Encoded DNA-Packaging RNAs During Phage Phi29 Genomic DNA Translocation. *J. Virol.* 71: 3864-3871

261. Kammerer RA, Schulthess T, Landwehr R, Lustig A, Fischer D, & Engel J (1998) Tenascin-C Hexabrachion Assembly Is a Sequential Two-Step Process Initiated by Coiled-Coil Alpha-Helices. *J. Biol. Chem.* 273: 10602-10608

262. Zhang Z, Lewis D, Strock C, Inesi G, Nakasako M, Nomura H, & Toyoshima C (2000) Detailed Characterization of the Cooperative Mechanism of Ca(2+) Binding and Catalytic Activation in the Ca(2+) Transport (SERCA) ATPase. *Biochemistry* 39: 8758-8767

263. Sun H & Squier TC (2000) Ordered and Cooperative Binding of Opposing Globular Domains of Calmodulin to the Plasma Membrane Ca-ATPase. *J. Biol. Chem.* 275: 1731-1738

264. Hiller R & Carmeli C (1990) Kinetic Analysis of Cooperative Interactions Induced by Mn2+ Binding to the Chloroplast H(+)-ATPase. *Biochemistry* 29: 6186-6192

265. Casjens, S. and Hendrix, R. (1988) Control mechanisms in dsDNA bacteriophage assembly. In Calendar, R., editor. *The Bacteriophages Vol.1*, Plenum Pubishing Corp., New York

266. Qian X, Ren Y, Shi Z, Long L, Pu P, Sheng J, Yuan X, & Kang C (2012) Sequence-Dependent Synergistic Inhibition of Human Glioma Cell Lines by Combined Temozolomide and MiR-21 Inhibitor Gene Therapy. *Mol Pharm.* 9: 2636-2645

267. Gillman S, Gillard M, & Strolin BM (2009) The Concept of Receptor Occupancy to Predict Clinical Efficacy: a Comparison of Second Generation H1 Antihistamines. *Allergy Asthma Proc.* 30: 366-376

268. Shu D, Zhang H, Jin J, & Guo P (2007) Counting of Six PRNAs of Phi29 DNA-Packaging Motor With Customized Single Molecule Dual-View System. *EMBO J.* 26: 527-537

269. Lee CS & Guo P (1994) A Highly Sensitive System for the Assay of in Vitro Viral Assembly of Bacteriophage Phi29 of Bacillus Subtilis. *Virology* 202: 1039-1042

270. Schwartz C, Fang H, Huang L, & Guo P (2012) Sequential Action of ATPase, ATP, ADP, Pi and DsDNA in Procapsid-Free System to Enlighten Mechanism in Viral DsDNA Packaging. *Nucleic Acids Res.* 40: 2577-2586

271. Han W, Shen Y, & She Q (2014) Nanobiomotors of Archaeal DNA Repair Machineries: Current Research Status and Application Potential. *Cell Biosci.* 4: 32

272. Swuec P & Costa A (2014) Molecular Mechanism of Double Holliday Junction Dissolution. *Cell Biosci.* 4: 36

273. Happonen LJ, Erdmann S, Garrett RA, & Butcher SJ (2014) Adenosine Triphosphatases of Thermophilic Archaeal Double-Stranded DNA Viruses. *Cell Biosci.* 4: 37

274. Junge W, Lill H, & Engelbrecht S (1997) ATP Synthase: an Electrochemical Transducer With Rotatory Mechanics. *Trends in Biochemical Sciences* 22: 420-423

275. DeRosier DJ (1998) The Turn of the Screw: the Bacterial Flagellar Motor. *Cell* 93: 17-20

276. Yoshida M, Muneyuki E, & Hisabori T (2003) ATP Synthase--a Marvellous Rotary Engine of the Cell. *Nat Rev Mol Cell Biol* 2(9): 669-677

277. Okuno D, Iino R, & Noji H (2011) Rotation and Structure of FoF1-ATP Synthase. *Journal of Biochemistry* 149: 655-664

278. Kaplan DL & Steitz TA (1999) DnaB From Thermus Aquaticus Unwinds Forked Duplex DNA With an Asymmetric Tail Length Dependence. *J. Biol. Chem.* 274: 6889-6897

279. LeBowitz JH & McMacken R (1986) The *Escherichia Coli* DnaB Replication Protein Is a DNA Helicase. *The Journal of Biological Chemistry* 261: 4738-4748

280. Itsathitphaisarn O, Wing RA, Eliason WK, Wang J, & Steitz TA (2012) The Hexameric Helicase DnaB Adopts a Nonplanar Conformation During Translocation. *Cell* 151: 267-277

281. Thomsen ND & Berger JM (2009) Running in Reverse: the Structural Basis for Translocation Polarity in Hexameric Helicases. *Cell* 139: 523-534

282. Di CE, Engel A, Stasiak A, & Koller T (1982) Characterization of Complexes Between RecA Protein and Duplex DNA by Electron Microscopy. *J. Mol. Biol.* 157: 87-103

283. VanLoock MS, Yu X, Yang SX, Lai AL, Low C, Campbell MJ, & Egelman EH (2003) ATP-Mediated Conformational Changes in the RecA Filament. *Structure* 11: 187-196

284. Ammelburg M, Frickey T, & Lupas AN (2006) Classification of AAA+ Proteins. *J Struct Biol* 156: 2-11

285. Guo PX & Lee TJ (2007) Viral Nanomotors for Packaging of DsDNA and DsRNA. *Mol. Microbiol.* 64: 886-903

286. Snider J & Houry WA (2008) AAA+ Proteins: Diversity in Function, Similarity in Structure. *Biochemical Society Transactions* 36: 72-77

287. Snider J, Thibault G, & Houry WA (2008) The AAA+ Superfamily of Functionally Diverse Proteins. *Genome Biol* 9: 216

288. Chemla YR, Aathavan K, Michaelis J, Grimes S, Jardine PJ, Anderson DL, & Bustamante C (2005) Mechanism of Force Generation of a Viral DNA Packaging Motor. *Cell.* 122: 683-692

289. Hwang Y, Catalano CE, & Feiss M (1996) Kinetic and Mutational Dissection of the Two ATPase Activities of Terminase, the DNA Packaging Enzyme of Bacteriophage Lambda. *Biochemistry* 35: 2796-2803

290. Guenther B, Onrust R, Sali A, O'Donnell M, & Kuriyan J (1997) Crystal Structure of the Delta' Subunit of the Clamp-Loader Complex of E. Coli DNA Polymerase III. *Cell* 91: 335-345

291. McNally R, Bowman GD, Goedken ER, O'Donnell M, & Kuriyan J (2010) Analysis of the Role of PCNA-DNA Contacts During Clamp Loading. *BMC. Struct. Biol.* 10: 3

292. Aussel L, Barre FX, Aroyo M, Stasiak A, Stasiak AZ, & Sherratt D (2002) FtsK Is a DNA Motor Protein That Activates Chromosome Dimer Resolution by Switching the Catalytic State of the XerC and XerD Recombinases. *Cell* 108: 195-205

293. Barre FX, Aroyo M, Colloms SD, Helfrich A, Cornet F, & Sherratt DJ (2000) FtsK Functions in the Processing of a Holliday Junction Intermediate During Bacterial Chromosome Segregation. *Genes Dev.* 14: 2976-2988

294. Yu XC, Weihe EK, & Margolin W (1998) Role of the C Terminus of FtsK in Escherichia Coli Chromosome Segregation. *J. Bacteriol.* 180: 6424-6428

295. Burton B & Dubnau D (2010) Membrane-Associated DNA Transport Machines. *Cold Spring Harb. Perspect. Biol.* 2: a000406

296. Pease PJ, Levy O, Cost GJ, Gore J, Ptacin JL, Sherratt D, Bustamante C, & Cozzarelli NR (2005) Sequence-Directed DNA Translocation by Purified FtsK. *Science* 307: 586-590

297. Crozat E & Grainge I (2010) FtsK DNA Translocase: the Fast Motor That Knows Where It's Going. *Chembiochem.* 11: 2232-2243

298. Massey TH, Mercogliano CP, Yates J, Sherratt DJ, & Lowe J (2006) Double-Stranded DNA Translocation: Structure and Mechanism of Hexameric FtsK. *Mol. Cell* 23: 457-469

299. Lowe J, Ellonen A, Allen MD, Atkinson C, Sherratt DJ, & Grainge I (2008) Molecular Mechanism of Sequence-Directed DNA Loading and Translocation by FtsK. *Mol. Cell* 31: 498-509

300. Casado V, Cortes A, Mallol J, Perez-Capote K, Ferre S, Lluis C, Franco R, & Canela EI (2009) GPCR Homomers and Heteromers: a Better Choice As Targets for Drug Development Than GPCR Monomers? *Pharmacol. Ther.* 124: 248-257

301. Makowska-Grzyska M, Kim Y, Maltseva N, Osipiuk J, Gu M, Zhang M, Mandapati K, Gollapalli DR, Gorla SK, Hedstrom L, & Joachimiak A (2015) A Novel Cofactor-Binding Mode in Bacterial IMP Dehydrogenases Explains Inhibitor Selectivity. *J. Biol. Chem.* 290: 5893-5911

302. Murakami S, Nakashima R, Yamashita E, & Yamaguchi A (2002) Crystal Structure of Bacterial Multidrug Efflux Transporter AcrB. *Nature* 419: 587-593

303. Sennhauser G, Bukowska MA, Briand C, & Grutter MG (2009) Crystal Structure of the Multidrug Exporter MexB From Pseudomonas Aeruginosa. *J. Mol. Biol.* 389: 134-145

304. Hu S, Chen Z, Franke R, Orwick S, Zhao M, Rudek MA, Sparreboom A, & Baker SD (2009) Interaction of the Multikinase Inhibitors Sorafenib and Sunitinib With

Solute Carriers and ATP-Binding Cassette Transporters. *Clin. Cancer Res.* 15: 6062-6069

305. Ziolo MT, Martin JL, Bossuyt J, Bers DM, & Pogwizd SM (2005) Adenoviral Gene Transfer of Mutant Phospholamban Rescues Contractile Dysfunction in Failing Rabbit Myocytes With Relatively Preserved SERCA Function. *Circ. Res.* 96: 815-817

306. Aker J, Hesselink R, Engel R, Karlova R, Borst JW, Visser AJWG, & de Vries SC (2007) *In Vivo* Hexamerization and Characterization of the Arabidopsis AAA ATPase CDC48A Complex Using Forster Resonance Energy Transfer-Fluorescence Lifetime Imaging Microscopy and Fluorescence Correlation Spectroscopy. *Plant Physiology* 145: 339-350

307. White SR & Lauring B (2007) AAA+ ATPases: Achieving Diversity of Function With Conserved Machinery. *Traffic* 8: 1657-1667

308. Willows RD, Hansson A, Birch D, Al-Karadaghi S, & Hansson M (2004) EM Single Particle Analysis of the ATP-Dependent BchI Complex of Magnesium Chelatase: an AAA(+) Hexamer. *J Struct Biol* 146: 227-233

309. Iyer LM, Leipe DD, Koonin EV, & Aravind L (2004) Evolutionary History and Higher Order Classification of AAA Plus ATPases. *J Struct Biol* 146: 11-31

310. Liu Y, Huang T, MacMorris M, & Blumenthal T (2001) Interplay Between AAUAAA and the Trans-Splice Site in Processing of a Caenorhabditis Elegans Operon Pre-MRNA. *RNA.* 7: 176-181

311. Watanabe R, Matsukage Y, Yukawa A, Tabata KV, & Noji H (2014) Robustness of the Rotary Catalysis Mechanism of F-1-ATPase. *J Biol Chem* 289: 19331-19340

312. Yasuda R, Noji H, Kinosita K, Jr., & Yoshida M (1998) F1-ATPase Is a Highly Efficient Molecular Motor That Rotates With Discrete 120 Degree Steps. *Cell* 93: 1117-1124

313. Kinosita K, Jr., Yasuda R, Noji H, Ishiwata S, & Yoshida M (1998) F1-ATPase: a Rotary Motor Made of a Single Molecule. *Cell* 93: 21-24

314. Stock D, Leslie AG, & Walker JE (1999) Molecular Architecture of the Rotary Motor in ATP Synthase. *Science* 286: 1700-1705

315. Boyer PD (1999) What Makes ATP Synthase Spin? *Nature* 402: 247-249

316. Adachi K, Yasuda R, Noji H, Itoh H, Harada Y, Yoshida M, & Kinosita K, Jr. (2000) Stepping Rotation of F1-ATPase Visualized Through Angle-Resolved Single- Fluorophore Imaging. *Proc. Natl. Acad. Sci. U. S. A* 97: 7243-7247

317. Hara KY, Noji H, Bald D, Yasuda R, Kinosita K, Jr., & Yoshida M (2000) The Role of the DELSEED Motif of the Beta Subunit in Rotation of F1- ATPase. *J. Biol. Chem.* 275: 14260-14263

318. Masaike T, Mitome N, Noji H, Muneyuki E, Yasuda R, Kinosita K, & Yoshida M (2000) Rotation of F(1)-ATPase and the Hinge Residues of the Beta Subunit. *J. Exp. Biol.* 203 Pt 1: 1-8

319. Wada Y, Sambongi Y, & Futai M (2000) Biological Nano Motor, ATP Synthase F(o)F(1): From Catalysis to Gammaepsilonc(10-12) Subunit Assembly Rotation. *Biochim. Biophys. Acta* 1459: 499-505

320. Okazaki K & Hummer G (2013) Phosphate Release Coupled to Rotary Motion of F-1-ATPase. *Proceedings of the National Academy of Sciences of the United States of America* 110: 16468-16473

321. Ito Y, Yoshidome T, Matubayasi N, Kinoshita M, & Ikeguchi M (2013) Molecular Dynamics Simulations of Yeast F-1-ATPase Before and After 16 Degrees Rotation of the Gamma Subunit. *Journal of Physical Chemistry B* 117: 3298-3307

322. Arai HC, Yukawa A, Iwatate RJ, Kamiya M, Watanabe R, Urano Y, & Noji H (2014) Torque Generation Mechanism of F-1-ATPase Upon NTP Binding. *Biophysical Journal* 107: 156-164

323. Trottier M, Zhang CL, & Guo P (1996) Complete Inhibition of Virion Assembly *in Vivo* With Mutant PRNA Essential for Phage Phi29 DNA Packaging. *J. Virol.* 70: 55-61

324. Sprowl JA, Ciarimboli G, Lancaster CS, Giovinazzo H, Gibson AA, Du G, Janke LJ, Cavaletti G, Shields AF, & Sparreboom A (2013) Oxaliplatin-Induced Neurotoxicity Is Dependent on the Organic Cation Transporter OCT2. *Proc. Natl. Acad. Sci. U. S. A* 110: 11199-11204

325. Furmanski BD, Hu S, Fujita K, Li L, Gibson AA, Janke LJ, Williams RT, Schuetz JD, Sparreboom A, & Baker SD (2013) Contribution of ABCC4-Mediated Gastric Transport to the Absorption and Efficacy of Dasatinib. *Clin. Cancer Res.* 19: 4359-4370

326. Hung ME & Leonard JN (2015) Stabilization of Exosome-Targeting Peptides Via Engineered Glycosylation. *J Biol Chem.* 290: 8166-8172

Curriculum Vitae

Pi Fengmei

Colleague of Pharmacy, University of Kentucky/ College of Pharmacy, The Ohio State University

(+1)859 317 0499 ● fengmei.pi@uky.edu

EXPERIENCE

01/2016-Now **College of Pharmacy, The Ohio State University**

Visiting Scholar in Dr. Peixuan Guo's Lab

- Research Area: Developing platforms of exosome based RNAi delivery system for targeted cancer therapy.

01/2012- Now **College of Pharmacy, University of Kentucky**

Ph. D Candidate/Graduate Student in Dr. Peixuan Guo's Lab

- Research Area: Developing platforms for cancer cell targeted drug delivery system, including selecting RNA aptamer targeting cancer cell protein marker, constructing RNA nanoparticles containing RNA aptamers for cancer treatment, and developing extracellular vesicle based RNAi delivery system. The projects are going on well under Dr. Peixuan Guo's mentorship.

09/2009-12/2011 **Tianjin Smith Kline & French Laboratories Co., Ltd.**

Consumer Healthcare R&D of Glaxo Smith Kline Co. in China

Senior Formulation Scientist, New Product Development, R&D

- Led "Bactroban Wound wash" innovation team in a key company project and I was in charge of the formulation design, process study and also technical transfer part. It is the first TSKF's self innovated consumer healthcare product. This product has been successfully launched to China market in July 2012.
- Led a research project about OTC product, studying on formula composition and process development. Cooperated with Manufacturing and Regulation Department of TSKF, resulting in successfully applying the New Project Permission and Manufacture License issued by SFDA.
- Supported the quality system with building up and maintenance of several SOPs regarding lab equipment operation and maintenance, material management system, significant figures and NPD excellence guideline document.
- Built up sensory study platform for NPD of TSKF R&D. Coworked with several project teams on the sensory study planning and implementation. Resulted good sensory test result to support patent application.
- Participated Knowledge and Methods Training of Innovation.

08/2007-09/2009 **Daewoong Pharmaceutical Co., Ltd. YongYin, Korea**

Research Scientist, Formulation Department of R&D

- Carried out formulation study and process development for a generic tablet dosage form drug which has passed the Bio Equivalence Test, and formulation study report has been submitted to KFDA for the Clinical Trial Permit.
- Led the formulation research of paediatric suspension syrup per oral. This formulation had passed sensory study and stability test.

07/2005-06/2010 **Argosi International Co., Ltd.**

Part-time, Translator

- Provided documentary translation between Chinese and English.

EDUCATION

01/2012-Now **University of Kentucky (UK)**

Ph.D candidate, Graduate student; Major: Pharmaceutical Science

Program: Graduate School, Doctor of Philosophy

- Cumulative GPA: 3.571

09/2000-06/2007 **China Pharmaceutical University (CPU)**

Master Degree; Major: Pharmaceutics, June 2007

- Overall GPA: 3.50

Bachelor Degree; Major: Traditional Chinese Medicine, June 2004

- Overall GPA: 3.50

PUBLICATION

1. **Pi F**, Zhang H, Li H, Thiviyanathan V, Gorenstein D, Sood A.k, Guo P. RNA Nanoparticles Harboring Annexin A2 Aptamer can Target Ovarian Cancer for Tumor Specific Doxorubicin Delivery. Molecular Therapy (under submission).
2. **Pi F**, Li H, Sun M, Haque F, Binzel D, Wang S, Guo B, Evers, B.M, Guo P. Nanoparticle Orientation to Control RNA Loading or Surface Display of Extracellular Vesicles for Efficient Cell Targeting, siRNA Delivery and Cancer Regression. Nature Nanotechnology (under revision).
3. **Pi F**, Zhao Z, Chelikani V, Yoder K, Kvaratskhelia M, Guo P. Development of Potent Antiviral Drugs Inspired by Viral Hexameric DNA Packaging Motors with Revolving Mechanism. Journal of Virology. 2016 pii: JVI.00508-16.
4. Li H, Zhang K, **Pi F**, Guo S, Shlyakhtenko L., Chiu W, Shu D, Guo P. Controllable Self-Assembly of RNA Tetrahedrons with Precise Shape and Size for Cancer Targeting. Advanced Material. 2016 doi: 10.1002.
5. **Pi F**, Vieweger M, Zhao Z, Wang S, Guo P. Discovery of a new method for potent drug development using power function of stoichiometry of homomeric biocomplexes or biological nanomotors. Expert Opinion on Drug Delivery. 2016. Jan; 13(1): 23-36.
6. Li H, Lee T, Dziubla T, **Pi F**, Guo S, Xu J, Li C, Haque F, Liang X, Guo P. RNA as a stable polymer to build controllable and defined nanostructures for material and biomedical applications. Nanotoday. 2015 Oct 1, 10(5):631-655.
7. Sharma A, Haque F, **Pi F**, Guo P. Controllable Self-assembly of RNA Dendrimers. Nanomedicine. 2016, 12(3):835-44.
8. Lee T, Ygati AK, **Pi F**, Sharma A, Choi JW, Guo P. Construction of RNA–Quantum Dot Chimera for Nanoscale Resistive Biomemory Application. ACS Nano. 2015, 9 (7), pp 6675–6682.
9. Li H, Rychahou PG, Cui Z, **Pi F**, Evers BM, Shu D, Guo P, Luo W. RNA Nanoparticles Derived from Three-Way Junction of Phi29 Motor pRNA Are Resistant to I-125 and Cs-131 Radiation. Nucleic Acid Ther. 2015 Aug; 25(4):188-97.
10. Shu D, **Pi F**, Wang C, Zhang P, Guo P. New approach to develop ultra-high inhibitory drug using the power-function of the stoichiometry of the targeted nanomachine or biocomplex. Nanomedicine , 2015, 10(12), 1881-1897.

11. Zhang H, **Pi F,** Shu D, Vieweger M, Guo P. RNA nanoparticles with thermostable motifs and fluorogenic modules for real-time detection of RNA folding and turnover in vivo. RNA Nanotechnology and Therapeutics: Methods and Protocols, Methods in Molecular Biology, Springer Press. 2015; 1297:95-111.
12. Shu Y, **Pi F,** Sharma A, Rajabi M, Haque F, Shu D, Leggas M, Evers BM, Guo P. Stable RNA nanoparticles as potential new generation drugs for cancer therapy. Adv Drug Deliv Rev. 2014 Feb; 66: 74-89.
13. Fang H, Zhang P, Huang LP, Zhao Z, **Pi F,** Montemagno C, Guo P. Binomial distribution for quantification of protein subunits in biological Nanoassemblies and functional nanomachines. Nanomedicine. 2014, 10(7): 1433-40.
14. Germer K, **Pi F,** Guo P and Zhang X. Conjugation of RNA Aptamer to RNA Nanoparticles for targeted drug delivery. RNA Nanotechnology and Therapeutics, CRC Press. 2013.
15. **Pi Fengmei,** Tu Xide, Wu Yue, Preparation of ATP-2Na Loaded Liposome and Its Effect On Tissues Energy State in Myocardial Ischemic Mice, Acta Pharmaceutical Sinica, 2010, 45 (10) 1322-1326.
16. **Pi Fengmei**, Tu Xide, Zhou Jianping, Recent Development in ATP-Loaded Liposome, Pharmaceutical and Clinical Research, 2007 Vol.15, No.1

ACADEMIC REASEARCH

04/2016 Attended the NIH Extracellular RNA Communication Consortium (ERCC) 6th Investigators' Meeting and presented poster "Non-destructive Purification of Exosomes Using Cushion Ultracentrifugation with Iso-osmotic Material", North Bethesda, MD, USA.

06/2015 Attended Pharmaceutical Graduate Student Research Meeting and Presented poster "New approach to develop ultra-high inhibitory drug using the power-function of the stoichiometry of the targeted nanomachine or biocomplex". Lexington, KY, USA

02/2015 Attended Gordon Research Conference frontiers of science RNA Nanotechnology and presented poster "New approach to develop ultra-high inhibitory drug using the power function of the stoichiometry of the targeted hexameric RNA and other components of nanomachine or biocomplex ". Ventura, CA, USA

10/2014 Attended Southeastern Regional Meeting of American Chemical Science and did Oral presentation "Multi-subunit RNA complex as potent drug target: Elucidating potency dependent on stoichiometry of the nano-machine". Nashville, TN, USA

05/2014 Attended Markey Cancer Research Day and presented poster "RNA nanotechnology approach to generate stable and high affinity RNA nanoparticle binds to T cell", Lexington, KY, USA

09/2013 Attended Annual Symposium on Drug Discovery and Development and presented poster "Assembly of therapeutic pRNA-siRNA nanoparticles using bipartite approach", Lexington, KY, USA

05/2013 Attended Markey Cancer Research Day and presented poster "Generation of 2'-Fluoro-RNA Aptamer that bind a cancer stem cell marker epithelial cell adhesion molecule", Lexington, KY, USA

04/2013 Attended Rho Chi Research Day and presented poster "Generation of 2'-Fluoro-RNA Aptamer that binds a cancer stem cell marker epithelial cell adhesion molecule", Lexington, KY, USA

04/2013 Attended 2nd international Conference of RNA Nanotehcnology and Therapeutics and presented poster "Assembly of therapeutic pRNA-siRNA nanoparticles using bipartite approach", Lexington, KY, USA.

08/2009 Sensory Study Method Review, my presentation in work

06/2007	Research on ATP-2Na Loaded Liposome, my presentation for Master Degree
04/2006	Research Progress on Solid Lipid Nanoparticle Drug Delivery System
03/2006	Preparation of Biodegradable Microcapsules Using for Antigen Delivery System
09/2005	Application of the Combination of Water-soluble Polymers in Drug Delivery System
05/2005	Central Composite Design-Response Surface Methodology, my presentation with a colleague
03/2005	Application of Micro-manufacturing Technology in Controlled Release System

ACTIVITIES

09/2012-09/2014	Served as Drug discovery division graduate student representative in AAPS student Chapter, Lexington, KY, USA
07/2011	Completed GSK High Performance Leadership Behaviors Training: Effective Presentation Skills. Beijing, China
08/2010	Completed HEART@HUB learning program by SDC Consulting, Beijing, China
08/2010	Sixth Annual Conference for Topical Medication Industry, Hangzhou, China
10/2008	Participated Global project leadership programme Impact Workshop, Beijing, China
10/2006-12/2006	Participated in the 1st Simcere Creative Intellectual Cultivation, organized by CPU and Simcere Co.
10/2005	Interviewed the excellent people's representative-Li Yuanlong
09/2000-06/2004	Serviced as private tutor for high school students
03/2004	Participated in and organized the volunteer activities to serve Nursing Home of CPU
09/2002-06/2003	Served as a member of English Salon, CPU, and exchanged with others
09/2002-06/2003	Served as Deputy Chief of Baili Fenlan Environmental Protection Association and organized various activities to protect environment
09/2001-06/2002	Served as student journalist of the university newspaper, CPU
05/2001	Participated in the university debate contest and obtained the Champion , CPU

AWARDS & NEWS RELEASE

07/2015	Scicasts News: New method to develop more efficient drugs described
07/2015	UKY News: UK Study Reveals New Method to Develop More Efficient Drugs
07/2015	Nanowerk News: A new approach to develop highly-potent drugs
05/2015	Markey Cancer Research Day, Researcher's Choice Award, University of Kentucky
12/2012	3T Ambassador, TSK&F
06/2012	GSK Spirit Recognition: High Performance Behavior-Build Confidence
10/2011	GSK Spirit Recognition: High Performance Behavior-Continuous Improvement
06/2009	Core Value Practice Award, Daewoong Pharmaceutical, Co. Ltd.
11/2005	International Specialty Products, Inc Scholarship, CPU
04/2004	Handan Scholarship, CPU
11/2003, 04/2001	Third-Class Scholarship, CPU
11/2001-04/2003	Second-Class Scholarship for 4 times, CPU
09/2002	Excellent Student Journalist Award, CPU
11/2001	First Prize of Campus Debate Contest, CPU
05/2001	First Prize of Campus Chorus Contest, CPU